Y 3. At7
22ANL-6301
AEC
RESEARCH REPORTS

ANL-6301

UNIVERSITY OF
ARIZONA LIBRARY
Documents Collection
MAR 22 1961

Argonne National Laboratory

IDAHO DIVISION

SUMMARY REPORT

July, August, September, 1960

metadc67212

LEGAL NOTICE

This report was prepared as an account of Government sponsored work. Neither the United States, nor the Commission, nor any person acting on behalf of the Commission:

A. Makes any warranty or representation, expressed or implied, with respect to the accuracy, completeness, or usefulness of the information contained in this report, or that the use of any information, apparatus, method, or process disclosed in this report may not infringe privately owned rights; or

B. Assumes any liabilities with respect to the use of, or for damages resulting from the use of any information, apparatus, method, or process disclosed in this report.

As used in the above, "person acting on behalf of the Commission" includes any employee or contractor of the Commission, or employee of such contractor, to the extent that such employee or contractor of the Commission, or employee of such contractor prepares, disseminates, or provides access to, any information pursuant to his employment or contract with the Commission, or his employment with such contractor.

Price $2.50 . *Available from the Office of Technical Services, Department of Commerce, Washington 25, D.C.*

ANL-6301
Reactor Technology
(TID-4500, 16th Ed.)
AEC Research and
Development Report

ARGONNE NATIONAL LABORATORY
9700 South Cass Avenue
Argonne, Illinois

IDAHO DIVISION
SUMMARY REPORT

July, August, September, 1960

Meyer Novick, Division Director
F. W. Thalgott, Associate Division Director

Operated by The University of Chicago
under
Contract W-31-109-eng-38

TABLE OF CONTENTS

TABLE OF CONTENTS

LIST OF FIGURES

LIST OF FIGURES

LIST OF FIGURES

LIST OF TABLES

LIST OF TABLES

ACKNOWLEDGMENTS

Project supervisors who have reported on the work of the Idaho Division are as follows:

F. D. McGinnis, EBR-I

J. K. Long, ZPR-III

J. F. Boland, TREAT

R. E. Rice, BORAX V

G. S. Brunson, Jr., AFSR

The report was edited by W. P. Rosenthal.

A. EXPERIMENTAL BREEDER REACTOR I

(F. D. McGinnis, Project Supervisor)

A. EXPERIMENTAL BREEDER REACTOR I

I. Stability Studies (R. R. Smith)

From the results of instability studies it may be concluded that the operational characteristics of the fully ribbed and rigid Mark III loading of EBR-I are governed by feedback processes which guarantee safe and stable operation under normal operating conditions. The influence of the stabilizing ribs is felt in two ways, both of which are in the direction of increased stability. The ribs provide strong radial coupling between fuel rods and between fuel rods and hexagonal subassemblies; consequently, a large radial contribution to the power coefficient is realized. The ribs have also eliminated, for all practical purposes, positive feedback effects arising from the inward bowing of fuel rods during power increases. Absolutely no evidence of positive reactivity effects was noted for the fully ribbed and rigid core.

The results of logical extrapolation of full-power, full-flow test data do indicate that the reactor could be brought into a resonant condition for power levels exceeding 1000 Mw. Since nominal full-power operation is limited to 1.2 Mw, the hypothetical instability is of mere academic interest. The limit to which power may be increased is dictated, not by matters of instability, but by matters of heat removal.

Strong nonlinearities in the power coefficient pose no serious operational problems, at least over the range of power associated with the tests. Except for the region between zero and 200 kw, in which the power coefficient is small but still negative, the power coefficient is everywhere very strongly negative. Whereas the nonlinearities are relatively unimportant from the stability viewpoint, they do greatly complicate the interpretation of test data in turns of a single unified model which may be applied over wide ranges of power, flow, and temperature. The origin of the nonlinearities appears to be a consequence of power-and-temperature-sensitive clearance systems in existence between rods, between rods and hexes, and between hexes.

The power coefficient has also been shown to be sensitive to the temperature of the inlet coolant. The explanation of this effect has been attributed to the strong temperature dependence of the expansion coefficient for the uranium-zirconium fuel material.

The influence of structural feedback has also been observed in Mark III, fortunately to a different and much less serious degree than in the earlier Mark II design. At the higher inlet temperature, approximately 13% of the net power coefficient is associated with a negative feedback

process which operates with a time constant of the order of 400 seconds. In view of the extreme slowness of action, the physical process responsible must certainly be one associated with some massive, and as yet unspecified, structural member located at some downstream location.

Attempts to enhance and measure possible feedback effects arising in the radial breeding blanket were unsuccessful. As a consequence it must be concluded that feedback mechanisms, based on the preheating of inlet coolant by the transfer of heat between one outlet and blanket inlet in series flow are unimportant. Since preheating possibilities are very nearly the same for Mark II and Mark III, it may also be concluded that strong blanket feedback mechanisms, postulated as the source of the delayed negative component for Mark II, are considerably discredited.

The results of removing the stabilizing ribs from fuel rods have demonstrated conclusively the existence of a strong positive effect which logically must be associated with the inward bowing of fuel rods. An extrapolation of the results obtained by shearing the rods from approximately one-third of the fuel rods effective in rod-bowing results in a value of $+2.06 \times 10^{-6}\ \Delta k/k/kw$ for the fully sheared core. Since the prompt negative component associated with fuel coolant and blanket expansion is $-.205 \times 10^{-6}\ \Delta k/k/kw$, the response of the reactor even when fully sheared would still be governed by a smaller, but still negative, prompt power coefficient. Under these conditions runaway excursions, such as the one which damaged the Mark II core, would be impossible. An application of the Nyquist stability criterion to the extrapolated, fully sheared data results in the conclusion that the reactor would attain resonance instability at full flow at approximately 11 Mw and for a frequency of 0.14 c/sec.

It has also been shown that rib-shearing resulted in an unexpected and unexplained increase in the magnitude of the delayed structural power coefficient. As a result of experienced analysis, it has been shown that the decrease in the prompt negative power coefficient is balanced in steady-state operation by an equal increase in the magnitude of the delayed structural component. The origin of the increased structural effect has been associated with wall deformation in those assemblies containing sheared rods.

The results of the Mark III tests have also proven beneficial in understanding the Mark II instabilities. As a result of the Mark III tests it now seems clear that the prompt positive coefficient so obviously present in Mark II was a consequence of two conditions: a strong prompt positive rod-bowing effect; and a greatly reduced prompt negative coefficient which is characteristic of an essentially uncoupled fuel rod system. As an additional item of information, the Mark III tests have also demonstrated that rod-bowing is a consequence of special conditions of fuel-rod restraint, which apparently were realized in Mark II through the expansive

action of the lower shield plate (the first perforated plate immediately above the core). Expansive action brought about by the temperature differential across the core was apparently sufficient to force the rod tips outward in the bottom plate until they formed an ordered system conducive to rod-bowing.

The results of experiments conducted on a shield plate similar to the one installed in the Mark I and II cores have indicated rather definitely that expansive motions induced through temperature changes may well be the source of the long postulated and hitherto unexplained delayed negative power coefficient. Immediately upon heating (with either air or water), the plate dishes. After a few seconds the dish disappears and begins to expand more slowly in a radial direction. The dishing effect is manifested by an amplified outward motion at core elevation by those fuel rods originally ambiguous with the plate perforations. Rough estimates of the extent of motions along with these amplifications are reasonably consistent with the amount of motion required to satisfy the Mark II test results.

II. 800-Mwh Irradiation Run (J. O. Zane)

During this period an 800-Mwh run was made to irradiate a number of samples for the Chemical Engineering (CEN) and Metallurgical (MET) Divisions of the Laboratory. Seventeen rod specimens for irradiation included: ten rods for CEN containing foils of U^{233}, U^{235}, and Pu^{239} to determine the ratio of capture-to-fission cross section (alpha); and seven rods for MET, three of which contained plutonium and uranium carbide samples, and four of which were plutonium prototypes for the Mark IV core. These latter seven rods will be inspected and analyzed to provide data on dimensional stability and fuel integrity of carbides under attainable temperatures and burnups in this reactor.

In addition to the sample rods, four CEN capsules containing U^{233} foils were located in separate thimbles, two on the inner and two on the outer periphery of one of the 84, stainless steel-jacketed, natural uranium bricks which make up the outer blanket. These keystone-shaped bricks, when fitted together, form a cup outside the reactor tank and surround the core and inner blanket of the reactor. Vertical movement of this outer blanket, combined with that of the control rods which penetrate holes in the bricks, is used to adjust the reactor reactivity.

The ten CEN rods were stainless steel-jacketed, NaK-bonded, and contained natural uranium and uranium highly enriched in the isotope U^{235}, alloyed with 2 w/o Zr. In Fig. 1, rods numbered 1 through 6 are fuel rods installed in the core section. Rods 7 through 10 are blanket rods loaded in a blanket subassembly. Slugs in both these types of rods were of varying numbers and lengths to allow spacing of the foil-containing aluminum capsules along the length of the rods as required.

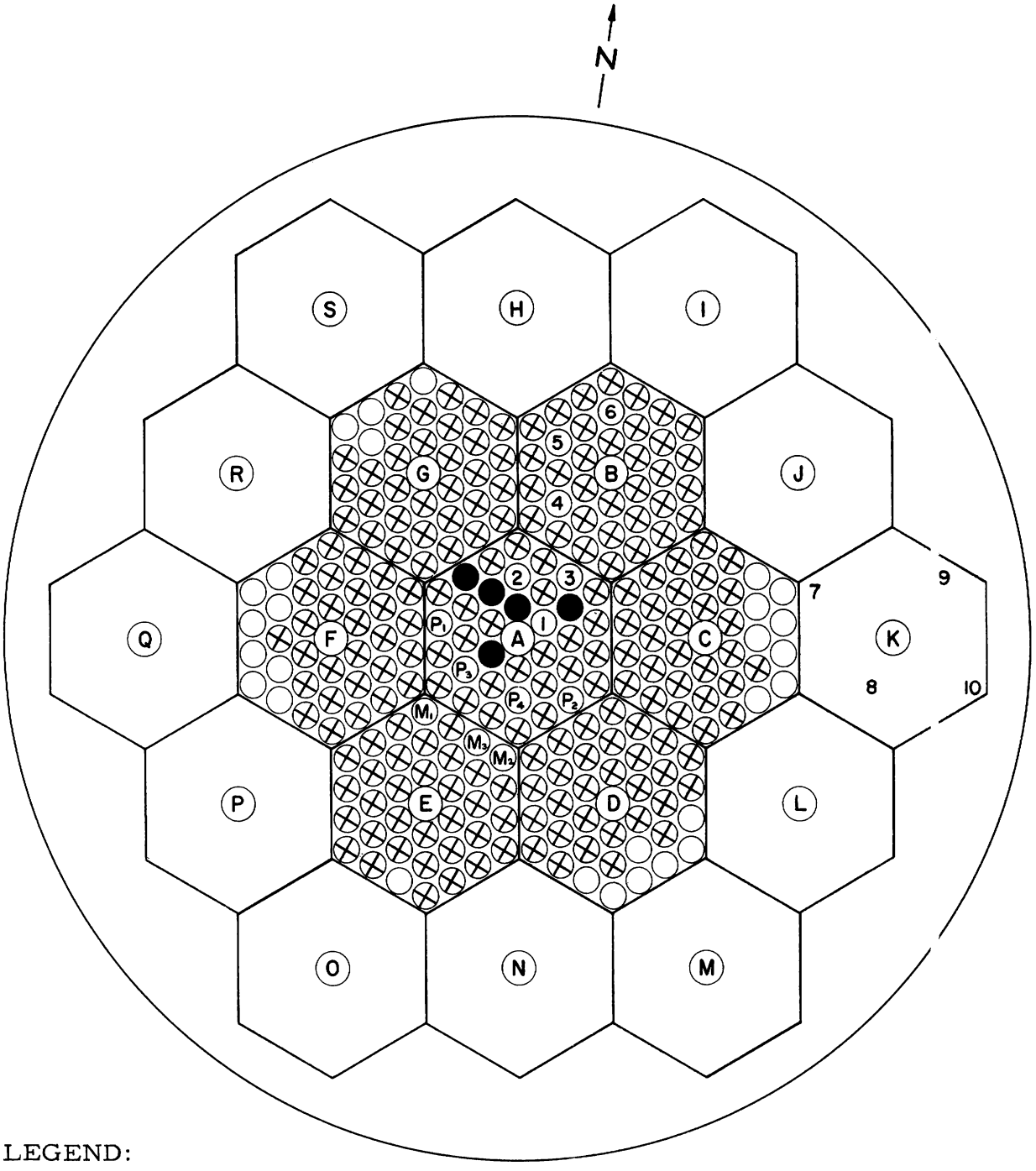

LEGEND:
X Fuel Rods
O Blanket Rods
P(1,2,3,4) Plutonium Prototype Rods
M(1,2,3) Metallurgy Specimen Rod
1 thru 10 CEN Irradiation Specimen Rods
● Mark III Fuel Rods being Monitored

Fig. 1

Loading Diagram
EBR-I, Mark III

The rods were distributed radially from the center to the edge of the reactor core and inner blanket, as shown in Fig. 1. This radial distribution of the rods was combined with a vertical distribution of the foils in the rods to provide radial and vertical sampling of the reactor.

Figure 2 shows the location of the special irradiation brick in position G-5. This places it at the vertical center of the reactor and in an angular position between two beam holes for minimum flux disturbance.

Locations of the rods irradiated for MET (M-1, 2, 3 and P-1, 2, 3, 4) are also shown in the loading diagram Fig. 1. Rod M-3 was loaded entirely with slugs of UC-20 w/o PuC, and had a thermocouple well within the fuel. Rods M-1 and M-2 were not provided with a thermocouple well. Their loadings consisted of alternating, one-inch slugs of PuC and UC-20 w/o PuC. As seen from Table I, a maximum temperature of 365°C was measured.

The plutonium prototype rods, P-1 through 4, were made with a fuel-to-slug diameter of 0.200 in. and jacket diameters from 0.280 down to 0.250 in., to give an annulus between the fuel and jacket of either 0.020, 0.010, or 0.005 in. These rods were slightly smaller than the final design diameter of the EBR-I, Mark IV rods. Two of these rods contained thermocouple wells. A maximum temperature of 349°C was measured (Table I). Temperature measurements of the PuC and the Pu-metal prototype rods were made throughout the 800-Mwh run. No change in steady-state temperature occurred between the beginning and the end of the run. In Table IV in Sect. IV below, the measured and calculated temperatures are compared. The calculated temperature differential was about 20 percent higher than that measured. Information on the dimensional stability of the fuel slug under operating conditions and the effect of the annular-liquid bond thickness will be obtained from inspection of the prototype fuel elements.

Also included in this loading were several Mark III fuel rods being monitored for rod-growth measurements and two stripped-rib subassemblies. The latter had been installed in the reactor in February, 1960, and were used through April during operation for the final phases of the kinetics studies without any resultant disturbance of the reactor stability. At the conclusion of the stability studies, these subassemblies remained in the reactor.

Loading of the reactor for the irradiation run was completed on May 23, 1960, and it was brought to a power of 1100 kw on the same day. The 800-Mwh run with this loading was completed September 10, 1960, and the reactor was shut down for removal of some of the samples.

The ten CEN sample rods, the sample brick, the two Pu prototype rods (without thermocouple), one PuC rod (without thermocouple), and one Mark III fuel rod from a stripped-rib subassembly were removed.

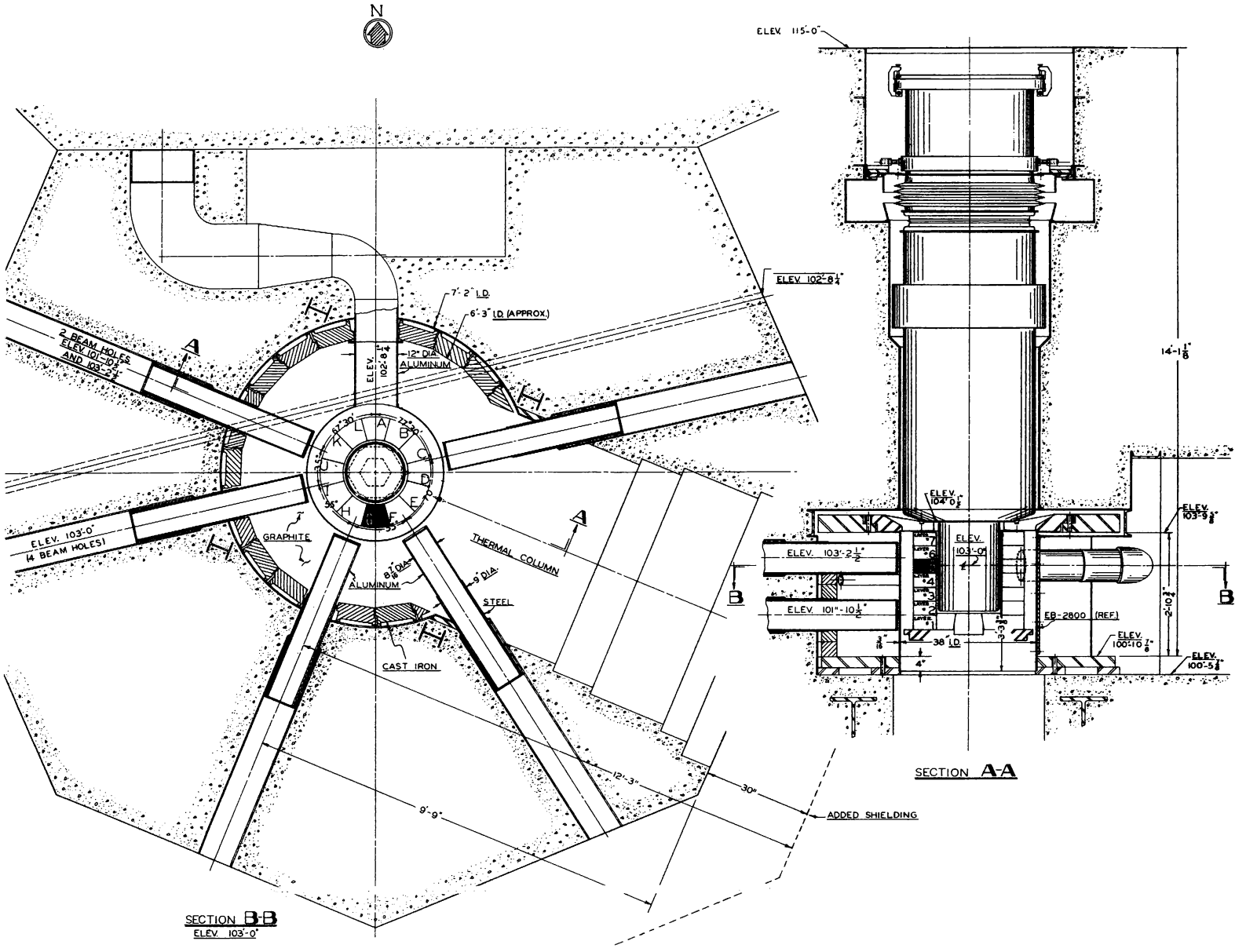

Fig 2. Reactor Layout Showing Location of Special Brick

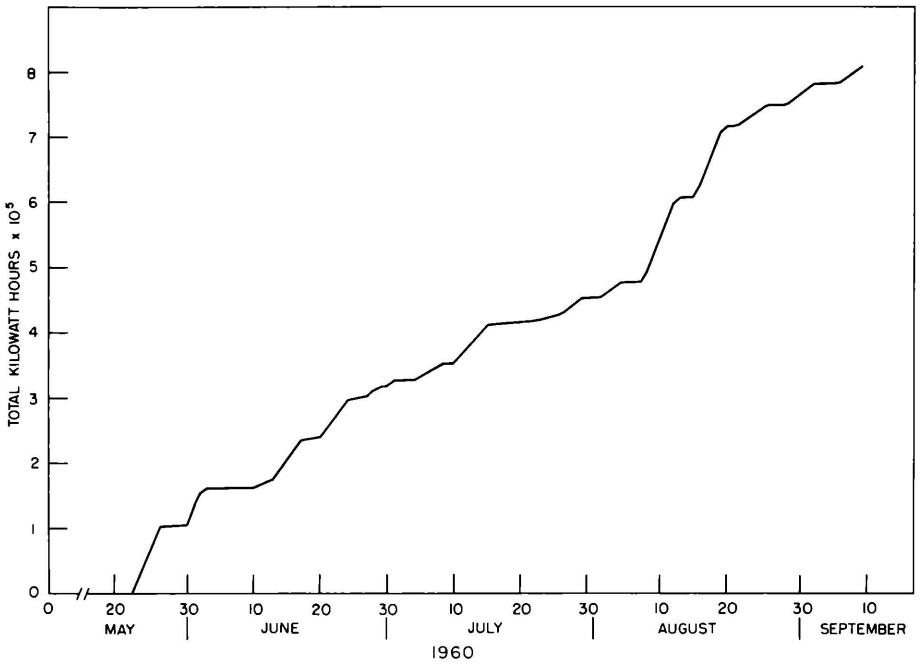

Fig. 3. Integrated Power Curve for Operation of EBR-I, Mark III during May-Sept. 1960.

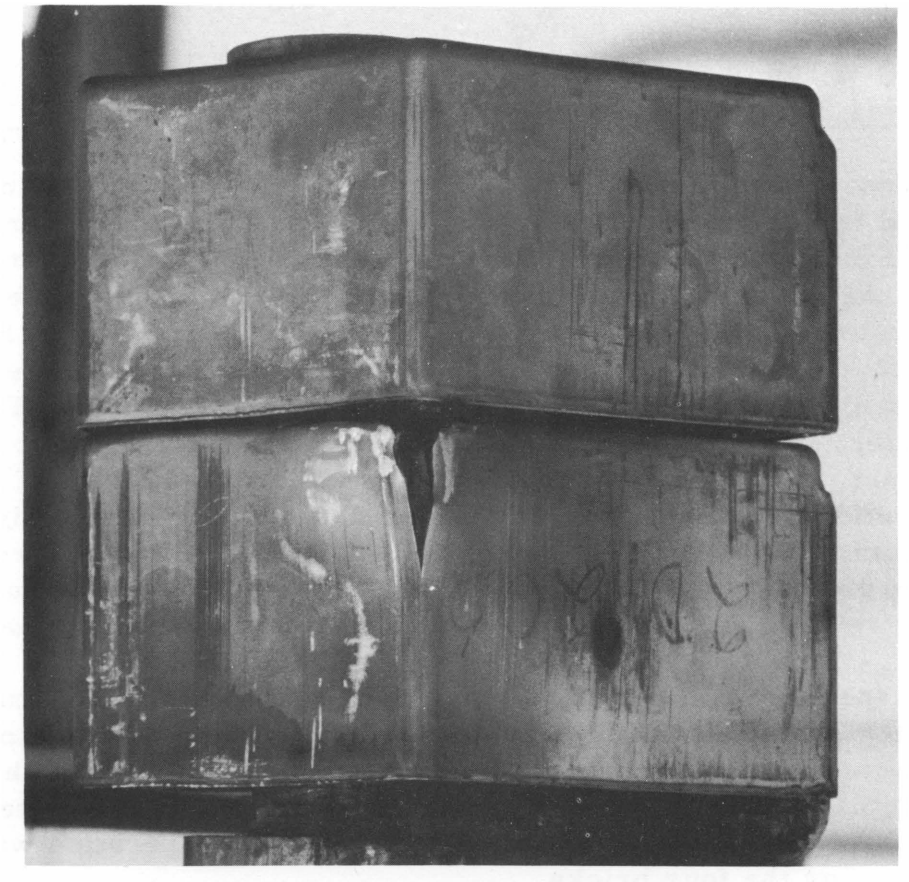

Fig. 4. Ruptured Brick Removed for Inspection

Table I

MEASUREMENT OF TEMPERATURES IN SELECTED RODS OF EBR I, MARK III AT A POWER OF 1120 kw

Rod	Location	NaK Temperature (°C)	Measured Temperature (°C)
P-4	A-20		
	1 in. above fuel $\mathbb{Q}_L$	305	348
	2.3 in. above fuel $\mathbb{Q}_L$	312	349
	Top of blanket	337	
P-3	A-8		
	1 in. above fuel $\mathbb{Q}_L$	305	342
	2.3 in. above fuel $\mathbb{Q}_L$	312	339
	Top of blanket	338	
PuC	E-28		
M-3	1 in. below fuel $\mathbb{Q}_L$	295	354
	2.9 in. above fuel $\mathbb{Q}_L$	330	365
	Top of blanket	350	

Most of the integrated power of the reactor was put on in periods of three- and two- shift operation with weekend shutdowns. Power operations were interrupted to some extent to give training in reactor operation to two groups of APDA operating people who were present for two-week periods for a four-week total. The integrated power curve is shown in Fig. 3. On two occasions, high activity levels in the outer-blanket exhauster-coolant air indicated brick cladding failures, necessitating shutdown. The first time, inspection revealed one brick with the entire inner jacket face broken open, a dent in the Al inner liner, and a considerable amount of uncontained uranium oxide. Apparently, a small hole developed in the cladding, allowing uranium oxide to form, causing swelling of the jacket, and resulting in the dented liner and eventual rupture of the brick. This situation was corrected by replacing the brick, the inner liner, and the contaminated filters.

Inspection on the second occasion revealed another ruptured brick stuck to the one below it. Two additional bricks, removed for inspection of a gap between them, revealed that the bricks above and below the gap were stuck together (see Fig. 4). Not enough uranium oxide had leaked from the ruptured brick to warrant replacing the filters, and operation was resumed after replacing the four bricks.

III. Summary of Measurements of Dimensional Changes in Coextruded Uranium-Zircaloy 2 Fuel Rods of EBR-I, Mark III (R. G. Matlock and J. D. Leman)

1. Observed Effects

The fifth set of measurements of dimensional changes in EBR-I, Mark III fuel rods were completed in September, 1960. These measurements have been taken over a period starting with May, 1959, during which time the majority of the rods measured have accumulated a total of 2,682 Mwh of operating time. A brief history of the fuel rods is presented in Table II, and some of the measurements in Table III.

The two most prominent effects observed were a diameter increase at the top of the fuel section and an overall decrease of rod length. In sheared rods the maximum diameter growth was large enough to be clearly visible. Figure 5 shows the comparison between a nonirradiated, sheared rod and a sheared rod which has been in the reactor for 2,682 Mwh. This particular rod showed a maximum diameter increase of 0.033 in.

Measurements of rod lengths showed decreases in length as large as 0.290 in. A comparison is made of the increase in rod jacket diameter and the decrease in rod length in Fig. 6. This figure indicates an approximately linear relationship between diameter increase and length decrease in the range of measurements taken.

Table II

EBR-I, MARK III
FUEL ROD HISTORY

Rod No.	Condition	Location	Distance from Core (inches)	Reactor Time	Rod No.	Condition	Location	Distance from Core (inches)	Reactor Time
F-54	Unsheared	A-17	0.90	1875 Mwh	F-8	Unsheared	D-5	1.72	1391 Mwh
	Unsheared	A-5	1.22	807 Mwh		Sheared	D-5	1.72	1269 Mwh
				Total 2682 Mwh					Total 2660 Mwh
F-215	Unsheared	A-20	0.90	1875 Mwh	F-72	Unsheared	D-11	2.06	1413 Mwh
	Unsheared	A-29	0.90	412 Mwh		Sheared	D-11	2.06	1269 Mwh
	Unsheared	A-11	0.80	395 Mwh					Total 2682 Mwh
				Total 2682 Mwh	F-76	Unsheared	C-8	2.14	1625 Mwh
F-18	Unsheared	A-15	1.22	1875 Mwh		Sheared	C-8	2.14	1057 Mwh
	Unsheared	A-11	0.80	412 Mwh					Total 2682 Mwh
	Unsheared	A-29	0.90	395 Mwh	F-165	Unsheared	C-2	1.72	1625 Mwh
				Total 2682 Mwh		Sheared	C-2	1.72	1057 Mwh
F-157	Unsheared	A-13	0.45	Total 807 Mwh					Total 2682 Mwh
F-86	Unsheared	A-18	0.45	Total 807 Mwh	F-47	Unsheared	D-7	2.56	1413 Mwh
F-140	Unsheared	G-26	2.06	Total 2682 Mwh		Sheared	D-7	2.56	1269 Mwh
									Total 2682 Mwh
F-21	Unsheared	D-6	2.14	1413 Mwh	F-111	Unsheared	D-30	3.36	1413 Mwh
	Sheared	D-6	2.14	1269 Mwh		Sheared	D-30	3.36	1269 Mwh
				Total 2682 Mwh					Total 2682 Mwh
F-239	Unsheared	C-6	2.14	1625 Mwh	F-176	Unsheared	G-23	3.36	Total 2682 Mwh
	Sheared	C-6	2.14	1057 Mwh	F-134	Unsheared	G-30	2.56	Total 2682 Mwh
				Total 2682 Mwh	F-182	Unsheared	G-36	1.80	Total 2682 Mwh

Table III

MEASUREMENTS OF FUEL ROD LENGTH AND MAXIMUM JACKET DIAMETER

Rod No.	Amount of Shrinkage ± 0.015 inches	Maximum Diameter Increase (in.)
F-54	0.126	0.0146
F-215	0.162	0.0167
F-157	0.022	0.0014
F-86	0.024	0.0017
F-18	0.100	0.0143
F-76	0.227	0.0259
F-176	0.020	
F-134	0.058	
F-182	0.061	
F-21	0.290	0.0345
F-8	0.204	0.0240
F-72	0.260	0.0334
F-47	0.171	0.0171
F-111	0.055	0.0067
F-239	0.178	0.0180
F-165	0.127	0.0151
F-140	0.082	0.0083

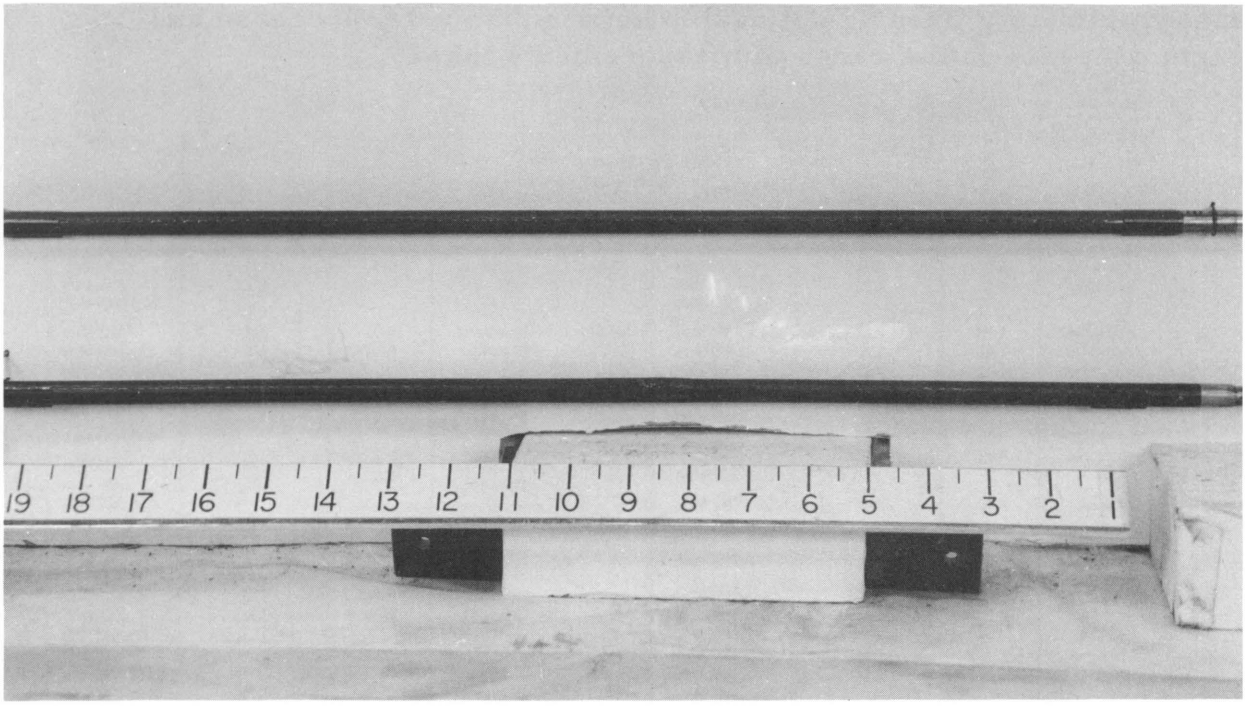

Fig. 5. Comparison between EBR-I, Mark III Sheared Fuel Rods, Irradiated (Bottom) and Nonirradiated (Top).

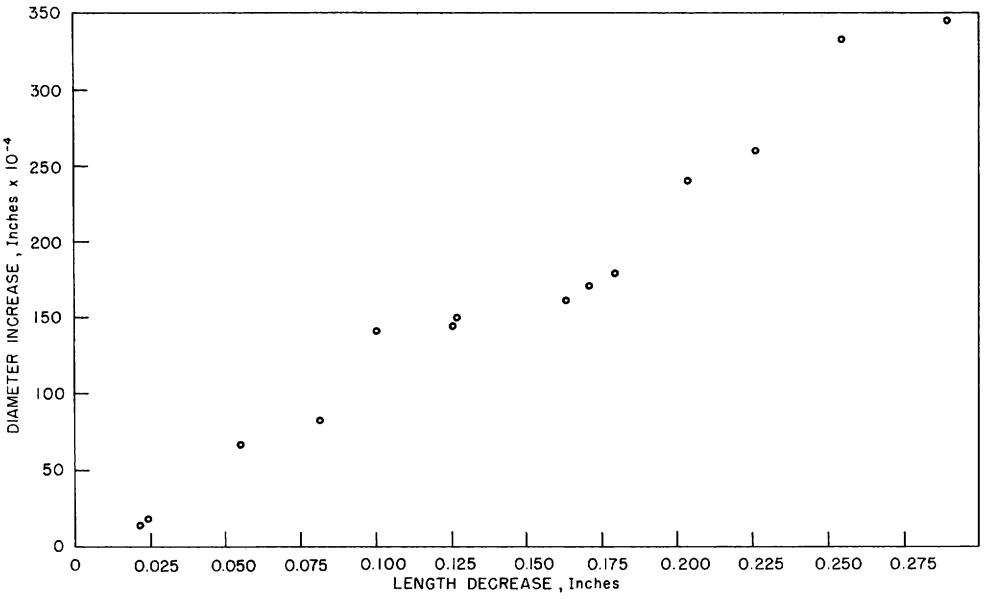

Fig. 6. EBR-I, Mark III Irradiated Fuel Rods - Length Decrease vs Jacket Diameter Increase

Figure 7 relates change in rod length with radial distance from the core centerline for four unsheared rods, each of which had 2682 Mwh in the reactor. Also, each of these rods remained at the radial distance indicated during this period.

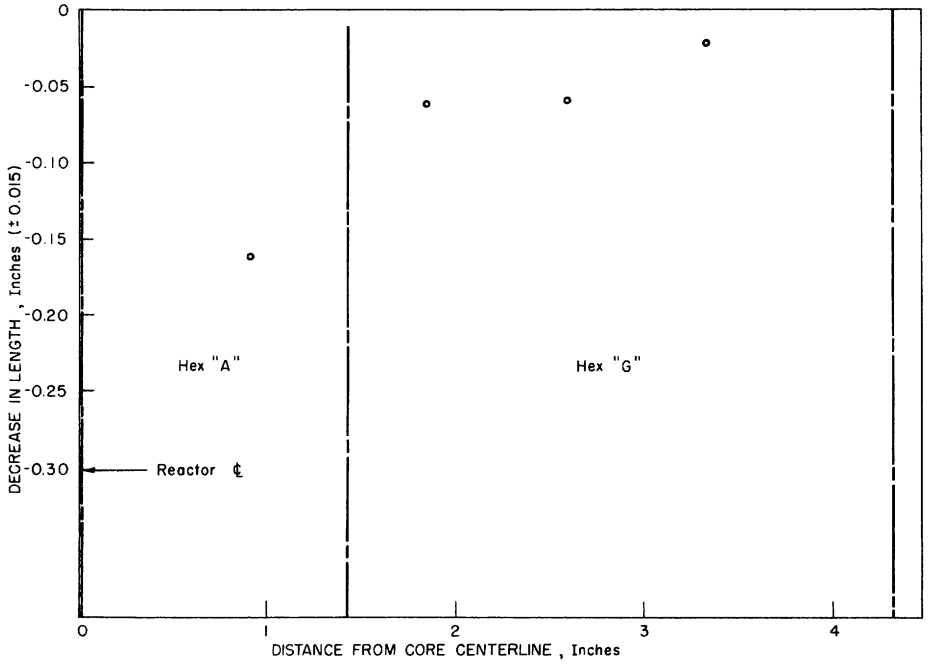

Fig. 7. EBR-I, Mark III Irradiated Fuel Rods - Change in Rod Length for 4 Unsheared Rods vs Radial Distance from Core Centerline.

During the period from about 1400 to 1600 Mwh of operation, the spacing ribs of fuel rods in Subassemblies C and D were sheared off in the fuel and blanket sections. Approximately one inch of each rib was left at each end of the rod (visible in Fig. 5) to insure proper positioning and to allow for tightening the ends of the rods in the subassemblies. Removal of these ribs eliminated radial contact in the fuel section between neighboring rods. In comparing the measurements taken on sheared rods with those taken on unsheared rods, it appears that the radial restraint imposed by the ribs had a pronounced effect on the growth characteristics of the rods.

Another effect observed in the fuel rods was bowing (see Fig. 8). Some bowing was observed in both sheared and unsheared rods. In some instances, rods were bowed to such an extent that they were unfit for reactor use. Most of the bowing occurred in the region of the junction between the fuel and upper blanket section of the rod. This is also the region in which the maximum diametrical changes take place. There does not seem to be a correlation between rod bowing and temperature, location, or time in the reactor.

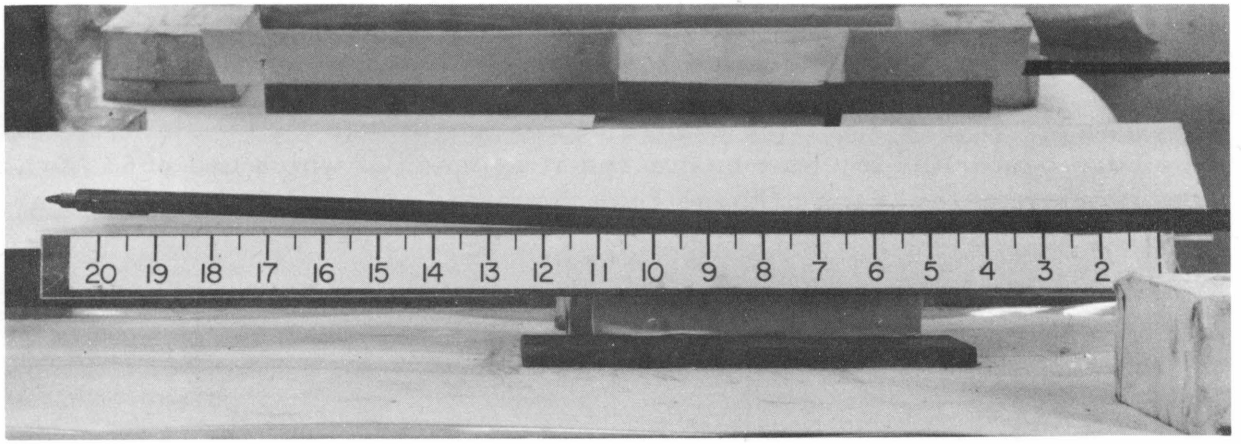

Fig. 8. Bowed Irradiated Mark III Fuel Rod

There is a possibility that the fuel and jacket were not concentric. A tolerance of 0.008 in. is allowed for the diameter of the fuel section. These conditions could lead to a nonuniform jacket thickness along the rod and bowing would be expected.

Figures 9 through 13 are plots of diameter increase versus length along the rod for five typical rods measured. Figure 9 is for rod F-21, which showed the largest diameter increase for all rods measured. Figure 10 is for rod F-140, which was unsheared and was located in Subassembly G. Figure 11 is for rod F-215 from Subassembly A. Figures 12 and 13 are rods F-157 and F-239. The former was located in Subassembly A, but spent only a comparatively small amount of time in the reactor. In Fig. 14 is a plot of diameter increase vs reactor time at high temperature.

Temperature seems to be an important factor in rod growth, and because about 450 Mwh of operation were carried out at a lower temperature, this period was subtracted from data in Fig. 14.

The noticeable decrease in growth rate is affected by several factors and is discussed in Section V.

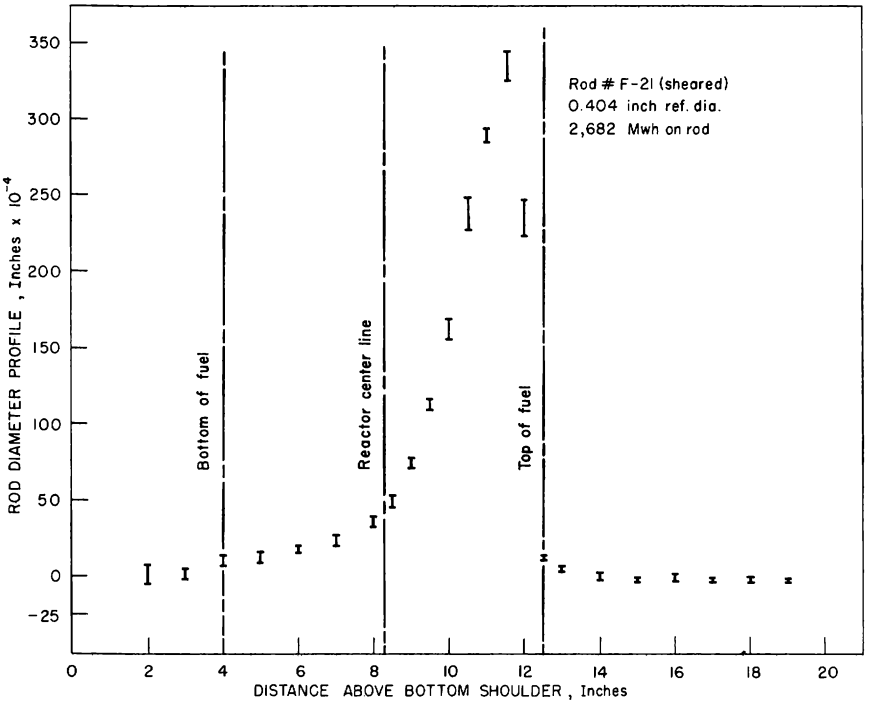

Fig. 9. Rod Jacket Diameter Measurements - Maximum and Minimum for 3 Angular Orientations on Rod # F-21.

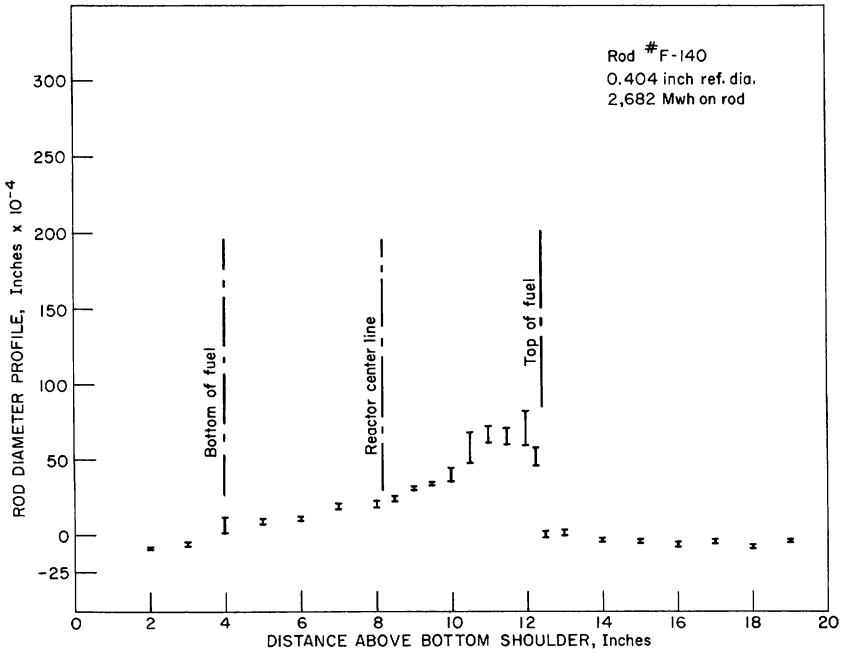

Fig. 10

Rod Jacket Diameter Measurements - Maximum and Minimum for 3 Angular Orientations on Rod # F-140.

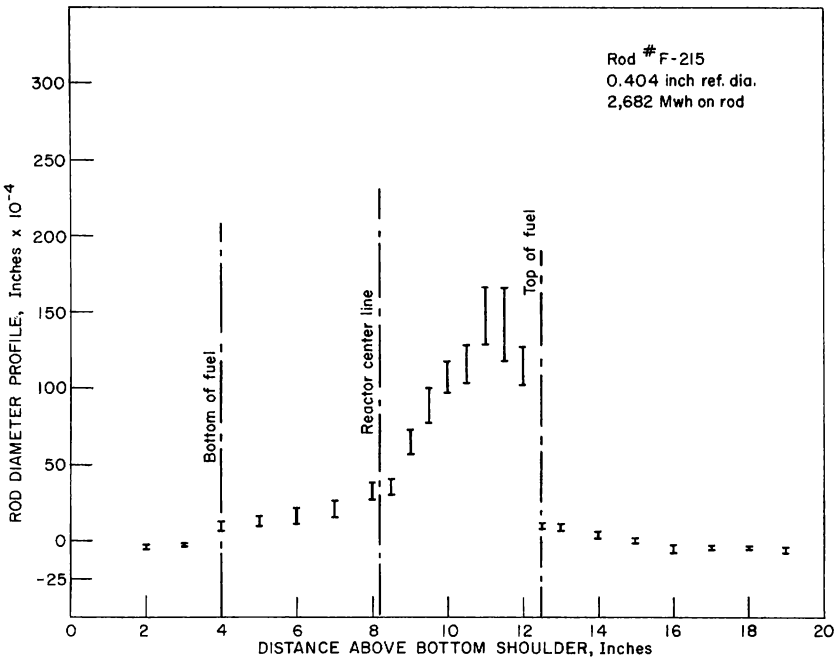

Fig. 11. Rod Jacket Diameter Measurements - Maximum and Minimum for 3 Angular Orientations on Rod # F-215

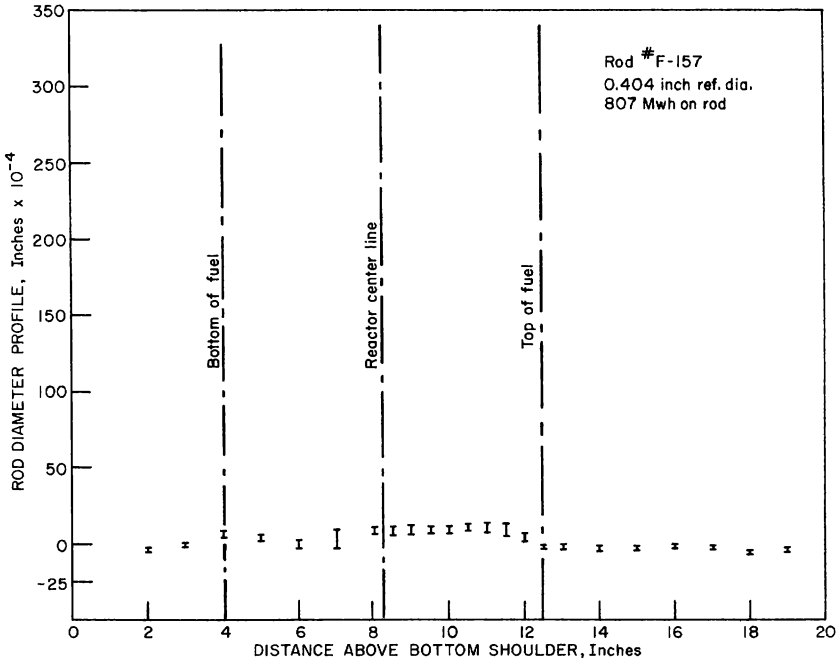

Fig. 12. Rod Jacket Diameter Measurements - Maximum and Minimum for 3 Angular Orientations on Rod # F-157.

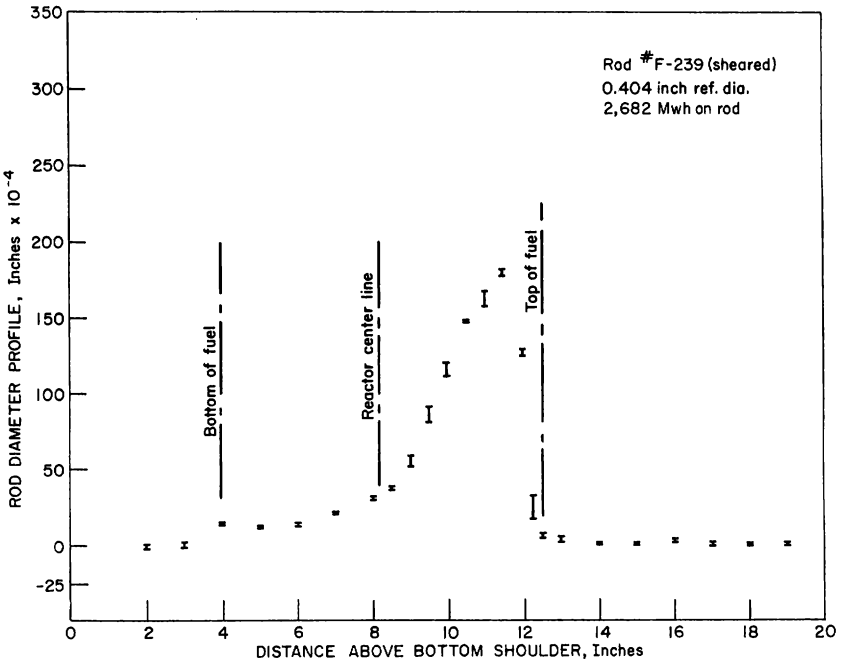

Fig. 13

Rod Jacket Diameter Measurements - Maximum and Minimum for 3 Angular Orientations on Rod # F-239.

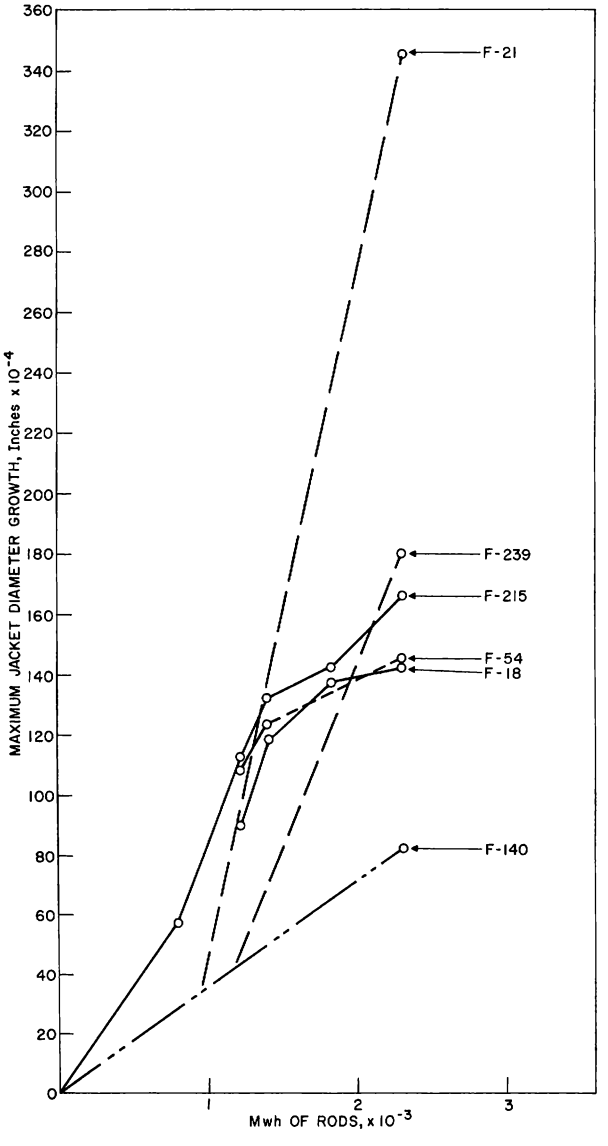

Fig. 14

Diameter Increase vs Reactor Time for Six EBR-I, Mark III Irradiated Fuel Rods.

2. Rod Structure and Fabrication

The fuel and blanket sections of the Mark III fuel rods contain a coextruded uranium-2 w/o zirconium alloy core within a Zircaloy-2 jacket. The fuel section is 8.5 in. long and contains enriched (93%) uranium-2 w/o zirconium. The lower blanket section is 3.562 in. long, and the upper blanket is 7.75 in. long. Each of these blanket sections contains natural uranium-2 w/o zirconium. The three sections are joined by welding and are separated by a 0.020-in. Zircaloy-2 disk. The disk is bonded, by induction-heating, to the fuel and blanket slugs.

The spacing ribs are of 0.056-in. diameter, of zirconium wire, and spot-welded at $\frac{1}{4}$-in. intervals to the rod jacket. Each rib is 0.046 in. high. Three such ribs are attached at 120° angular spacings, as shown in the fuel rod assembly drawing (see Fig. 15). A stainless steel handle, weighing $3\frac{1}{8}$ lb and $85\frac{3}{4}$ in. in length, is attached to the upper end of the fuel rods for handling purposes.

3. Fuel Assembly

Each hexagonal fuel assembly contains 36 fuel rods. The radial position of each rod tip is controlled by the locating holes in the fuel rod support plate (see Fig. 16). Spacing between the fuel rods is maintained by longitudinal ribs attached to each rod. A tightening rod located in the center of each hexagonal subassembly serves to hold the fuel rods in contact with each other.

In Subassembly A, two different rods were used during the period of measurements. For the first 1857 Mwh of operation, an expanding rod was used to exert an outward radial force over the entire length of the fuel and blanket sections of the fuel rods. During the 800-Mwh run, this subassembly was loosened by interchanging rods with outer subassemblies, and the expanding rod was replaced with a positioning rod. This positioning rod limits movement only at the top and bottom of the fuel rods. In the sheared subassemblies the rods were tightened at the top and bottom only.

4. Discussion of Results

In reviewing the observed growth effects in the fuel rods, it is interesting to compare the growth profiles and the temperature profiles. A comparison of a typical rod diameter profile with the axial rod temperature traverse of Fig. 17 shows that the maximum rod growth and the maximum rod temperature occur at about 11.5 in. above the bottom shoulder. At the upper junction between the fuel and blanket sections, the temperature drops abruptly to a fairly constant value, and the rod diameter decreases abruptly at this point also.

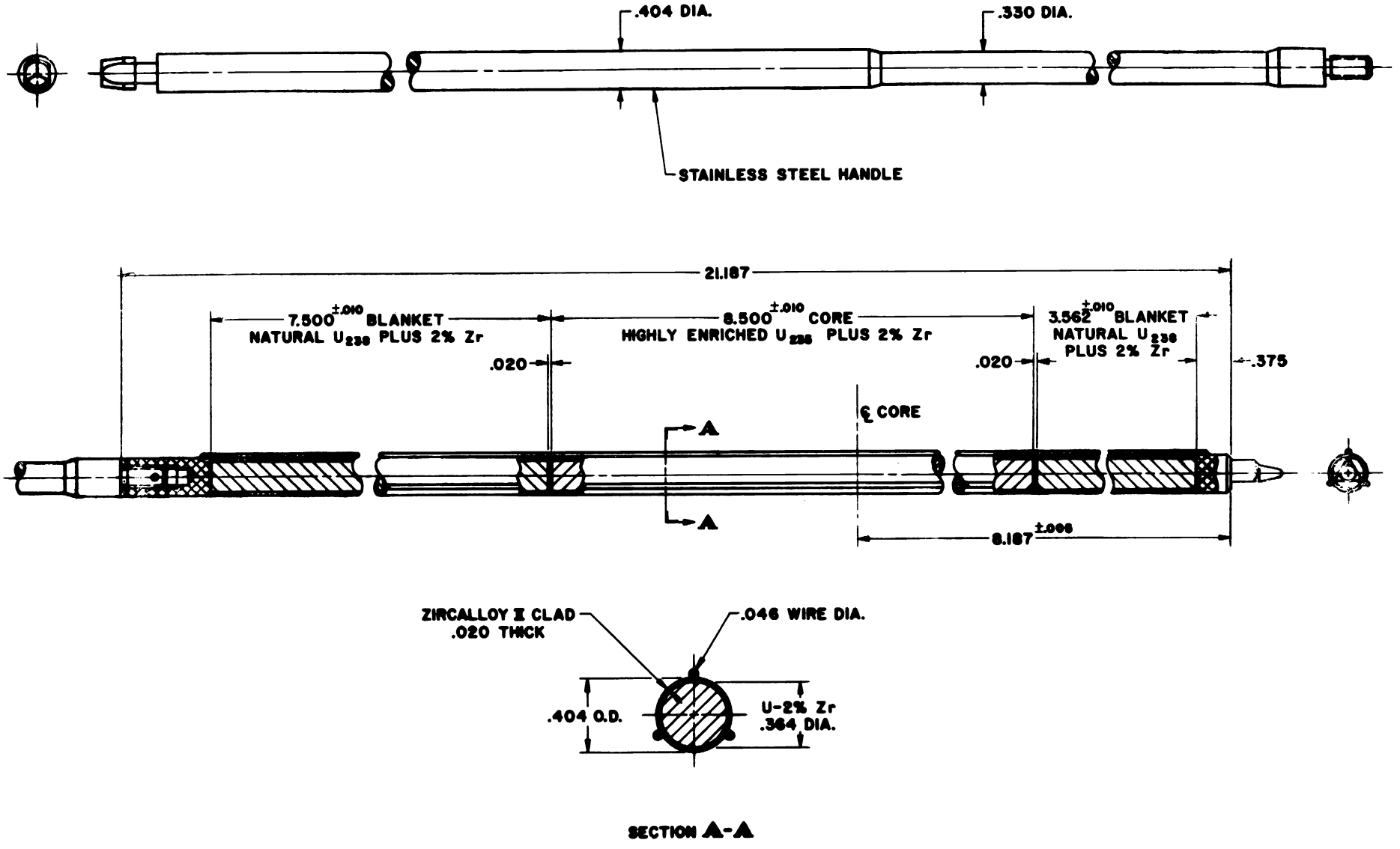

Fig. 15. EBR-I, Mark III Fuel Rod

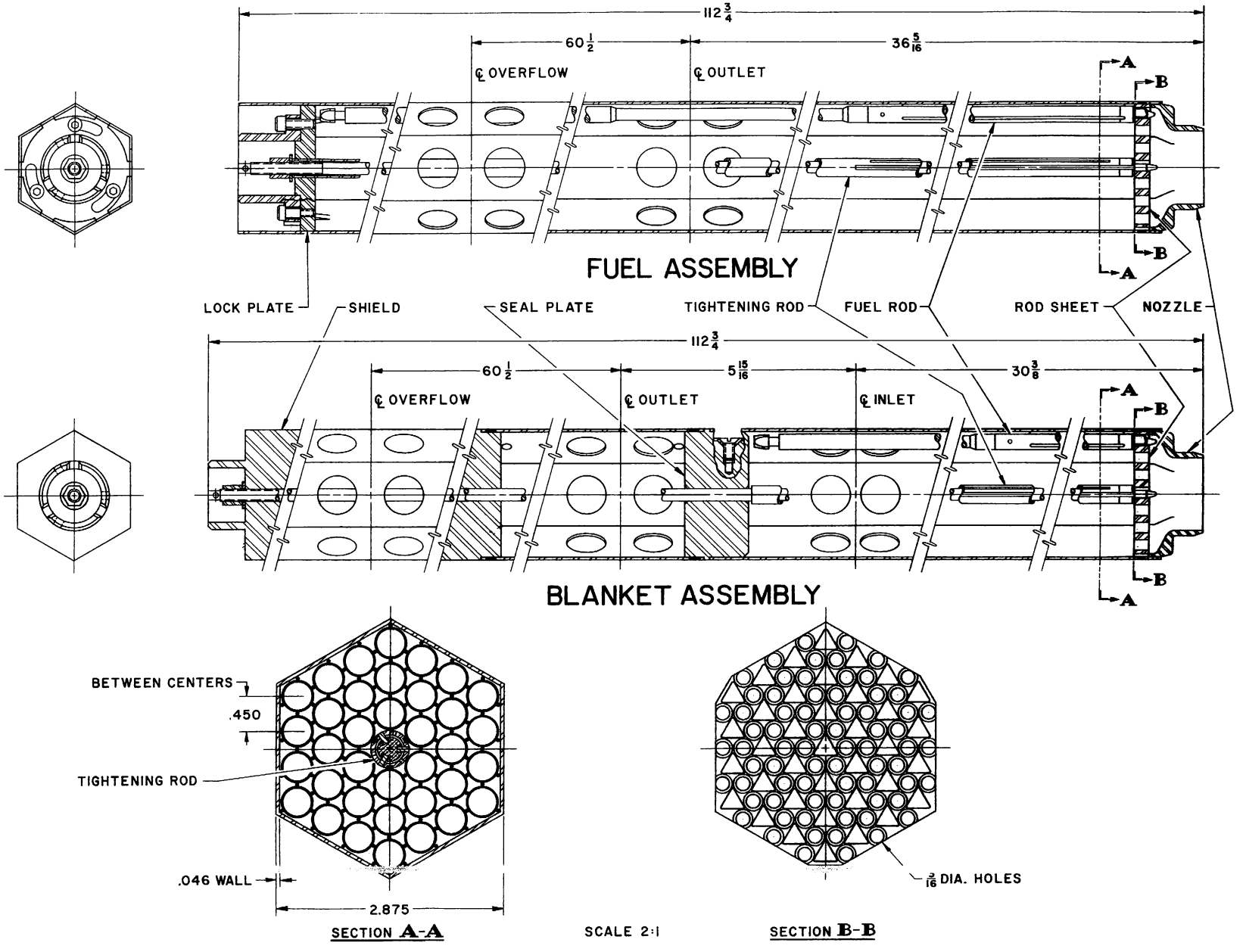

Fig. 16. EBR-I, Mark III Fuel and Blanket Assembly

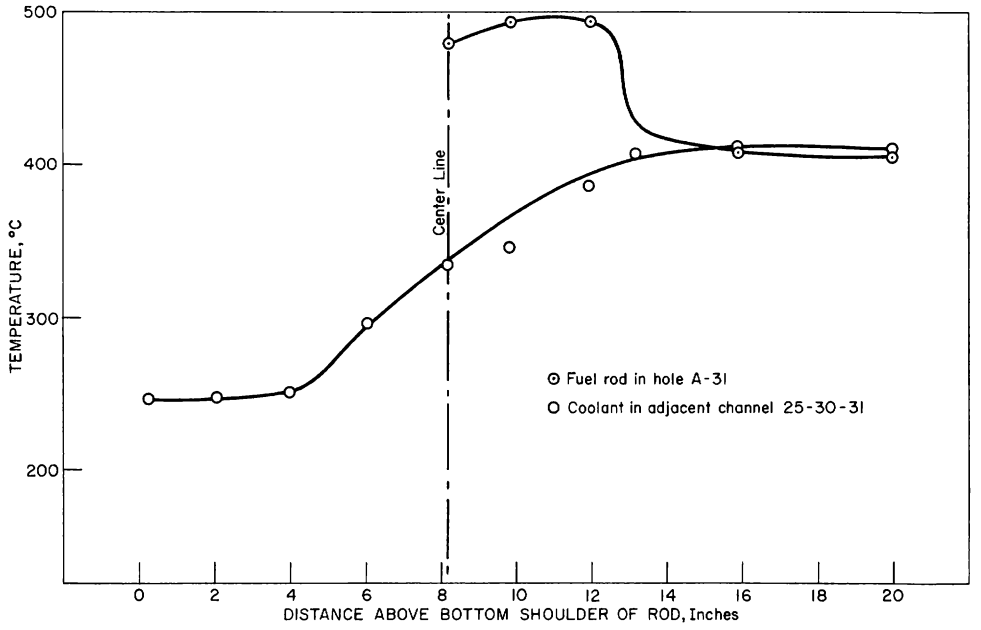

Fig. 17. Rod and Coolant Temperature vs Axial Distance in One Subassembly

A comparison of the radial temperature traverse across the reactor core (see Fig. 18) with the length measurements across the core (Fig. 7) shows that the maximum length changes occur in the high-temperature region and the minimum length changes occur in the region of lower temperature. A comparison of more complete data on the growth of the rod diameter across the core with this temperature traverse shows that diameter growth also varies directly with temperature. Another temperature growth correspondence is evident in Fig. 14. A decreased growth rate for rods F-215, F-18, and F-54 is clearly indicated. These rods were located in Subassembly A (the central subassembly) during the entire run. This decreased growth rate is apparent for the last 800 Mwh of reactor operation.

During the last 800 Mwh, the reactor power level was maintained at about 100 kw below the previous operating level. The lower outlet temperature observed in Subassembly A was too much below that with the standard loading to be attributed to the lower power level only. Seven irradiation sample rods were present in this region during the last 800 Mwh. The plutonium prototype rods were about 0.140 in. smaller in diameter than the regular fuel rods and provided more area for coolant flow. All contained less fuel and contributed less to heat generation. Further, they flattened the flux across this subassembly. The combined effects of lower power, more coolant flow, and lower flux level due to less fuel reduced the temperature in this subassembly.

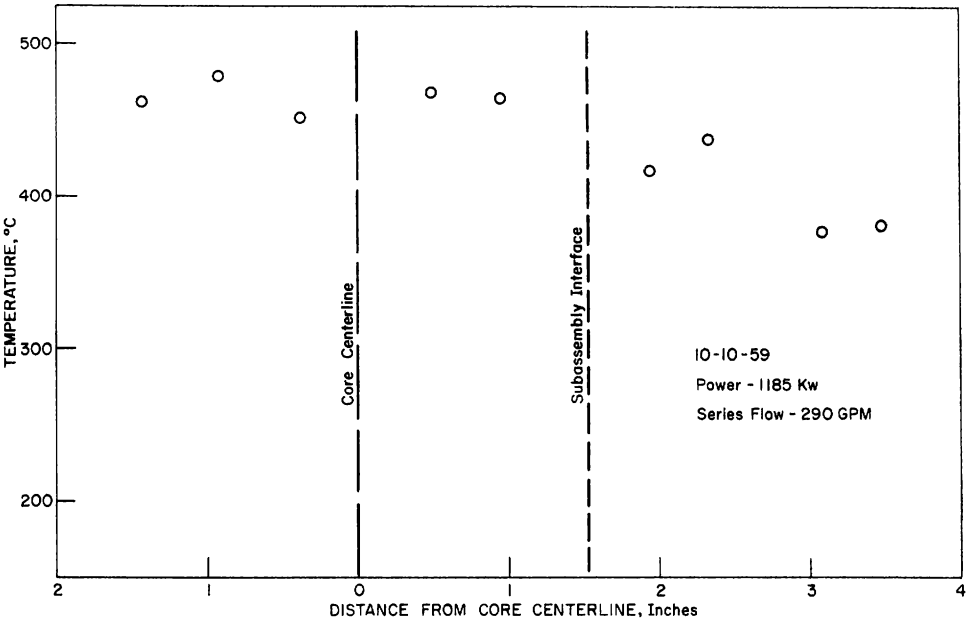

Fig. 18. Radial Temperature Distribution at Fuel Vertical Center Line

More complete data for diameter growth of sheared rods showed a decreased growth rate in the row adjacent to the central subassemblies. The temperature in this row was lower due to an increased area for coolant flow at the edge.

Another factor exerting influence on rod growth is radial restraint. In comparing the sheared rod which grew the most (F-21) with the unsheared rod which grew the most (F-215), the former grew twice as much as the latter. Also, rod F-21 was unsheared for the first 1400 Mwh of operation as well as being located in a region of lower temperature. Comparing rod F-239 (see Fig. 13) with rod F-21 shows a difference of 0.018 in. in maximum growth. These two rods had the same amount of accumulated time in the reactor; however, F-21 was sheared for 200 Mwh more than F-239.

Rods F-140 (unsheared) and F-21 were in the reactor the same amount of time and were located at about the same radial distance from the core. A comparison of maximum diameter showed a difference of 0.026 in., that for F-21 being larger.

An attempt has been made in Fig. 14 to indicate the increased growth rate of the sheared rods. Although diameter measurements were not made on the sheared rods before their ribs were removed, an initial growth rate for these rods is approximated from the growth rate of an unsheared rod in Subassembly G, located at about the same radial distance

from the core centerline as the sheared rods. The increased growth rate of the sheared rods should begin at equivalent reactor operating times of 1400 Mwh and 1628 Mwh for rods F-21 and F-239, respectively. This figure shows that the growth rates for the sheared rods were considerably larger than for the unsheared rods.

As is illustrated in Fig. 16, an unsheared rod, when placed in a hex, is restrained radially at six points on its circumference. Tests performed to determine the effectiveness of the tightening rods in holding the fuel rods indicated that most of the rods were held fairly snugly. In contrast, a sheared rod has no ribs and no radial contact with its neighboring rods, except for a one-inch section at the top of the upper blanket and the bottom of the lower blanket. The radial restraint imposed by the ribs on unsheared rods evidently exerts considerable influence on the extent of radial growth. That high pressures are exerted between unsheared rods is illustrated by the fact that in the central part of Subassembly A some ribs have been flattened and pushed to one side in the upper fuel section.

IV. EBR I, Mark IV Core Design (J. D. Leman)

The design criteria of the Mark IV core required that a critical mass be obtained while limiting the fuel temperature to about 500°C. This requirement is necessitated because a delta-to-epsilon-plus-delta phase change occurs in Pu-10 a/o Al at approximately 600°C. With a fuel slug 0.235 in. in diameter, the maximum calculated fuel temperature is 505°C. This should allow a hot spot temperature of approximately 95°C under the limiting temperature at full power (1200 kw). The 0.235-in. fuel slug size with 60 rods per subassembly, instead of 36 as in Mark III, provides the smaller temperature differential in each rod that is required and provides the necessary material for critical loading.

Four Pu-10 a/o Al prototype fuel rods were put in the Mark III core. Two of these rods (Pu4 and Pu3) were drilled so that a thermocouple could be used to measure the fuel temperature under actual operating conditions. Rod Pu4 had a fuel slug of 0.200-in. diameter, a jacket 0.280 in. in diameter, and a NaK-filled annular clearance of 0.019 in. Rod Pu3 had a fuel slug 0.200 in. in diameter, a jacket of 0.250-in. diameter, and a NaK-filled annular clearance of 0.004 in.

The NaK coolant channel outlet temperatures were measured by thermocouples located in the rod handle above the upper blanket slug, whereas coolant temperatures adjacent to the fuel thermocouples were determined from a vertical temperature profile drawn below the measured vertical temperature traverse for Subassembly A with a uniform loading of Mark IV fuel rods.

A comparison of the measured and calculated fuel temperatures are contained in Table IV. The discrepancy between the two values is possibly explained by the uncertainty as to the actual adjacent coolant temperature.

Table IV

COMPARISON OF MEASURED AND CALCULATED FUEL TEMPERATURES

Rod (in.)	Location	Power (kw)	NaK Temp (°C)	Fuel Temp Calculated (°C)	Fuel Temp Measured (°C)	Temp Drop Calculated (°C)	Temp Drop Measured (°C)
Pu-4; 0.280 Jacket	A-20 1 in. above fuel centerline	1118	305	358	348	53	43
Pu-3; 0.250 Jacket	A-8 1 in. above fuel centerline	1118	305	354	342	49	37
	Core inlet		248				
	Channel outlet		338				

The final design of the Mark IV loading has been set. Some minor details may be altered due to fabrication methods and procurement of materials. This work is now being done by the Metallurgy Division in Argonne, Illinois

1. Fuel Rods

The Mark IV fuel rod is shown in Fig. 19. It consists of a Zircaloy-2 tubular jacket with an OD of 0.299 in. and a 0.020-in. wall. Three Zircaloy-3 ribs, 0.049 in. in height, are equispaced around the jacket to maintain uniform spacing and a coolant channel between the rods in the assembly. The jacket is filled with six slugs, of which the upper and lower are of depleted uranium, 7.745 and 3.552 in. long, respectively, and constitute part of the longitudinal blanket. The center core section is composed of four plutonium-10 a/o aluminum slugs, each 2.121 in. long to give a total length of 8.484 in. All the slugs are 0.235 in. in diameter and are held concentrically in the jacket by spacers die-formed on their surfaces. The 0.011-in. annular clearance between the slugs and the jacket is filled with NaK for thermal bonding. A gas space is provided within the element to allow for thermal expansion of the NaK and for the accumulation of fission gas.

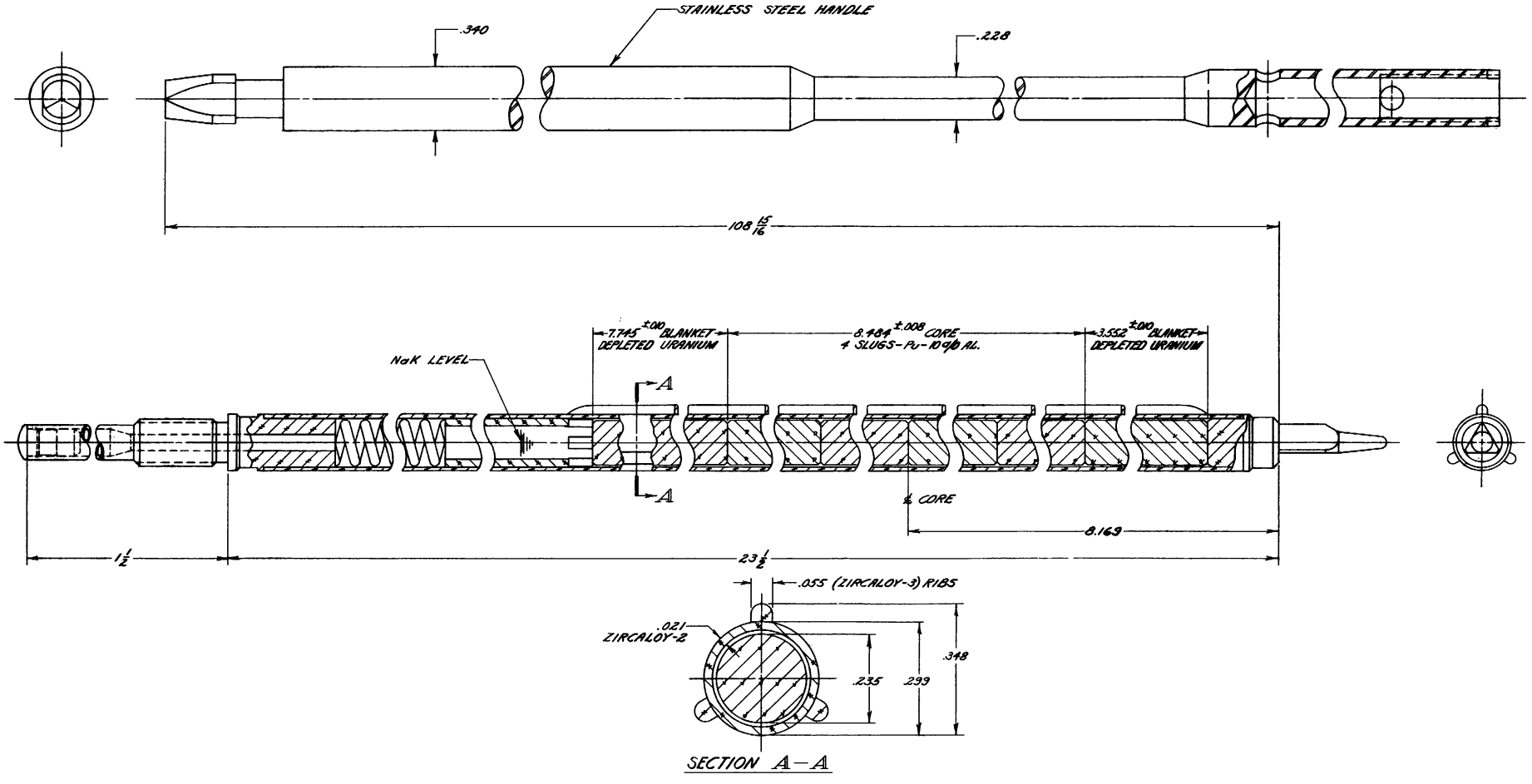

Fig. 19. Fuel Rod EBR-I, Mark IV

A Zircaloy-2 transition piece is welded to the upper end of the jacket. It contains the NaK-fill tube, which is finally seal-welded and is threaded at its top. A Type 304 stainless steel handle is screwed and locked into this. This extension is used for handling purposes and as part of the upper shield. It has a reduced section from connector to plenum chamber to reduce flow resistance and a special head on the upper end to receive the handling tool. On the bottom end of the jacket is a Zircaloy-2, triangular tip for locating and orienting the fuel rod in the hex assembly.

2. Blanket Rods

The blanket rods and subassemblies used in the outer hexes are the same ones that were used in the Mark III loading (see ANL-5836).

The blanket rods used in the inner hexes are identical to the fuel rods except for the replacement of the fuel by blanket material. This is in the form of four depleted uranium slugs. The upper slug is 1.745 in. long, two center slugs are 4.247 in. long, and the lower slug is 3.552 in. long.

3. Thermocouple Rods

Special fuel and inner blanket thermocouple rods will be used in the core. These rods are the same as the standard fuel and blanket rods except that a thermocouple thimble down through the length of the handle to the position of the centerline of the fuel section is provided in each of them. A special tubular handle in some of the fuel rods will allow a thermocouple to be placed in the bottom of the handle for measurement of coolant channel outlet temperatures.

4. Tightening Rods

Each fuel assembly contains one tightening rod of a modified design used in Mark III at the center of the assembly (see ANL-5836). The tightening rod is essentially an expandable rod, consisting of an outer split tube which may be expanded by means of a series of Woodruff-key-type wedges riding in modified, Woodruff key slots in the center shaft. Expansion is actuated by means of a nut on the center rod at the top of the assembly, which moves the center rod relative to the wedges on the split tube.

5. Fuel Assemblies

The fuel assembly of the Mark IV loading will be similar to that of the Mark III. There will be seven hexagonal, Type 304 stainless steel tubes, $2\frac{7}{8}$ in. OD across flats with a wall thickness of 0.040 in. At the bottom of the assembly tube is a nozzle which reduces from the hexagonal shape to that of a cylinder. Resting on the nozzle is a rod sheet

which supports, locates, and orients the rods. The triangular holes in the rod sheets receive the triangular tips of the rods. The round holes around the triangular holes allow the NaK coolant to pass through the sheet and into the space between the rods.

Each fuel assembly contains 60 rods plus one tightening rod on a lattice spacing of 0.348 in. The inner seven assemblies will contain the fuel elements required for critical loading and power operation. Lattice positions which are unused for this purpose will be filled out with similar elements that contain depleted uranium only.

There is a nominal clearance of 0.017 in. between the edge of the fuel rod bundle and the hexagonal wall. The tightening rod located in the center of the assembly will take up the clearance, thus leaving a rigid assembly. All of the rods in the fuel assemblies have long handles reaching to the top of the reactor tank. Fuel may be handled either by replacing the whole assembly or by loosening the tightening rod and replacing individual rods.

A summary of design characteristics is given in Table V.

Table V

SUMMARY OF DESIGN CHARACTERISTICS FOR EBR-I, MARK IV

1. Flow and Temperature Conditions - Reactor Core and Inner Blanket - Series Flow

Inlet Temperature of NaK	230°C
Outlet Temperature of NaK	322°C
Flow Rate in Series	291 gpm
Reactor Power to NaK Coolant	1203 kw 4.11×10^6 Btu/hr
Core Inlet Temperature	246°C
Core Outlet Temperature	342°C
Reactor Inlet Plenum	232°C
Fraction of Total Reactor Coolant Flow through Core and Blanket	0.838
Flow through Core and Blanket	244 gpm
Fraction of Total Reactor Coolant Flow that is Bypassed	0.162
Bypass Coolant Flow	47 gpm
Fraction of Power to Coolant in Core	0.876
Power to Coolant in Core	1054 kw 3.6×10^6 Btu/hr
Fraction of Power to Coolant in Blanket	0.124
Power to Coolant in Blanket	149 kw 0.51×10^6 Btu/hr
Reynolds Number	14,600

Table V (cont'd)

2. Dimensional Data - Reactor Core

Fuel Rod Lattice Spacing	0.348 in.
Number of Rods per Subassembly	60
Total Number of Rods in Core	420
Number of Rods for Critical(at ρ = 15.06 gm/cm^3)	314
Number of Rods for Operation	325
Jacket OD	0.299 in.
Jacket ID	0.257 in.
NaK Bond	0.011 in.
Fuel Slug Diameter	0.235 in.
Fuel Weight per Rod	90.1 gm Pu
Total Fuel Alloy Weight per Rod	91.0 gm
Maximum Fuel Loading	37.8 kg Pu
Calculated Critical Loading (Cold, wet)	28.3 kg Pu
Calculated Operating Fuel Loading	29.3 kg Pu
Cross-sectional Area for Coolant Flow	0.0972 ft^2
Coolant Velocity, Series Flow	5.6 fps
Parallel Flow	5.3 fps
NaK Flow Area per Lattice Triangle	0.0137 in.^{2}
Flow Area of Lattice	26.1%
D_e = 4 x Hydraulic Radius	0.0944 in.
Percent NaK Flow Area of Total Area	29.4
Core Volume, Critical	5.19 ℓ
Core Volume, Operating	5.31 ℓ
Total Area of Core Section	0.348 ft^2
Total Fuel Rod Surface Area	18.0 ft^2
Jacket Wall	0.021 in.

3. Heat Transfer Data - Reactor Core

Average Heat Flux	15.6 cal/(cm^2)(sec)
	207,000 Btu/(ft^2)(hr)
Average Specific Power	35.9 kw/kg Pu
Ratio of Maximum to Average Power	1.35
Max Specific Power	48.5 kw/kg
Max Heat Flux	21.0 cal/(cm^2)(sec)
	279,000 Btu/(ft^2)(hr)

Temperatures at Reactor Center

Temperature Difference in Slug, Center to Surface	86°C
Temperature Difference across NaK Bond	11°C
Temperature Difference across Jacket	35°C
Temperature Difference across Coolant Film	13°C
Total Temperature Difference	145°C
NaK Coolant Temperature	338°C
Fuel Slug Temperature at Reactor Centerline	483°C
Maximum Fuel Temperature	505°C

V. Critical Mass of EBR-I, Mark IV (A. R. Baker*)

1. Introduction

The critical mass of EBR-I, Mark IV was estimated by PDQ and SNG calculations on the IBM 704 and by calculations using the RE-7 code on UNIVAC. Diffusion theory calculations (using the PDQ code) were performed for a cylindrical model of the reactor. Diffusion theory calculations are known to overestimate the critical mass for systems as small as EBR-I. The PDQ estimate of the criticality factor, k, was therefore corrected by an amount equal to the difference between criticality factors obtained for the same spherical model of EBR-I from calculations using both SNG (transport theory) and RE-7 (diffusion theory).

2. Results of Calculations

PDQ calculations have been performed for the first proposal for a Mark IV core in EBR-I and for a proposed mockup of this core in ZPR-III. The principal dimensions assumed in the calculations are given in Table I. The other dimensions and compositions were the same as those of Mark III and its mockup.[1]

Table VI

DIMENSIONS USED IN THE CALCULATION OF EBR-I, MARK IV (FIRST PROPOSAL†)

	Mark IV (Mockup Core)	Mark IV (Actual Core)
Number of plutonium plates per drawer	11	-
Fuel Pin diameter, in.†	-	0.220
Percentage of Pu^{240} in total plutonium†	4.55	4.55
Volume fraction of plutonium, %	25.44	24.84
Core length, in.	8.0	8.5
Core radius, in.	3.878	3.992
Mass of Total plutonium in core, kg	30.0	33.0

† The final design for Mark IV will have a different pin diameter and percentage of Pu^{240}.

*On loan from AERE, Harwell, England; work done at Argonne National Laboratory, Idaho Division.

[1] J. K. Long et al., Fast Neutron Power Reactor Studies with ZPR-III, Proc. of the Second UN Intn'l. Conf on the Peaceful Uses of Atomic Energy, Geneva (1958), Vol. 12, p. 119.

The machine problems are described in Table VI. The one-dimensional models of ZPR-III mockups were spherical versions of the two-dimensional ones. Other calculations for this spherical Mark IV mockup have been described elsewhere (see ANL-6217). The eleven-group constants used were Set 58 as given by Loewenstein and Okrent; the four-group constants, Set 122, were derived from Set 58 using an EBR-I core spectrum as a weighting function.

The values of the criticality parameters, k, obtained by the machine calculations are given in the fifth and sixth columns of Table VII. As expected for reactors with such small cores, diffusion theory predicted too low a value of k in all cases. For the spherical model of the Mark III mockup, the 11-group SNG calculation gave a value of k that was higher by 0.0958 than the value by a 4-group diffusion theory calculation. All the values of k from PDQ calculations have therefore been increased by 0.0958, giving the adjusted values of k in Table VII. These are the best wholly theoretical estimates of k for the two mockups and the two reactors.

Table VII

CALCULATED VALUES OF CRITICALITY PARAMETERS, k

Reactor or Mockup	Code	No. of Dimensions	No. of Groups	k		Adjusted k		$k(IV)/\overline{k(III)}$
				Mark III	Mark IV	Mark III	Mark IV	
Mockup	SNG	1	11	1.0389	1.0254			
Mockup	RE-7	1	4	0.9431				
Mockup	PDQ	2	4	0.9454	0.9216	1.041	1.017	0.980
Reactor	PDQ	2	4	0.9400	0.9253	1.036	1.021	0.983

The calculations therefore predict that all four models are supercritical, but cross-section Set 58 overestimates k for small systems. If it is assumed that k for a plutonium system is overestimated by the same amount as k for a similar U^{235} system, then the best estimate of k for the Mark IV reactor or mockup is $k(IV)/\overline{k(III)}$, where $\overline{k(III)} = 1.0385$ is the mean value of k for the two Mark III systems, both known to be just critical.

3. Critical Mass of EBR-I, Mark IV

All the calculations for Mark IV specified in Table VI were for models of the first proposal for the core design, with plutonium pins of 0.220-in. diameter. First, a best estimate will be made of k for the first proposal and then corrections will be made for the increased pin diameter, 0.235 in., and other small changes.

It can be seen from Table VI that the best estimate of k for the first proposal was 0.983. It was shown by a one-group perturbation theory calculation that, on increasing the mass of total plutonium (4.55% Pu^{240}) in the core, keeping the core volume constant, there would be an increase in reactivity given by

$$\frac{\Delta k}{k} = 0.66\left(\frac{\Delta M}{M}\right) \quad .$$

Thus the increase in pin diameter gives an increase in k of 0.093.

The effects of the reduction in core height from 8.5 to 8.484 inches and of the reduction in Pu^{240} content from 4.55 to 4.50% were considered. The corrections to k are in opposite senses and both are negligible. Hence the final estimate for seven hexagons, loaded with pins of 0.235-in. diameter was

$$\underline{k = 1.076} \quad .$$

The core radius was reduced to make the reactor just critical, using the formula

$$\frac{\Delta k}{k} = 0.54\left(\frac{\Delta r}{r}\right) \quad .$$

In this way it was shown that EBR-I, Mark-IV will be just critical and cold at a core radius of 8.71 cm, which corresponds to a critical mass of 27.7 kg.

Finally, it was shown by a comparison of published calculations using Set 58 for Popsy (a small Pu^{239} system) and Topsy (a similar U^{235} system) that k was likely to be overestimated by 0.6% more for a small plutonium reactor than for the corresponding U^{235} system. Making a correction for this leads to a final value of cold critical mass given by

$$\underline{M = 28.3 \text{ kg of total plutonium}} \quad .$$

This estimate of critical mass will be valid only if the Pu^{240} fraction is made exactly 4.5% and the density of the alloy is exactly 15.00 g/cm^3. Since the alloy will contain 1% by mass of aluminum, the actual plutonium density assumed was 14.85 g/cm^3, which corresponds to a mass of plutonium of only 89.55 g per fuel pin. If the fraction, f, or the pin mass, m, departs from these values, it can be shown that the critical mass is given by

$$M = 28.3\,[1 + 1.5\,\Delta f - 2.4\,(\Delta m/m)]\ \text{kg of total plutonium.}$$

The cold critical loading will require 316 fuel pins and 104 natural uranium pins in the central seven hexagons.

For Mark III, an additional $1\frac{1}{2}$ kg of U^{235} is required to allow for the temperature coefficient and for control. The normal operating load for Mark IV will therefore be about 1 kg (of plutonium) greater than the cold critical mass; that is, will be 29.3 kg of total plutonium 327 fuel pins).

B. ZERO-POWER REACTOR III (ZPR-III)

(Reviewed by J. K. Long, Project Supervisor)

B. ZERO-POWER REACTOR III (ZPR-III)

(W. P. Keeney and J. K. Long)

I. Introduction

During the period covered by this report a mockup of the EBR-II reactor was under study in ZPR-III. The work reported here was actually begun in April 1960 and proceeded throughout the summer.

The configuration studied at this time was identical with a mockup that had been in the reactor in 1957. Redesign of some of the components of the reactor and the need for more detailed mapping of the worth of materials necessitated the present study. The following points were of principal interest in the present mockup:

1. In Sect. III the worth of control rods was reevaluated. Previous studies had evaluated control rods without any poison follower. The present study investigated the effects of tantalum and boron carbide followers.
2. The worth of a reactivity oscillator was determined and is reported in Sect. IV.
3. The worths of sodium, aluminum and stainless steel were mapped throughout the core and blanket for their effects on power coefficient. These experiments are covered in Sect. V. During the course of these experiments, the sodium worth at the center of the core was found to be larger than expected. The study was therefore extended to develop additional information on the equivalence of substituting aluminum for sodium in this type of reactor mockup. The conclusion was reached that there are some spectral differences between cores containing aluminum and those with sodium.
4. A two-dimensional mapping of the worth of U^{235} and U^{238} was also performed in order that more reliable estimates of the power coefficient could be made. Fission rates for U^{235} and U^{238} were also determined throughout the mockup. These results are given in Sect. VI.
5. The startup instrumentation for EBR-II and its associated shielding have been redesigned since 1957. A mockup of eight variations of the new design was therefore studied so that the response level of the instrumentation during the initial approach to criticality could be estimated. Section VII covers this work.

After a general description of the mockup, these five subjects will be considered in order.

II. Description of ZPR-III Mockup of EBR-II

The reactor was made critical with the configuration shown in Figs. 20 - 23.

Figure 20 is an interface view of the entire assembly. Three different blanket regions are indicated, containing different degrees of coarseness in the size of pieces approximating the EBR-II blanket composition. The finest approximation is closest to the core, but the limitation of the number of available small pieces required that outer regions of the blanket be mocked up more coarsely.

Figure 21 shows both halves of the core interface. The shaded regions are mocked up according to the composition of the 61-pin control rods. The rest of the core region has the same enrichment but higher uranium concentration, as given in Table VIII. The dashed lines show the original proposal to approximate the hexagonal outlines of the core. This loading did not go critical, so the increments indicated by the solid outline were added. The crosses show the location of the ZPR control rods.

Figure 22 gives a more detailed picture of one-quarter of the interface on one-half of the reactor. The core is assembled of $\frac{1}{8}$-in. plates of enriched and depleted uranium, aluminum and stainless steel, in a matrix of stainless steel as shown. The plates were placed horizontally or vertically, as required, to best approximate the core and control rod regions. The numbers shown on the matrix squares refer to the master drawings for the drawers inserted in these squares. In Fig. 22 a diagram of the interface of any one master drawing is shown only once, the numbers in the blank squares indicating that the proper master drawing can be inserted there. The hexagonal outline of the EBR-II core is shown in broken lines. Locations of control and safety rods in the EBR-II core are shown by completed hexagons, while the rest of the core region is just shown in its farthest outline.

Figure 23 shows diagrammatically a sectional view of the midplane of the mockup seen from above. The regions there indicated are prefixed with the letters "C" for core, "G" for gap, "B" for blanket, or "S," which designates the region at the top and bottom of the safety and control rods. Two safety rods in the horizontal midplane are shown. Control rods were built up with the same configuration as safety rods. For simplicity, the two control rods in the horizontal midplane are not shown in Fig. 23. Half No. 1, the fixed half of ZPR, represents the top half of EBR-II, and Half No. 2, the movable half of ZPR, represents the bottom half of EBR-II. Table VIII gives the compositions by volume percent of the regions shown in Fig. 23.

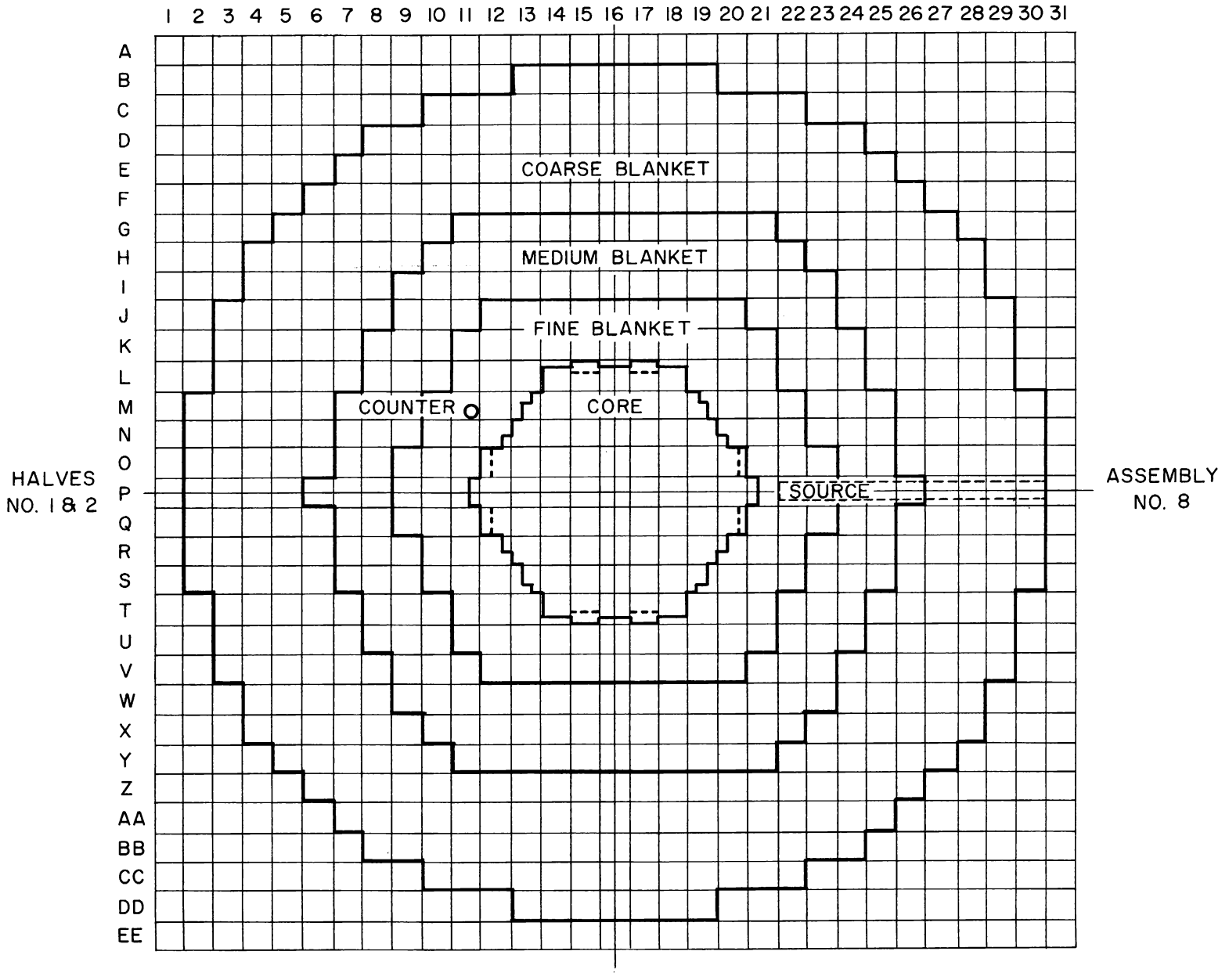

Fig. 20. Interface View of EBR-II Mockup Assembly in ZPR-III

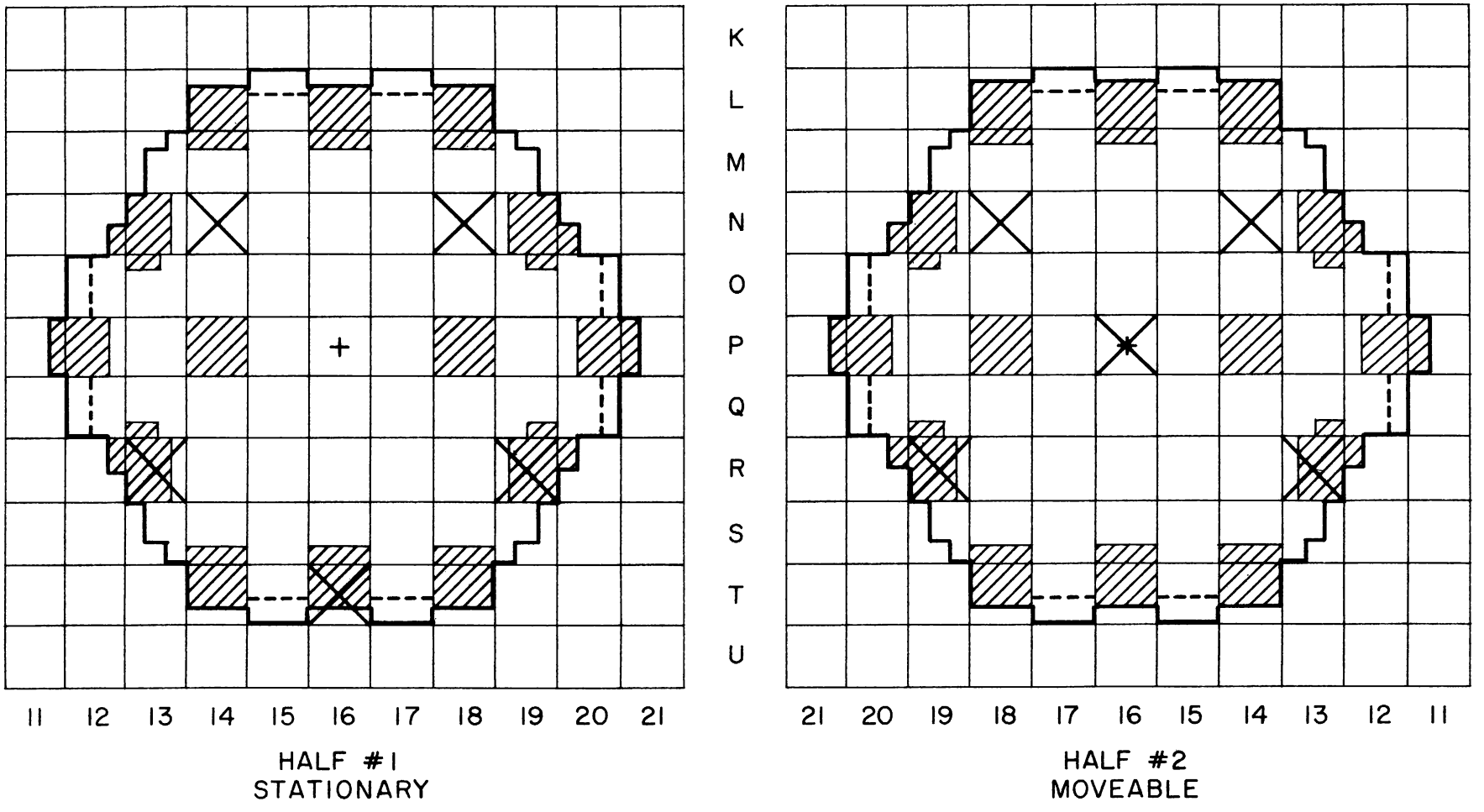

Fig. 21. Interface View of Each Core Half of EBR-II Mockup in ZPR-III

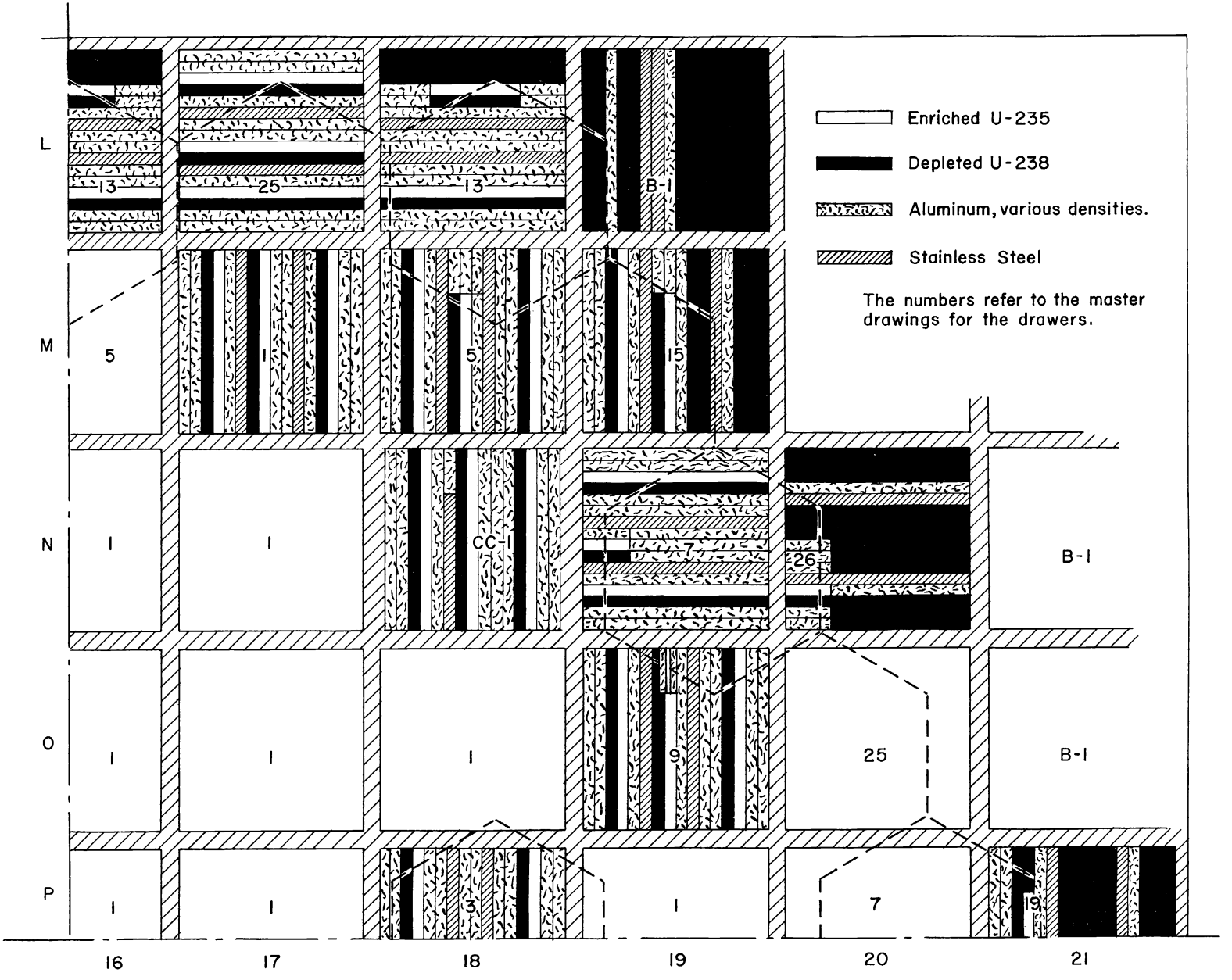

Fig. 22. Loading of One Core Octant of EBR-II Mockup

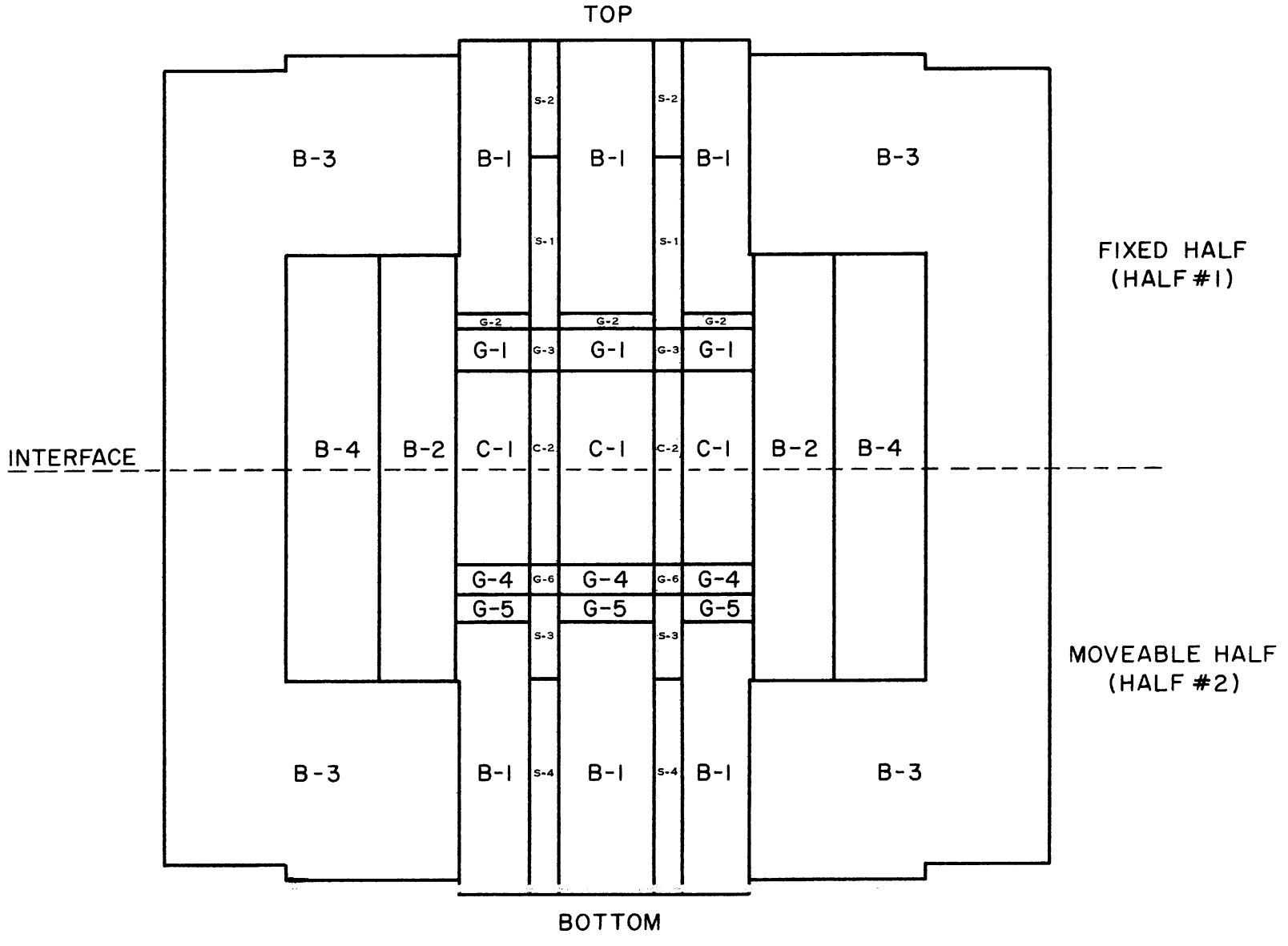

Fig. 23. Sectional View of EBR-II Mockup at Midplane from Above

Table VIII

COMPOSITION AND DIMENSIONS OF MOCKUP AND REACTOR

		ZPR-III Mockup						EBR-II				
		Composition, Vol %				Dimensions, in.		Composition, Vol %			Dimensions, in.	
		U^{235}	U^{238}	SS	Al	Effective Radius	Length	U^{235} + U^{238}	SS	Sodium	Effective Radius	Length
Core Regions	C1	13.93	15.84	19.4	26.47	9.73	14.08	29.27	18.5	49.5	9.52	14.22
	C2	9.35	10.55	19.4	31.05		14.08	19.58	20.3	58.3		14.22
Gap Regions	G1			30.0	27.0	9.73	3.0		29.6	55.7	9.52	3.50
	G2			56.3	9.0	9.73	1.0		56.9	43.1	9.52	0.87
	G3			30.0	27.0		3.0		29.4	59.5		3.09
	G4			40.5	22.3	9.73	2.0		41.3	58.7	9.52	2.06
	G5			24.6	29.0	9.73	2.0		26.1	51.8	9.52	1.88
	G6			35.1	24.6		2.0		34.8	65.2		1.63
Blanket Regions	B1	.06	29.9	19.5	17.9	9.91	19	32	20.4	47.6	9.52	18
	B2	.13	61.26	19.6	6.43	15.50	30	60	17.6	22.4		
	B3	.13	59.5	7.31	3.70	31.70	56-58	60	17.6	22.4	30.75	55.0
	B4	.13	55.2	14.3	6.74	21.68	30	60	17.6	22.4		
Safety and Control Rod Back Regions	S1			12.3	35.4		12.0		12.2	87.8		12.66
	S2			49.1	24.8		8.0		50.1	49.9		6.62
	S3			72.1	8.94		6.0		73.1	26.9		20.31
	S4			69.8	13.4		15.0		73.1	26.9		

The compositions of Table VIII are based on the average weights of pieces, drawers, and matrix tubes, and the following theoretical densities:

U^{235}	18.75 gm/cc
U^{238}	19 gm/cc
Stainless Steel	7.85 gm/cc
Aluminum	2.70 gm/cc

In computing the compositions the spring gaps were neglected.

Also shown in Table VIII is a comparison between the dimensions of the mockup and EBR-II. The regions designated in Table VIII correspond to those shown in Fig. 23. EBR-II Data of Table VIII are taken from design

information. The fuel concentration has been reduced by an amount corresponding to the fissium.* The effective radii given in the table are the outer radii of the respective regions measured from the center of the core. No radii are given for regions C2, G3, G6, or S1-S4, since these are control and safety rods and do not represent regions centered at the core center. The actual control rods in EBR-II are to have a cross section of 4.68 square inches, whereas in the mockup the cross section is 4.75 square inches.

The effective radius which is given for the core, 9.73 inches, is the actual radius built into the mockup. The critical radius would be slightly less, about 9.71 inches.

The critical mass of the mockup was 166.2 kg U^{235} to be compared with 165.2 reported for the 1957 mockup.

III. Worth of Control Rods in EBR-II Mockup

1. Description of Control Rod

Starting from the bottom (Half No. 2 in ZPR-III) the drawer representing an EBR-II control rod contains the amounts of materials indicated in Table IX.

Table IX

DESCRIPTION OF MOCKUP CONTROL ROD

Region (in.)	SS (g)	Al (g)	Other Materials (g)	
0-15	5741	362		
15-21	2311	112.7		
21-23	318.8	103.3		
23-37 (core)	868.3	917.8	1902.6 U^{235}	2206.4 U^{238}
37-40	373.1	169.9		
40-44	62.3	291.2		
44-51 (follower)				
Reference	217.1	494.1		
Heavy Ta	0	262.9	3668 Ta	
Light Ta	0	394.4	1834 Ta	
$B_4{}^{10}C$	217.0	267.7	339.8 gross $B_4{}^{10}C$†	
51-53	61.9	140.8		
53-60	1784	337.6		

† The $B_4{}^{10}C$ weight is the gross weight of material, 69.34% boron, 90.7 a/o enriched.

* Fissium is the equilibrium mixture of fission products alloyed with the fuel.

The materials listed were distributed uniformly over the length of each region. Note that the list contains only the contents of the drawers which were actually moved. The weights of the matrix tube and the drawer itself are not included.

The control rod was evaluated in its full in position and 14 in. out with each of the followers listed. In addition, several intermediate positions were taken with the heavy tantalum follower. As the mockup rod was moved outward (which would correspond to a downward motion in EBR-II, or movement into Half No. 2 in the ZPR-III), the space behind the 60-in. position was filled with 30.9 g steel per inch, 70.4 g aluminum per inch.

The experimentally determined worths are given in Table X.

Table X

WORTH OF MOCKUP CONTROL RODS

Follower Material	Position[1] (in.)	Reactivity in ZPR-III[2] (Ih)	Temp (°C)	Reactivity at 23.5 °C, (Ih)	Reactivity Difference from Zero Position (Ih)
Reference	0	302.6	23.6	302.75	0
Heavy Ta	0	303.7	23.4	303.55	0
Light Ta	0	303.55	23.4	303.40	0
$B_4{}^{10}C$	0	298.2	23.5	298.2	0
Heavy Ta	3	288.85	23.3	288.55	15.0
Heavy Ta	7	243.1	23.2	242.65	60.9
Heavy Ta	11	190.15	23.3	189.85	113.7
Reference	14	177.25	22.6	175.90	126.85
Heavy Ta	14	159.4	23.2	158.95	144.60
Light Ta	14	167.9	22.7	166.7	136.70
$B_4{}^{10}C$	14	47.20	22.4	45.55	252.65

[1] Zero is full-in position.

[2] Arbitrary zero.

2. Corrections for Location and Enrichment

The mockup control rod was located in ZPR-III drawers 1 L 18 and 2 L 18. This is a little further out in the radial direction than the actual corner control rods in EBR-II would be located, about 9.65 in. from center of mockup rod to center of assembly, compared to about 9.2 in. in the actual reactor. The enrichment in the mockup is somewhat less than is required in the actual reactor, as is evidenced by the slightly oversize

loading of the mockup compared to EBR-II. Thus the mockup control rod in the present experiment would have less worth than in the reactor.

In the previous mockup of EBR-II, done in 1957, a more accurate construction of the EBR-II control, both in regard to location and enrichment, was made. The fine detail used in the previous mockup, which required quite extensive handling, was not repeated this time. The reference loading of the control rods can be compared, however, to estimate the difference between the worths of the recent control rod mockups and the more accurate mockup done previously. Thus the 126.8-inhour worth of the reference in the present loading should be compared with 141 inhours for the worth of a 61-pin control rod at the hex corner measured previously. If the same factor is assumed to apply to the rods with the poison follower, then the worth of the heavy tantalum rod would be 160.7 inhours, that of the light tantalum would be 152 inhours, and that of the boron carbide rod would be 281 inhours.

IV. EBR-II Oscillator Rod Experiment

In order to evaluate and define the design of the boron carbide oscillator rod for the EBR-II, the Reactor Engineering Division provided a zero-power oscillator assembly to be used in ZPR-III. The oscillator assembly consisted of a square box, approximately 2 x 2 x $15\frac{1}{2}$ in. long, which contains a rotating cylinder of $1\frac{7}{8}$ in. OD (see Fig. 24). Mounted eccentrically in the cylinder was a boron carbide section, $\frac{1}{2}$ x $\frac{1}{2}$ x 14 in. long. Two filler strips were provided to permit the removal of one-half of the boron carbide, resulting in a boron carbide section of $\frac{1}{4}$ x $\frac{1}{2}$ x 14 in. long, which could be rotated. The cylinder was indexed at 15° intervals and keyed for the rotator attachment.

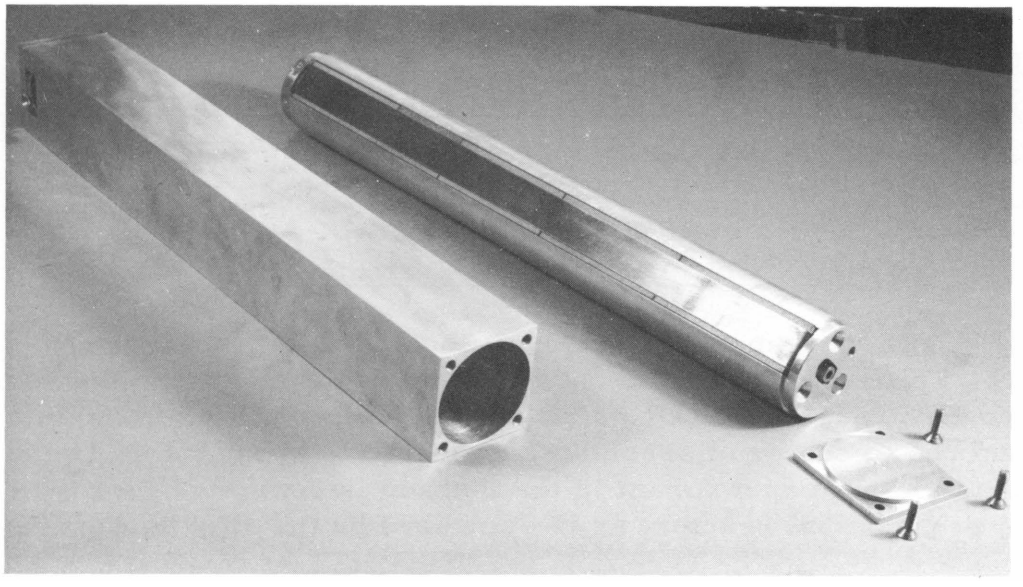

Fig. 24. EBR-II Oscillator Rod Assembly

The oscillator was rotated by means of a selsyn motor supported at the rear of the stationary matrix of the reactor. The motor was coupled to the oscillator by means of a steel shaft, the length of which was varied as various axial oscillator positions were investigated. A position indicator was affixed to the shaft of the selsyn generator located in the reactor control room. This arrangement permitted the oscillator angular position to be varied while the reactor was critical. The error in the angular position of the oscillator was less than ±1°.

Three axial oscillator positions were evaluated in the L-16 and L-18 matrix positions of ZPR-III. The axial positions are designated as 14, 10, and 6 in., the number of inches indicating the length of the boron carbide that was in the core. The remaining length of the rod occupied the axial position that would be above the actual EBR-II core.

In all, three different configurations of boron carbide of various masses were used. The oscillator, as described above and designated as Modification 0, was initially run in the L-16 and L-18 matrix elements with loadings of 116 and 59 g of boron carbide.

In an effort to increase the worth of the rod, it was reworked to Modification I and the loading increased to 230.5 g of boron carbide.

Modification II was a rearrangement of the 230.5 g of boron carbide to a greater average radial position within the rod. Figure 25 shows the arrangement of the boron carbide for each modification.

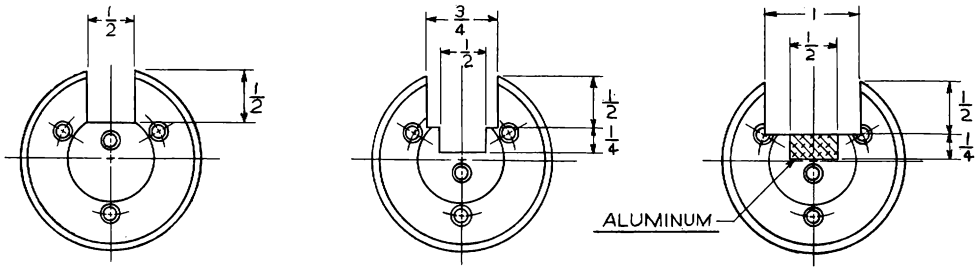

Fig. 25. End View of EBR-II Oscillator Rod Mockup (dimensions in inches).

Table XI presents the experimentally determined excess reactivity in the reactor as a function of the angular position of the oscillator. As the angular index of the rod with respect to the indicator varied from run to run, the shift in phase of the fundamental from one run to another is not significant.

Table XI

REACTIVITY (IN INHOURS) VERSUS OSCILLATOR ANGULAR POSITION

	Loading Position							
ϕ, deg	116 g* 14 in. -L-16	116 g* 10 in. -L-16	116 g* 6 in. -L-16	59 g* 14 in. -L-16	116 g* 14 in. -L-18	230.5 g** 14 in. -L-16	230.5 g** 6 in. -L-16	230.5 g† 1[illegible] in. -L-16
0	43.50	54.75	53.25	84.00	114.25	1.26	1.48	22.33
15	43.00	53.75	52.40	83.50	115.75	0.48	2.60	28.27
30	42.60	52.25	51.60	83.40	117.10	0	3.85	28.63
45	43.00	50.00	50.50	83.50	117.50	0.71	5.40	27.93
60	43.75	48.25	49.00	83.75	117.75	2.18	7.00	26.62
75	45.00	46.00	47.75	84.50	117.25	4.08	8.58	24.12
90	46.75	44.50	46.50	86.00	116.60	6.58	10.00	21.37
105	49.00	43.00	45.50	87.00	115.00	9.52	11.10	17.86
120	51.25	41.75	44.50	88.50	113.20	12.37	11.85	14.18
135	53.50	40.80	44.25	89.75	111.00	15.37	12.28	10.39
150	55.50	40.75	44.20	91.00	108.80	17.95	12.38	7.01
165	57.00	40.80	44.25	92.00	106.50	20.27	11.98	4.10
180	58.50	42.00	44.60	92.80	104.75	21.69	11.48	2.00
195	59.25	42.75	45.40	93.25	102.90	22.50	10.55	0.58
210	59.75	44.50	46.20	93.50	101.50	22.71	9.05	0.46
225	59.75	46.50	47.50	93.25	101.40	22.06	7.68	1.26
240	59.20	48.75	48.80	93.00	101.00	20.69	5.90	2.79
255	58.00	50.75	50.00	92.00	101.50	18.87	4.30	5.47
270	56.50	52.50	51.00	91.00	102.20	16.66	2.80	8.40
285	54.25	54.00	52.00	89.60	104.20	13.69	1.45	12.07
300	52.00	55.20	52.50	88.00	106.00	10.45	0.60	15.65
315	49.50	55.50	52.75	86.80	108.20	7.55	0.15	19.23
330	46.75	55.50	52.80	85.75	110.50	4.76	0	22.53
345	44.80	55.50	52.80	84.00	112.20	2.63	0.23	25.33
360	43.50	55.00	52.60	83.50	113.00	0.84	1.10	27.33

*Modification 0
**Modification I
†Modification II

Table XII is a listing of the calculated Fourier coefficients for a series of the form

$$f(x) = a_0 + \sum_{1}^{\infty} (a_n \cos nx + b_n \sin nx) \quad ; \quad n = 1, 2, \ldots$$

Combining the components of each harmonic,

$$f(x) = a_0 + \sum_{1}^{\infty} C_n \sin (nx + \theta_n) \quad ; \qquad n = 1, 2, \ldots$$

$$C_n^2 = a_n^2 + b_n^2 \quad ; \quad \theta_n = \tan^{-1} (a_n/b_n) \quad .$$

The coefficients and phase angle for the sine expression are given in Table XIII. The units are inhours.

Table XII

FOURIER SERIES COEFFICIENTS

116 g* 14 in. -L-16		116 g* 14 in. -L-18	
$a_0 = 51.338$		$a_0 = 109.460$	
$a_1 = -7.412$	$b_1 = -4.639$	$a_1 = 4.822$	$b_1 = 6.913$
$a_2 = -0.330$	$b_2 = -0.027$	$a_2 = -0.029$	$b_2 = -0.129$
$a_3 = -0.022$	$b_3 = +0.198$	$a_3 = 0.014$	$b_3 = -0.071$
$a_4 = -0.062$	$b_4 = +0.079$	$a_4 = -0.048$	$b_4 = 0.011$
116 g* 10 in. -L-16		**230.5 g** 14 in. -L-16**	
$a_0 = 48.335$		$a_0 = 11.459$	
$a_1 = 6.502$	$b_1 = -3.973$	$a_1 = -10.285$	$b_1 = -4.852$
$a_2 = 0.129$	$b_2 = 0.054$	$a_2 = -0.056$	$b_2 = -0.016$
$a_3 = 0.057$	$b_3 = 0.133$	$a_3 = 0.008$	$b_3 = 0.109$
$a_4 = 0.063$	$b_4 = 0.065$	$a_4 = 0.080$	$b_4 = 0.021$
116 g* 6 in. -L-16		**230.5 g** 6 in. -L-16**	
$a_0 = 48.752$		$a_0 = 6.362$	
$a_1 = 4.094$	$b_1 = -2.133$	$a_1 = -5.076$	$b_1 = 3.574$
$a_2 = 0.0003$	$b_2 = 0.241$	$a_2 = 0.005$	$b_2 = 0.177$
$a_3 = 0.026$	$b_3 = 0.208$	$a_3 = 0.017$	$b_3 = -0.018$
$a_4 = 0.050$	$b_4 = 0.036$	$a_4 = 0.028$	$b_4 = 0.049$
59 g* 14 in. -L-16		**230.5 g† 14 in. -L-16**	
$a_0 = 88.327$		$a_0 = 14.733$	
$a_1 = -8.398$	$b_1 = -2.501$	$a_1 = 12.626$	$b_1 = 6.379$
$a_2 = -0.025$	$b_2 = 0.073$	$a_2 = -0.152$	$b_2 = -0.137$
$a_3 = 0.070$	$b_3 = 0.104$	$a_3 = 0.035$	$b_3 = -0.036$
$a_4 = -0.002$	$b_4 = 0.050$	$a_4 = 0.021$	$b_4 = -0.019$

Table XIII

FOURIER SINE EXPRESSION (C_n IN INHOURS)

Loading Position	Harmonic							
	Fundamental		Second		Third		Fourth	
	C_n	θ_n	C_n	θ_n	C_n	θ_n	C_n	θ_n
116 g* 14 in. -L-16	8.74	238°	0.331	265°	0.198	355°	0.100	322°
10 in. -L-16	7.61	121°	0.140	293°	0.145	23°	0.091	44°
6 in. -L-16	4.62	117.5°	0.241	0°	0.210	7°	0.062	54°
59 g* 14 in. -L-16	5.17	241°	0.076	337°	0.122	35°	0.050	358°
116 g* 14 in. -L-18	8.43	35°	0.133	181°	0.071	171°	0.051	281°
230.5g** 14 in. -L-16	11.37	245°	0.058	254°	0.109	4°	0.083	75°
6 in. -L-16	6.208	305°	0.177	0°	0.025	137°	0.056	30°
230.5 g† 14 in. -L-16	14.146	63°	0.205	228°	0.050	136°	0.028	132°
	$f_n(x) = a_n \cos nx + b_n \sin nx = c_n \sin (nx + \theta_n)$							
	$C_n^2 = a_n^2 + b_n^2$			$n = \tan^{-1}(a_n/b_n)$				

*Modification 0
**Modification I
†Modification II

V. Sodium, Aluminum and Stainless Steel Worths in the EBR-II Mockup

A series of sodium, stainless steel, and aluminum substitutions have been made, which essentially map the worth of these materials throughout various mockups of EBR-II. Three different core variations were constructed, as summarized in Table XIV. In the so-called clean mockups, all core drawers were loaded with the standard (1) pattern of Fig. 22.

Table XIV

CORE MOCKUPS FOR SUBSTITUTION EXPERIMENTS

	Na-filled, Clean Core	Al-filled, Clean Core	Al-filled Engineering Core
Critical Mass, kg U^{235}	161.6	161.0	166.2
Composition, Vol %			
U^{235} (18.75 g/cc)	13.92	13.92	see Table VII
U^{238} (19.0 g/cc)	15.83	15.83	
SS (7.85 g/cc)	16.86	19.31	
Al (2.70 g/cc)		17.77	
Na (0.97 g/cc)	39.94		

In each core three radial regions, designated by Roman numerals, were chosen for the substitutions in the core, and a fourth radial region was studied in the inner blanket. Each of these radial regions was divided into five two-inch-long axial increments, numbered 1-5 (Arabic numerals) from the center out to the gap. The core was 7 in. long in each half of the mockup; thus, if distances are measured from the center, increment No. 1 extends from 0 to 2 in., and No. 5 is in the gap, from 8 to 10 in. The average radii of the radial regions is given in Table XV. Although the cores are roughly hexagonal, the radii are those of the circles having equal cross-sectional area. Figures 26 and 27 show the substituted regions in detail.

Table XV

INNER AND OUTER RADII OF SUBSTITUTION REGIONS (IN.)

Region	Na-filled Clean Core and Al-filled Clean Core	Al-filled Engineering Core
I	0-3.69	0-3.69
II	3.69-6.62	3.69-6.62
III	6.62-9.39	6.62-9.70
IV	10.21-12.96	9.70-15.50

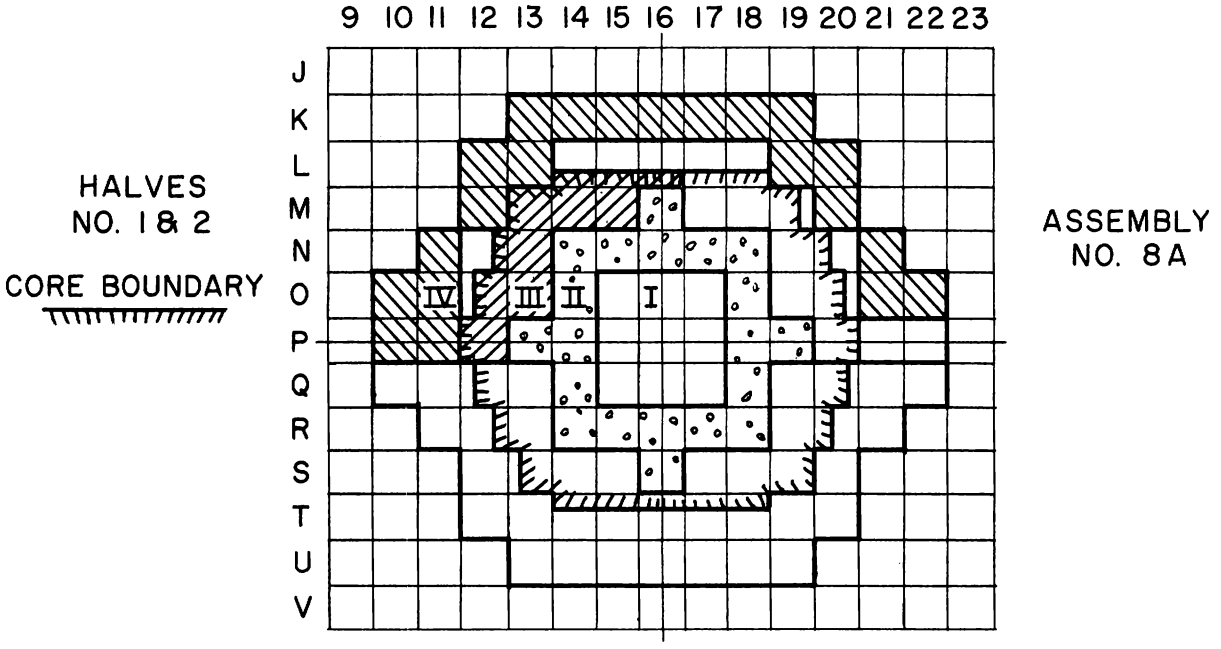

Fig. 26. Radial Regions of EBR-II Clean Core Mockup

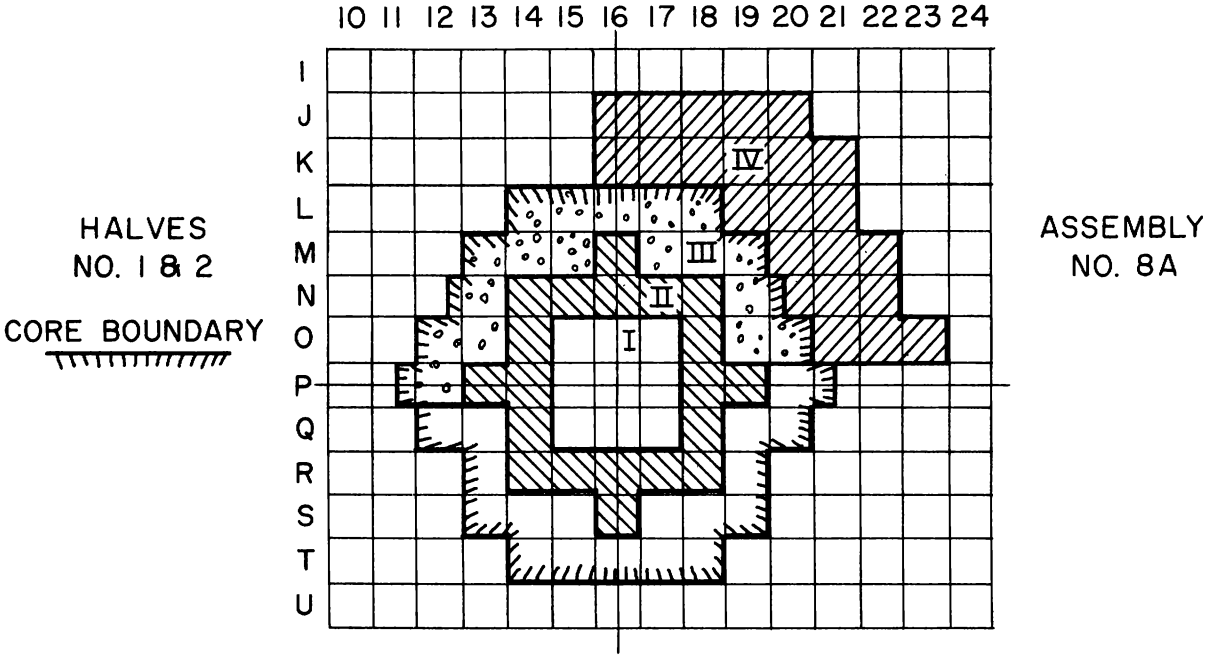

Fig. 27. Radial Regions of EBR-II Engineering Core Mockup

The results of the substitutions are shown in Table XVI. It is worth noting that there is good agreement between the worth of sodium in the two clean cores in regions I-4 and IV-4, but a significant difference in regions I-1 and I-2. The difference in region IV-1 is just slightly larger than the expected experimental uncertainty, and may not be significant.

Table XVI

SODIUM, STAINLESS STEEL, AND ALUMINUM WORTHS IN EBR-II MOCKUPS (Ih/kg OF MATERIAL COMPARED TO VOID)

Region (radial-axial)		Na-filled Clean Core	Al-filled Clean Core	Al-filled Engineering Core		
		Na Worth	Na Worth	Na Worth	Al Worth	SS Worth
I	1	25.4	34.5	40.9	7.5	-4.9
I	2	36.8	51.0	54.0	20.5	2.6
I	3	65.4		79.6	44.6	14.6
I	4	92.2	95.7	94.8	60.0	24.3
I	5	53.9		57.7	33.3	13.0
II	1	39.6		51.3	18.8	2.4
II	2	44.6		56.4	26.0	6.6
II	3	58.7		70.0	37.5	13.2
II	4	69.7		47.2	45.9	18.5
II	5	43.6		47.6	27.3	11.8
III	1	54.8		55.5	31.2	10.4
III	2	50.1*		52.2	30.3	10.7
III	3	49.8		50.1	31.3	11.7
III	4	42.0		46.0	31.0	12.1
III	5	35.8		30.2	19.2	8.4
IV	1	21.5	18.3	15.9	10.7	4.6
IV	2	21.5		9.2	10.6	4.5
IV	3	18.9		7.4	9.2	3.8
IV	4	9.0	10.0	4.0	6.0	2.6
IV	5	5.4		3.8	4.2	1.8

* First determination at this location was a value of 41.5, which does not fit any reasonable pattern. Upon rechecking, the figure in the table was determined and the earlier value is assumed to be in error.

The sodium substitutions in the aluminum-filled engineering core were made in three $\frac{1}{4}$-in. columns per drawer, with two $\frac{1}{8}$-in. columns of aluminum and two $\frac{1}{8}$-in. columns of stainless steel unsubstituted. In the clean reactor mockups, however, all eight columns of aluminum and two columns of stainless per drawer were substituted with a total of five $\frac{1}{4}$-in. columns of sodium per core drawer. In the radial blanket only two $\frac{1}{4}$-in. columns of sodium per drawer were used.

Analysis of the sodium from selected cans showed them to contain less than 100 ppm of hydrogen.

1. Worth of Fissile Materials

Several additional experiments were performed with these cores to aid in the interpretation of the Na and Al substitutions. Fissile materials were evaluated in the front $\frac{1}{4}$ inch of the central drawers. Values are given in Table XVII.

Table XVII

WORTH OF FISSILE MATERIALS
(Ih/kg RELATIVE TO VOID)*

	Na-filled Clean Core	Al-filled Clean Core
Enriched U	238.1	256.8
Depleted U	4.55	3.18
Plutonium	474.5	496.8
U^{233}	488.6	504.5

* Values reported are experimental worths of the materials substituted without correction for the presence of other isotopes.

2. Distributed Worth of Aluminum

The distributed worth of aluminum was determined in the Na-filled clean core in a composition predominantly Na. The worth was found to be 31.7 Ih/kg.

3. Sodium Worth in Region I-1 as a Function of the Quantity Substituted

In the Na-filled clean mockup, one can of Na per drawer in region I-1 was replaced by an empty can. Next, two additional cans in each drawer at this region were substituted by empty cans, and finally the remaining two cans per drawer were substituted. The worth of Na for each of the three changes was 20.7, 24.6 and 17.6 Ih/kg, respectively. Although the spread among the results is larger than desired, no consistent trend is observed, and one must conclude that the sodium worth is not a function of the amount substituted in this case.

4. Worth of Polyethylene

The worth of polyethylene was determined by placing 2 x 2-in. squares on top of the drawers in region I-1, where a value of 2.8 Ih/g was obtained. In region III-1, the worth of polyethylene, determined in a similar fashion, was 1.2 Ih/g.

5. Worth of a Single Column

In the Na-filled clean core, the worth of a single column of enriched uranium relative to void was +100.3 Ih at the center of drawer 2P-16. A column of depleted was worth +4.0 Ih relative to void.

6. Conclusions Drawn from the Substitution Experiments

There appears to be some spectral difference at the center of the clean cores, depending on whether the core is filled with Na or Al, even though the geometrical outlines of the cores and their critical masses are essentially the same. This is demonstrated by the different worths of fissile materials (Table XVII) and is further reflected in the different maps of the worth of sodium (Table XVI). The change in stainless steel content between the two cores may contribute to the effect. Analysis of the sodium showed it to be essentially hydrogen-free in comparison with the amounts of hydrogen that would be required to produce significant reactivity effects.

VI. Reactivity Traverse Measurements with Fissionable Materials

Reactivity coefficient traverses in the axial direction were made at positions approximately four inches apart, starting from the core central axis. A radial traverse was also made about $\frac{1}{4}$ in. from the core midplane. These were done in the engineering version of the mockup to provide power coefficient data.

The measurements were made using the fission counter traverse mechanism to drive a slug of enriched or natural uranium through a one-half-inch void in the assembly. The uncertainty of positioning the reactivity coefficient sample was found by experiment to be less than $\frac{1}{8}$ in.

An arbitrary zero reference at some point well out in the blanket was established, and the difference in control rod critical position between this position and any other position was interpreted as the combined worth of sample, sample holder, and traverse rod. The worths of the sample holder and traverse rod were determined in the same way and the difference was attributed to the sample. The error in the worth is thought to be in the order of $\pm$0.1 Ih.

The masses of the enriched and natural uranium reactivity coefficient samples were 22.93 and 32.15 g, respectively.

For traverses in the engineering core, Tables XVIII and XIX are tabulations of the axial worths of the samples at various radial distances. Table XX gives the radial worths at the core midplane. Figure 28 is a plot of the axial traverses, each adjusted at its center to correspond to the radial traverse.

Table XVIII

ENRICHED (93%) URANIUM AXIAL REACTIVITY COEFFICIENT TRAVERSE (WORTH IN INHOURS/SAMPLE)

Axial Position (in. from midplane)	Matrix Position (in. from center)			
	P-16 0	N-16 4.36	L-16 8.73	J-16 10.9
-15	0.148	0.154	0.310	0
-13	0.592	0.231	0.310	0
-11	0.918	0.666	0.394	0
-9	1.69	1.025	0.874	0
-7	2.49	1.97	1.212	0.206
-5	4.26	3.46	2.2	0.412
-3	5.92	4.34	2.90	0.353
-1	6.81	4.82	3.38	0.441
0	6.75	4.82	3.30	0.441
1	6.72	4.85	3.02	0.441
3	6.10	4.30	2.82	0.500
5	4.62	3.36	2.28	0.441
7	3.11	2.26	1.66	--
9	1.84	1.41	1.043	-0.029
11	0.83	0.795	0.761	-0.059
13	0.681	0.461	0.564	--
15	0.533	0.128	0.226	-0.059

Reference for reactivity zero is -41.0 in.

Table XIX

NATURAL URANIUM AXIAL REACTIVITY COEFFICIENT TRAVERSE
(WORTH IN INHOURS/SAMPLE)

Axial Position (in. from midplane)	Matrix Position (in. from center)			
	P 0	N 4.36	L 8.73	J 10.9
-15	0	0	-0.169	0
-13	0.148	-0.077	0	--
-11	0.207	-0.180	0.099	0
-9	0.444	0.051	0.141	--
-7	0.504	0.513	0.197	0.063
-5	0.592	0.513	0.310	0.097
-3	0.681	0.487	0.423	-0.015
-1	0.474	0.231	0.480	-0.170
0	0.237	0.308	0.465	-0.176
1	0.296	0.410	0.310	-0.206
3	0.296	0.436	0.310	-0.206
5	0.533	0.308	0.169	--
7	0.830	0.539	0.113	-0.273
9	0.356	0.410	0.031	-0.258
11	0	0.231	0.212	-0.232
13	0.207	0.077	-0.310	0.47
15	0.296	-0.103	-0.282	0.47

Reference for reactivity zero is -41.0 in.

Table XX

RADIAL REACTIVITY COEFFICIENT TRAVERSES AT
REACTOR MIDPLANE (WORTH IN INHOURS)

Radial Distance (in. from center)	Enriched Uranium	Natural Uranium
15	0.324	-0.005
13	0.540	0.119
11	1.38	0.081
9	2.52	0.378
7	3.62	0.527
5	4.40	0.419
3	5.46	0.481
1	6.03	0.470
0	6.06	0.460
-1	6.06	0.460
-3	5.60	0.406
-5	4.81	0.487

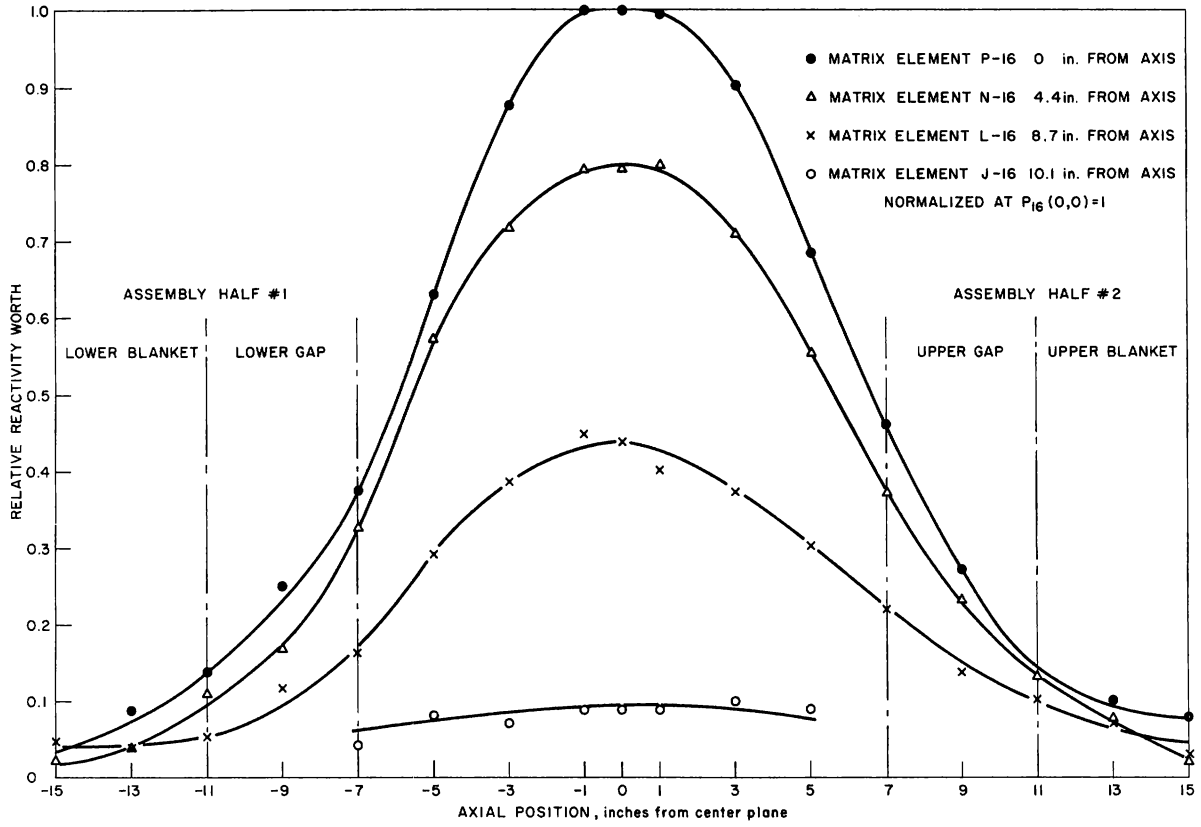

Fig. 28. Axial Reactivity Worth Traverses with Enriched Uranium

The enriched uranium reactivity coefficient sample was also used to determine the worth at the core center and the core-blanket axial interface in the Na clean core and the Al clean core. These values are given in Table XXI. It is interesting to note the possibility of a larger gradient for the worth in the Al core, with the two curves crossing somewhere between the core center and the axial core-blanket interface.

Table XXI

ENRICHED (93%) URANIUM REACTIVITY COEFFICIENT TRAVERSE

0 in. is core center
-7 in. is axial core blanket interface

Traverse taken along core axis at r = 0

Position (in.)	Worth in inhours/sample	
	Na Clean Core	Al Clean Core
-46.0	0	0
-7.0	2.74	2.35
0	5.66	5.79

Axial fission traverses along the core center were made with U^{235}, U^{234}, and natural uranium fission counters. These were done in both the Al and Na clean cores and are tabulated in Tables XXII and XXIII. Table XXIV lists the loading of each of the counters.

To normalize all of the points on the traverse to the same power, a U^{235} fission counter was installed at the core-blanket interface. All points on each traverse were normalized to 10,000 or 20,000 counts on this counter.

Table XXII

AXIAL FISSION TRAVERSES IN Al CLEAN CORE

Axial Position (in.) $\mathbb{C}_L$ = 0	Counts/10,000 on Standard Counter		Counts/20,000
	U^{234}	U^{235}	Natural Uranium
-46.9	61	495	11
-25.0	391	4988	143
-21.0	824	9989	285
-19.0	1172	13224	489
-17.0	1911	18332	773
-15.0	2830	24824	1270
-13.0	4239	32483	2060
-11.0	6293	41097	3488
-9.0	9156	49497	5841
-7.0	13714	62107	10289
-6.0	17527	71428	14358
-5.0	21400	81073	17346
-4.0	23851	86553	19868
-3.0	25739	94162	21813
-2.0	27547	98735	22360
-1.0	28206	101701	23706
0	28081	101110	23979
1.0	29167	101078	24294
2.0	27925	101422	23445
3.0	27171	98092	22617
4.0	25311	93533	21379
5.0	23223	86230	19473
6.0	20309	78226	16915
7.0	16836	71415	13569
9.0	10975	56186	7261
11.0	7517	45880	4371
13.0	5056	35228	2661
15.0	3293	27305	1510
17.0	2211	20562	906
19.0	1371	14511	561
21.0			

Table XXIII

AXIAL FISSION TRAVERSES IN Na CLEAN CORE

Position (in.) $\mathbb{C}_L = 0$	Counts/10,000 Counts on Standard Counter		
	U^{234}	U^{235}	Natural Uranium
-46.9	33	442	7
-25.0	334	4907	69
-21.0	752	9351	161
-19.0	1140	13031	246
-17.0	1860	18817	414
-15.0	2808	25437	674
-13.0	4073	33048	1121
-11.0	6129	42541	1883
-9.0	8914	51894	2967
-7.0	14371	63508	5583
-6.0	17785	71208	7506
-5.0	20640	78994	8952
-4.0	22843	83903	9717
-3.0	24309	89059	10394
-2.0	25949	93824	11231
-1.0	26598	95541	11524
0	26714	97109	11451
1.0	25891	96698	11485
2.0	25926	96779	11232
3.0	24795	91683	10908
4.0	22890	86896	10170
5.0	21193	81479	8995
6.0	18528	75235	7885
7.0	15175	66178	6190
9.0	9723	55496	3290
11.0	6531	45554	1988
13.0	4973	35995	1151
15.0	2773	26192	696
17.0	1972	19699	416
19.0	1175	13780	262
21.0	786	10187	160

Table XXIV

FISSION COUNTER LOADINGS

Counter	Loading Mass, mg	Thickness, mg/cm^2	Composition (%)		
			U^{238}	U^{235}	U^{234}
Natural U	4.34	0.51	99.29	0.71	--
U^{235}	5.1	0.60	93.2	6	1
U^{234}	3.15	0.37	2.89	7.72	89.39

It is interesting to compare graphical presentations of the fission rates in the sodium- and aluminum-filled cores, and this is done for enriched U^{235} in Fig. 29 and for natural uranium in Fig. 30. The four curves of Figs. 29 and 30 were constructed from separate fission traverses, individually normalized to unity at the center and plotted to the same scale on individual graphs. The two enriched curves were then superimposed and adjusted to match as symmetrically as possible around their peaks, and this result is shown in Fig. 29. The differences between the curves, especially in the region of the gaps, are believed to be significant. Figure 30 was constructed in similar fashion from the natural uranium traverses, which are more sensitive to the high end of the spectrum, and there is very little difference between the aluminum- and sodium-filled cores. It is concluded that there are apparently spatial differences in the spectral distribution of the two assemblies.

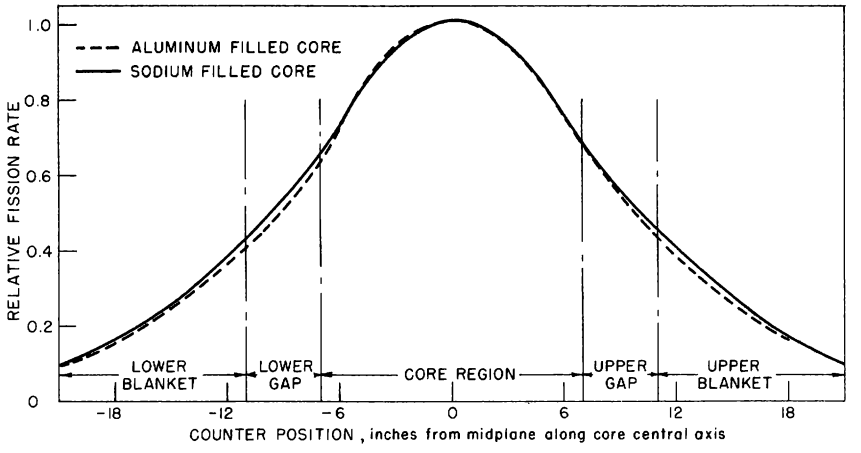

Fig. 29. Enriched U^{235} Fission Counter Traverses in Aluminum and Sodium-filled Cores

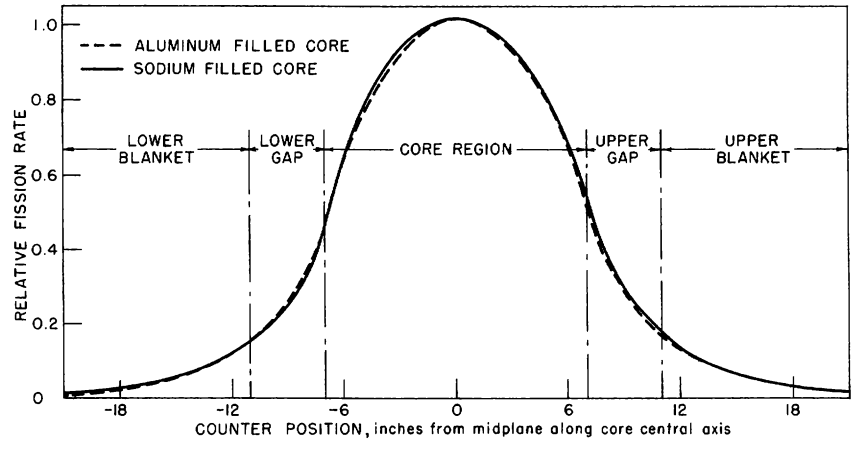

Fig. 30. Natural Uranium Fission Counter Traverses in Aluminum and Sodium-filled Cores

This would indicate that although a density of aluminum may be chosen so that its worth over the whole core will reproduce the worth of a uniform density of sodium coolant, nevertheless spatially varying spectral differences exist so that the aluminum is not a true mockup of the sodium in all regions.

It is suggested that calculations of the two assemblies be examined to see if this difference in space-energy distribution is computable. Furthermore, the calculations should be examined for any information they might provide on the interpretation of Table XVII, where it was observed that reactivity coefficients for fissionable materials were different at the center of the two cores.

VII. The Second EBR-II Source Experiment

Between the time of the first mockup of EBR-II, December 1957, and the recent EBR-II critical experiments in the summer of 1960, the design of the shield and thimble holes for EBR-II has evolved considerably. Since there is still a great deal of uncertainty about calculated counter responses in the shield region, it seemed advisable to mock up some of the most promising current designs on ZPR-III and investigate counter response.

The principal design changes since the previous experiment are the introduction of the steel reactor vessel between the source thimble and the inner shield, and an increase in the amount of steel in the thimble itself. Since both of these changes are expected to reduce the thermal flux at the thimble, more effective moderating materials than graphite were sought, and zirconium hydride was therefore proposed. In addition, the instrument placed at 71 inches from the core center is no longer of interest and our 1960 mockup considered a startup instrument in a thimble 58 inches from the core center. Other counters were spotted between this location and the core center to give some indication of flux variation.

1. Mockup Shield

Figure 31 gives a diagram of the ZPR-III with the mockup shield placed next to the east face of the matrix. Three principal regions which were mocked up outside the normal ZPR-III matrix are:

1. The inner shield. Spaced $\frac{1}{2}$ in. from the steel matrix tubes is 1 in. of aluminum and $\frac{1}{2}$ in. of steel plate. Beyond this is a 8-$\frac{1}{4}$-in. space which, during various experiments, was filled either with aluminum or 93 v/o graphite-7 v/o steel. Beyond this is the reactor vessel, represented by 1-$\frac{1}{8}$-in. steel plate.

2. The outer shield. This region extends from the reactor vessel 25-$\frac{1}{4}$ in. outward in our mockup. It includes the 15-in. diameter thimble shown in Fig. 32. In some of the experiments zirconium hydride powder in rectangular aluminum cans was stacked around the thimble to a depth of three to four inches (see Fig. 33). This amounted to about 188.15 kg of ZrH in 76.1 kg of Al, covering 24 in. of the thimble, starting from 2 in. from the lower end of the thimble. Solid aluminum filled the remainder of the outer shield region.

   An alternative composition for the outer shield region consisted of 93 v/o graphite-7 v/o steel replacing the aluminum and zirconium hydride around the thimble.

3. The bulk sodium region. In our mockup 12 in. are available beyond the outer shield for this region. This was filled either with 12 x 60 x 60 in. of solid aluminum, or alternatively with 12 x 28 x 60 in. of graphite-steel directly behind the thimble and the remainder with aluminum (see Fig. 34).

   All steel used in the shield mockup was low carbon. It is believed that low carbon steel in the amounts used here will behave toward neutrons approximately like stainless steel in the reactor concentrations and at reactor temperatures.

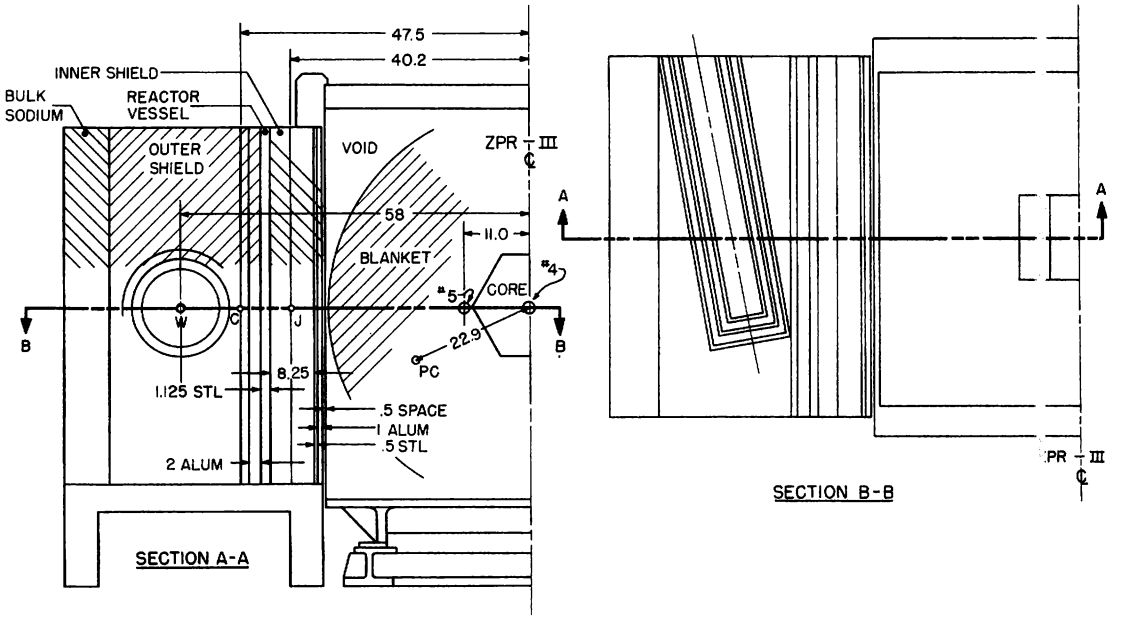

Fig. 31. Shield Mockup of EBR-II in ZPR-III (Dimensions in inches)

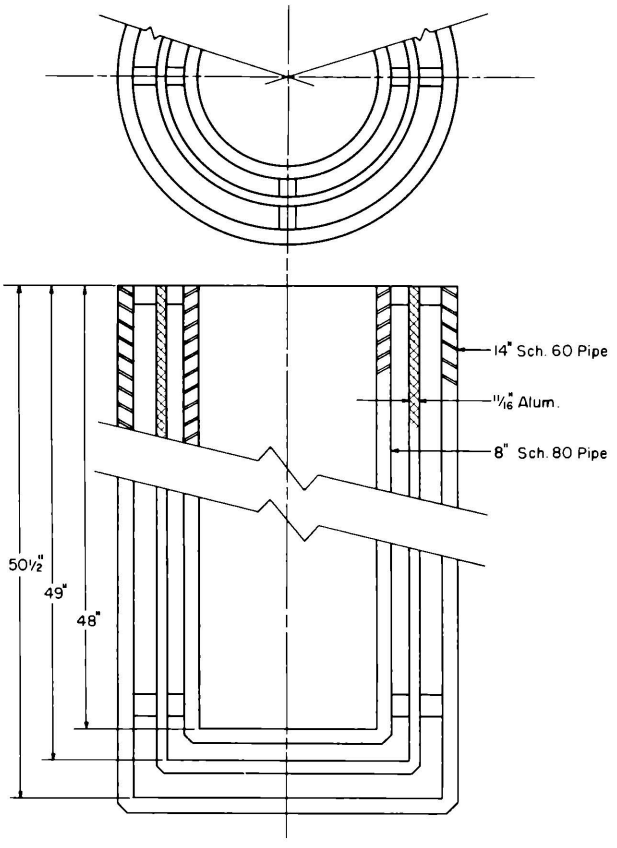

Fig. 32

Instrument Thimble of EBR-II Mockup (Dimensions in inches)

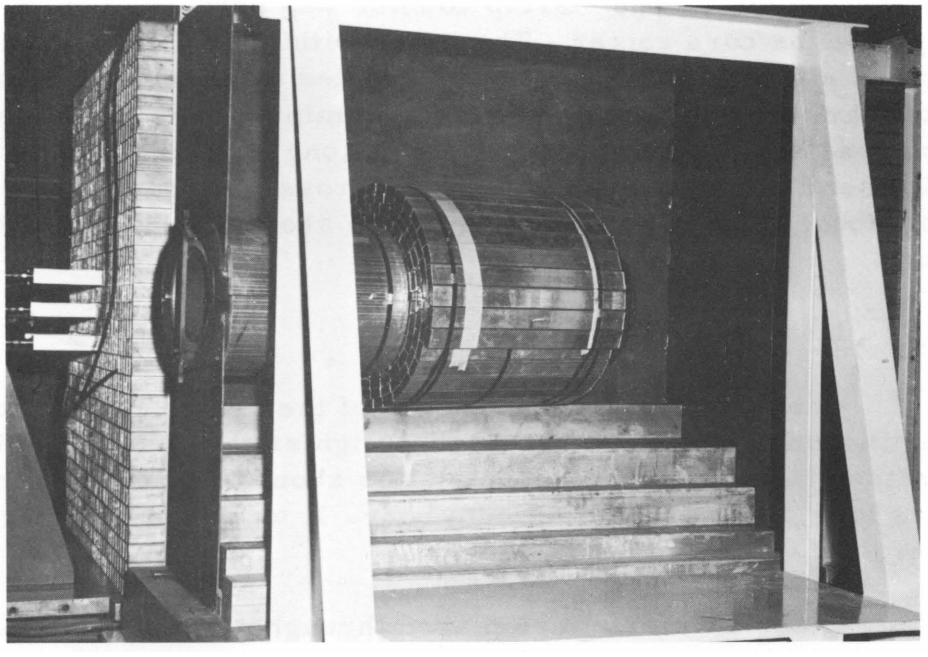

Fig. 33. Zirconium Hydride Stacked Around Instrument Thimble

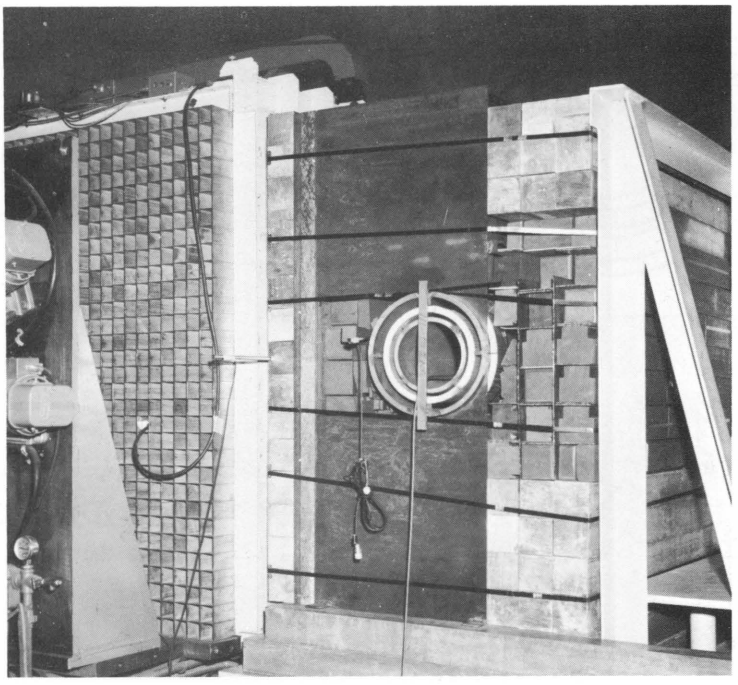

Fig. 34. Shield Configurations 7 and 8 with Graphite Behind the Thimble

2. Thimble

The thimble, which is shown in Fig. 32, represents a J-thimble of the actual reactor. The startup counter was positioned on the thimble axis opposite the core center. The space within the thimble and around the counter was either left void or partially filled with ZrH. The ZrH for use within the thimble was contained in two aluminum cans, each having a triangular cross section and about 10 inches long. The two cans contained 4.1 kg ZrH and 1.2 kg Al. The combined cross-sectional area of the two cans was about 9.8 square inches, of which about 2 square inches are aluminum.

3. Instrumentation

The counter proposed as one of the principal startup instruments is a Westinghouse fission counter with a lighter than usual uranium loading, 0.92 g rather than 2.0 g. The counter was about 2 inches in diameter, 10 inches long, and had an aluminum body. It was used both bare and Cd-covered, 0.031 in. thick.

Other counters were placed throughout the core, blanket, and shield for the purpose of ascertaining if the subcritical multiplied fluxes were the same in space and energy distribution as the critical fluxes with

the reactor at power. If this proved to be the case, it would be an easy matter to scale up the counter responses from small sources, using the information gained at power. These counters were not identical and cannot reliably be used for determination of flux patterns, since their efficiencies differ and are energy-dependent. In order that some approximate picture of the flux pattern could be obtained, however, the counters were intercompared in the thimble, with and without cadmium, and also in several spectra of the AFSR. Results are tabulated in Table XXV. Descriptions of the counters are given in Table XXVI.

TABLE XXV

COUNTER RESPONSES WITH VARIOUS SHIELD CONFIGURATIONS

Configuration		1	2	3	4	5	6	7	8
Inner Shield		Al	Al	Al	Al	C	C	Al	Al
Outer Shield		ZrH	ZrH	C	C	C	C	C	C
Bulk Sodium		Al	Al	Al	Al	Al	Al	C	C
Thimble		Void	ZrH	Void	ZrH	Void	ZrH	Void	ZrH
Counter Designation	Inches from Center	Critical (relative count rates)							
4	0	1.00	1.00	1.00	1.00	1.00	1.00	1.00	1.00
5	11.0	0.46	0.46	0.49	0.48	0.46	0.46	0.46	0.47
J	40.2	0.027	0.028	0.037	0.034	0.39	0.38	0.034	0.035
C	47.5	0.15	0.14	0.057	-	0.051	0.055	0.058	0.056
W	58.0	5.35	8.40	4.56	12.6	2.47	5.16	4.68	11.50
W(Cd)	58.0	1.09	0.96	2.47	2.32	1.01	0.75	2.51	2.22
PC	22.9	-	-	17.2	17.6	18.6	18.8	18.4	18.0
		1170-Ih Subcritical (counts per minute)							
4	0	180		180		190		200	
5	11.0	-		-		170		77	
J	40.2	6		6		-		7	
C	47.5	-		-		24		-	
W	58.0	780		670		370		710	
PC	22.9	2560		2410		2720		2580	
		2340-Ih Subcritical (counts per minute)							
4	0	110		110		110		110	
5	11.0	36		-		49		39	
J	40.2	2.5		4.3		-		2.9	
C	47.5	-		-		19		-	
W	58.0	395		365		190		350	
PC	22.9	1290		1290		1450		1290	

Table XXVI

DESCRIPTION OF COUNTERS IN MOCKUP SHIELD

Counter	Type	Loading, mg	Active Surface	Counter Body	Relative Count Rate			
					1	2	3	4
					AFSR Thermal Column	Beam Hole	Thimble	Thimble (Cd)
4	U^{235} fission counter	0.802	Flat	Stainless	1.83	1.55	1.70	1.71
5	U^{235} fission counter	0.804	Flat	Stainless	1.68		1.70	1.81
J	U^{235} fission counter	5.1	Cylinder	Brass	8.96		8.22	-
C	U^{235} fission counter	5.1	Cylinder	Brass	7.55		6.94	7.65
W	U^{235} fission counter	920	Cylinder	Aluminum	1000	1000	1000	1000
PC	$B^{10}F_3$ proportional counter	-	-	Aluminum	-	-	-	-

Since the cylindrical fission counters have no plateau, the following procedure was used for adjusting the gain of the amplifiers:

A plot of counts versus discriminator setting was made for each cylindrical fission counter at fixed gain with no neutrons present. This was very nearly a straight line on semilog paper. The operating point was chosen as the discriminator setting at which the background alpha count was 0.1 c/sec. On subsequent days the count rate at some lower discriminator setting was checked to see that it matched the corresponding point on the original plot, small adjustments in the gain being made if necessary to bring the circuit into agreement with previous characteristics. Then, with the adjusted gain setting, the discriminator was set at the previously selected operating point.

The validity of this method of adjusting the gain setting was checked as follows. With a constant flux of neutrons, the gain was varied over the entire range which had been used during the experiment, about ±2% gain change. The response of the various counters changed by not over ±3% under this adjustment. Since the counter reproducibility is within 3% over the range of gain settings when no change in amplifier characteristics was occurring, it is felt that the reproducibility must be even better when the gain changes are employed only to compensate for amplifier drift.

The five fission counters were intercompared in four different spectra, indicated under relative count rate in Table XXVI by columns 1, 2, 3, and 4. The relative count rates in column 1 were obtained in the AFSR thermal column with the counters wrapped in cadmium. The fact that counters 4 and 5 disagreed by about 8% probably indicates that the cadmium wrapping was not done carefully enough to give the same flux depression in each case. Column 2 values were determined in the AFSR beam hole. Since there is a steep flux gradient in this hole, the count rates for counter No. 4

were determined at a number of positions and averaged together to get a figure comparable to the Westinghouse fission counter rate. These counters were also wrapped in cadmium. The values in column 3 were obtained with all the fission counters placed simultaneously in the thimble. There was no cadmium in the thimble. The thimble was surrounded with the graphite-steel mixture and the inner shield region was filled with aluminum as in configuration 7. Column 4 comparisons were made with the same configuration as the Column 3 comparison, except that all the counters were wrapped in cadmium. In all these intercomparisons, the same cables, preamplifiers and amplifiers were used, as had been used in the source experiment.

4. Sources

The source for EBR-II will be an antimony slug enclosed in beryllium. In our mockup an antimony slug was inserted in a beryllium jacket in each half of the assembly, drawers 1P21 and 2P21. These locations are alongside a corner of the hexagonal core, just outside the core boundary. The beryllium jackets were 0.446 in. thick. We had available irradiated antimony slugs and inactive slugs, the latter being used just to give the proper geometrical mockup when the reactor was operating. The activated slugs were fabricated in Argonne and irradiated in CP-5. Unfortunately, the exact amount of antimony in the Argonne fabricated slugs is unknown because they used an alloy of undetermined composition. The samples will be too hot for chemical analysis, probably for a few more months. Meanwhile, for the purpose of preliminary estimates, they are considered to be about 50% antimony, or a total of about 370 g Sb total for the two slugs. With this assumption, the antimony had about 9.7 curies of Sb-124 activity on June 3, 1960.

5. Notes on Table XXV

Eight Configurations Studied: Taking into account the variations in inner and outer shield, bulk sodium region, and presence or absence of ZrH inside the thimble, a total of eight configurations were studied.

In configuration 1, the thimble was surrounded by three to four inches of zirconium hydride, with aluminum filling the rest of the outer shield region. The inner shield region was filled with aluminum as was the bulk sodium region. Configuration 2 was the same except for the addition of ZrH inside the thimble.

In configuration 3, the ZrH and aluminum in the outer shield region were replaced with graphite and steel. ZrH was removed from inside the thimble. The inner shield and bulk sodium regions still had aluminum. Configuration 4 was the same with ZrH again inserted inside the thimble.

In configurations 5 and 6, 8-$\frac{1}{4}$ in. of aluminum in the inner shield was replaced with the graphite-steel mixture. Outer shield and bulk sodium regions were unchanged from the previous loading. Configuration 5 was without ZrH and configuration 6 had the ZrH in the thimble.

In configuration 7 and 8 the graphite-steel in the 8-$\frac{1}{4}$ in. region of the inner shield was replaced with aluminum. The outer shield still had graphite-steel. In the bulk sodium region a 12 x 28 x 60-in. region directly behind the thimble was loaded with graphite steel, the remainder of this region being aluminum, as shown in Fig. 35. Configuration 7 was tested with no ZrH inside the thimble while configuration 8 had ZrH in the thimble.

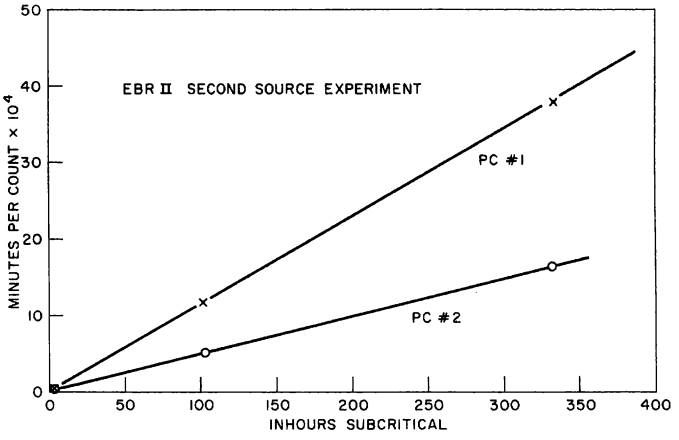

Fig. 35. Subcritical Counter Calibrations

Normalizations: The critical measurements listed in Table XXV are the responses on the counters relative to counter No. 4 at the core center. All critical measurements were made with the dummy (inactive) antimony source.

The subcritical measurements are corrected for decay of the source to June 3, but are not normalized to the central counter. Therefore, the figures given are the actual count rates, counts per minute, for a total 9.7-curie source.

All the figures in Table XXV are rounded off so that the number of significant figures reported is indicative of the estimated accuracy. Both the statistical accuracy of the counts and the observed reproducibility of counts expected to be identical have been taken into consideration in estimating the accuracy of the data.

Nomenclature: The designation W refers to the Westinghouse fission counter in the thimble and W (Cd) refers to the response of this counter when wrapped in 0.031-in. cadmium.

6. Power Calibration

The count rate on counter No. 4 at the core center can be converted to a measure of the fission power of the U^{235} in the core by means of the following assumptions:

1. The ratio of fissions per gram of U^{235} at center to the core average value is 1.51. This is consistent with foil activation maps run on the previous EBR-II mockup.
2. One watt = 3.1×10^{10} fissions per second. This figure omits most of the delayed gamma and beta power.
3. Fission counter No. 4 contains 0.802 mg 93% U^{235}.
4. The critical mass of the mockup is 166.2 kg U^{235}.

Then, one count per minute on counter No. 4 at the center represents

$$\frac{1}{60} \times \frac{1.662 \times 10^{5}}{8.02 \times 10^{-4} \times .93} \times \frac{1}{1.51 \times 3.1 \times 10^{10}} =$$

7.9×10^{-5} watt of fission power in the core U^{235}.

The foil activation maps also indicate that for one watt of fission power generated in the core U^{235},

0.066 watt is generated in the core U^{238}
0.002 watt is generated in the axial blanket U^{235}
0.010 watt is generated in the axial blanket U^{238}
0.024 watt is generated in the radial blanket U^{235}
0.138 watt is generated in the radial blanket U^{238}

7. Subcriticality Measurements

Control rods were calibrated by period measurements in the usual fashion. The reactor was made known amounts subcritical by moving out control rods and inverse count rates were recorded for two $B^{10}F_3$ proportional counters. These gave good straight lines as shown in Fig. 35. The extrapolations of these straight lines were used to estimate the degree of subcriticality reported in Table XXV.

The loadings used to achieve subcriticality consisted of the replacement of enriched by depleted uranium in peripheral core drawers. Thus, the subcritical loadings in our mockup achieve a composition comparable to a reactor loading in which some outer fuel pins are replaced by blanket pins.

The 1170-Ih subcritical loading had enriched replaced by depleted in nine outer core drawers and the 2340-Ih subcritical loading had 15 drawers substituted.

C. TRANSIENT REACTOR TEST FACILITY

C. TRANSIENT REACTOR TEST FACILITY

I. Review (J. F. Boland)

The Transient Reactor Test Facility (TREAT) is a graphite-moderated reactor constructed by Argonne National Laboratory to generate integrated thermal neutron flux bursts up to a maximum of 10^{16} nvt. This may be done repeatedly without damage to the facility.

The reactor went critical in February 1959. Physics measurements were conducted until September, 1959, when transient testing was started. Two hundred transient tests have been satisfactorily run in the reactor. The results of the physics measurements made to determine the static and dynamic characteristics of the reactor have been reported in ANL-6173, and the theoretical work performed in conjunction with these measurements was reported in ANL-6174.

Experimental work in the facility during its first year of operation has been divided between experiments designed to investigate meltdown characteristics of fast reactor fuel elements and metal-water reaction experiments designed to measure reaction rates of various metals used in reactor core construction.

II. Tests Conducted for Other Divisions (J. F. Boland)

During the period covered by this report, tests were run for the Reactor Engineering, Chemical Engineering, and Metallurgy Divisions. A total of 20 samples was tested under the fast reactor fuel element test program being conducted by the Reactor Engineering Division. Of these, 15 were stainless steel-clad EBR-II type elements, one was a Nb-clad prototype EBR-II element, and 4 were Zr-clad Fermi-I-type elements. The Chemical Engineering Division program consisted of seven experiments designed to obtain data on metal-water reactions, with small fuel elements of various materials, and to make observations of changes in geometry which take place during a transient. The Metallurgy Division test program consisted of 4 tests on stainless steel-clad EBR-II-type fuel elements.

III. Reactor Operations (J. F. Boland)

Operation during the period of this report consisted primarily of transient testing of fuel element samples using pulse-shaped bursts.[1,2] However, a few transients were run utilizing "constant power" or "flat top" types of bursts. Since this type of transient has not been previously reported, a description of the equipment and procedures used to obtain the

[1] D. R. McFarlane et al., Hazards Summary Report on the Transient Reactor Test Facility, ANL-5923 (Oct., 1958).

[2] F. Kirn et al., Physics Measurements in TREAT, ANL-6173 (Oct., 1960).

"flat top" shape, problems associated with this type of operation, the reason for using this shape of burst, and typical results will be discussed.

The normal TREAT transient releases energy at a changing rate determined by the initiating reactivity and the negative temperature coefficient. Therefore, a reasonable simulation of the failure of a fuel element resulting from operation of a reactor at a steady power exceeding the capabilities of the coolant for heat removal cannot be obtained from this normal type of transient. In order to provide a reasonably constant high power for a reasonable length of time during transient operation of a reactor with a large negative temperature coefficient, it is necessary to add reactivity, at a rate equal to the rate that the negative temperature coefficient is removing reactivity, from the time that the temperature-limited power peak is reached until the desired energy release has been obtained. In TREAT this is accomplished by dropping a transient rod[1] at a predetermined rate which is set by adjusting the downward force on a transient rod-drive air cylinder and the opening of a needle valve in a hydraulic system connected to the bottom of the cylinder. Since the transient rod does not have a constant worth per inch over its entire length and since the reactor temperature-energy relationship is nonlinear, the instantaneous rate of reactivity addition can only be made to approximately the rate required to give a truly "constant power" type of burst.

Initially the sustaining rod was released by a programmed time signal based on the time required for the reactor to reach its temperature-limited peak power for a given initiating k_{ex}. But experience showed that a small error in initial period caused a relatively large error in release time, since 8 to 14 periods are required for the power to reach the peak. Therefore, a circuit was designed to release the sustaining rod when the rate of change of power with respect to time went negative by a predetermined amount. A schematic block diagram of this circuit is shown in Fig. 36. It was found necessary to block the positive derivative of power signal in order to maintain the desired sensitivity without saturating the amplifier. Such saturation would introduce an unacceptable time delay in the release of the rod. The diode connected across the feedback resistor in the amplifier circuit blocked this undesirable signal very effectively.

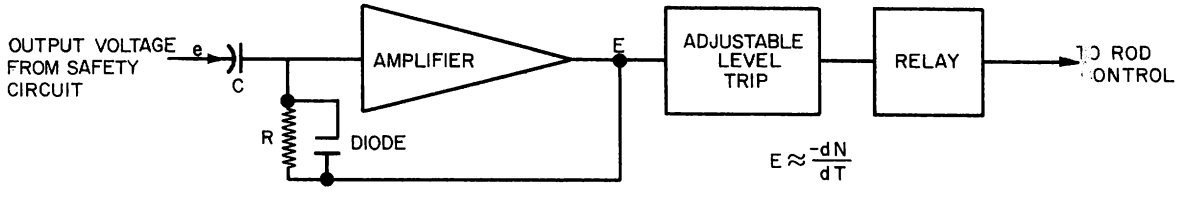

Fig. 36. Negative Derivative Trip Circuit Diagram

Figures 37 and 38 show data for power vs time obtained for two typical flat-top-type transients, together with data from the normal type of transient with the same initial period. The magnitude of the power peaks is very sensitive to initiating reactivity additions. Typically, an error of 0.01 percent k_{ex} will cause an error of 5 percent in the power peak. Therefore, a "constant power" type of burst, which maintains the power within ±10 percent of the desired value, is about the best than can be expected on a routine basis.

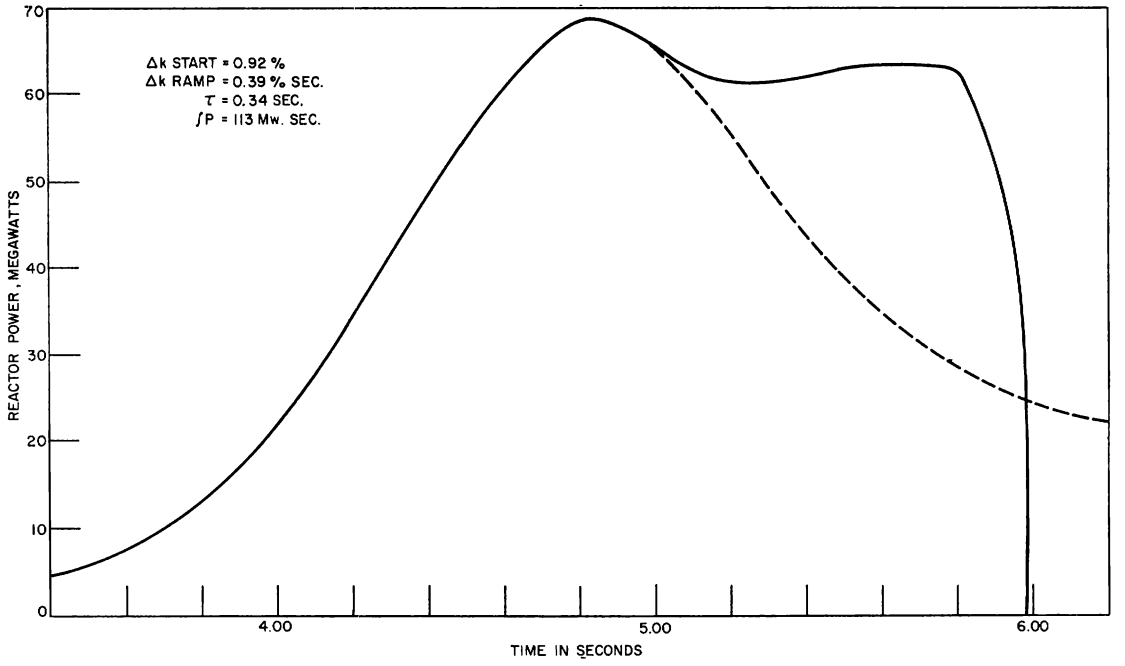

Fig. 37. Typical Flat-top Transient, Reactor Power vs Time

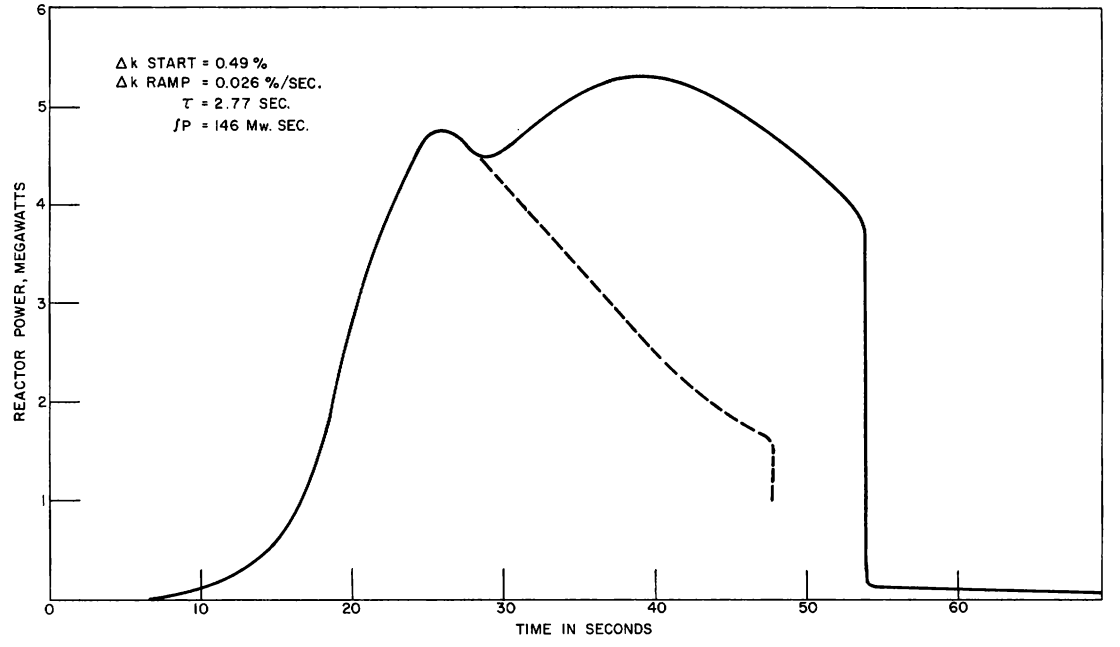

Fig. 38. Typical Flat-top Transient, Reactor Power vs Time

IV. Control Rod Modification (H. Lawroski)

The poison sections of the TREAT reactor control rods were modified by mixing epoxy resin with graded boron carbide to prevent movement of the poison in the control rods during operation of the reactor. Previously, some erratic reactivity additions were obtained for transients based on control rod positioning. These deviations could be explained by movement of the boron carbide in the poison sections.

New poison sections were examined by X-raying the internals of the rods. Figure 39 is a positive copy of the X rays of the rods as received from Argonne, Illinois. These rods had not been in the reactor previously and had not received any shocks other than in normal shipping. The rods had been filled by vibrating the tubes while adding the boron carbide. The rods shown in Fig. 39 were in a vertical position. Rod C appeared to be well compacted, whereas Rods A, B, and D showed slight void spaces at the top.

The rods were jarred vertically, similar to the motion of the rods in use in the reactor, but less vigorously. Figure 40 shows the rods after this treatment. This jarring further compacted the boron carbide to increase the void spaces. Rod C showed only a slight effect, but Rod A appeared to have a void space of approximately $\frac{3}{8}$ in. It was expected that further shocking of the rods would increase the voids.

The rods were inverted, jarred once, and X-rayed again. The results are shown in Fig. 41. The powder moved back into the voids.

A qualitative experiment to observe the movement of the compact powder was made using a 500-cc glass graduate, whose inner diameter was approximately the same as that of the rods. The powder, after compaction by vibrating, moved in slugs when the graduate was inverted. This indicated that there could be separation of the B_4C in the rods and that the void space might vary (depending upon the friction) to maintain the position of the compaction in the rod. Also, in the case of the rods in the reactor, by stopping and starting the rod drives the poison could move during reactor operations.

Two fillers were tested to fix the B_4C powder in the rods: Bakelite 2600, which was a thermosetting resin; and epoxy resin ERL 2774 with hardener ZZL 0816. Both plastics were obtained from the Union Carbide Plastics Company. Bakelite 2600 is a phenolic resin and is set by heating to 300°F for approximately 60 minutes. The epoxy resin ERL 2774 when mixed with its hardener ZZL 0816 starts to harden in approximately 30 minutes at 77°F. The short workable period of the epoxy resin requires rapid handling of any mixtures once the hardener has been added. Both plastics have good shock properties and, when mixed with solids, the epoxy (75 vol % solid) has a base shrinkage of less than 0.1%. No data were available on the radiation resistance of these two resins.

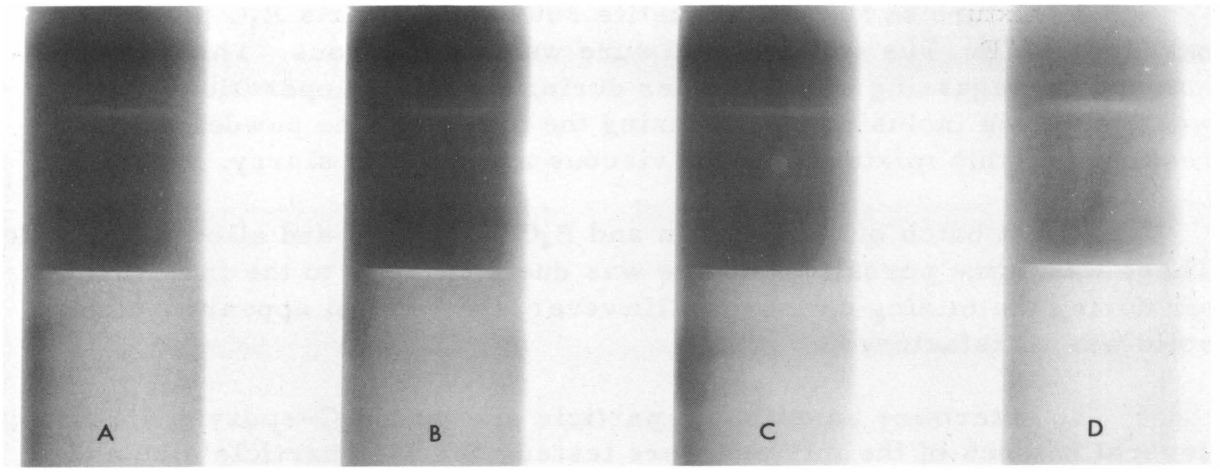

Fig. 39. X-ray Photograph of TREAT Control Rods

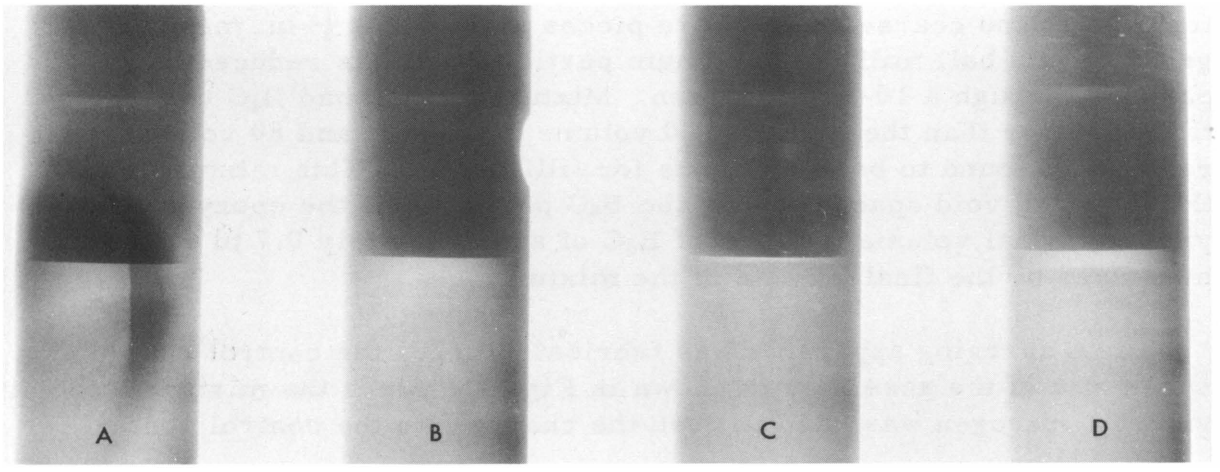

Fig. 40. X-ray Photograph of TREAT Control Rods after Vertical Jarring

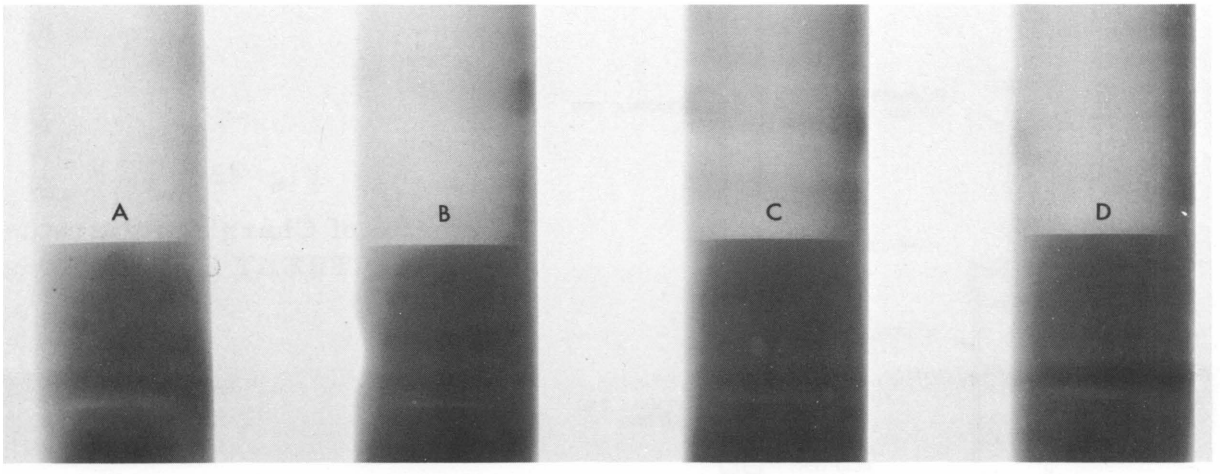

Fig. 41. X-ray Photograph of TREAT Control Rods after Inversion and Jarring

A mixture of 50 parts Bakelite 2600 and 50 parts B_4C powder was baked at 300°F. The solidified mixture was quite porous. This was probably due to degassing of the powder during the baking operation. There was also some inclusion of air during the mixing of the powder with the resin, since this mixture is very viscous and a dense slurry.

A test batch of epoxy resin and B_4C was made and allowed to harden. There was some porosity, but this was due primarily to the inclusion of air during the mixing operation. However, the general appearance of the solid was satisfactory.

To determine an optimum particle size and B_4C-epoxy resin ratio, several batches of the mixture were tested. Smaller particle size and lower B_4C-epoxy resin ratio yielded more fluid, easier-working slurries. However, higher concentrations of B_4C are desirable to maintain the reactivity worth of the rod. The B_4C powder as removed from the rod was found to be too coarse (there were pieces as large as $\frac{1}{4}$-in. mesh). By grinding in a ball mill the maximum particle size was reduced to allow passage through a 10-mesh screen. Mixtures which had B_4C concentrations greater than the ratio of 100 volume parts B_4C and 80 volume parts resin were found to be too viscous for filling rods. This mixture, due to the filling of void spaces among the B_4C particles by the epoxy resin, yielded a final volume fraction of B_4C of approximately 0.7 to 0.75 as measured by the final volume of the mixture.

A charging apparatus was fabricated to fill the control rods. A schematic of the assembly is shown in Fig. 42. Since the mixture was quite viscous, nitrogen was used to push the charge into the control rod.

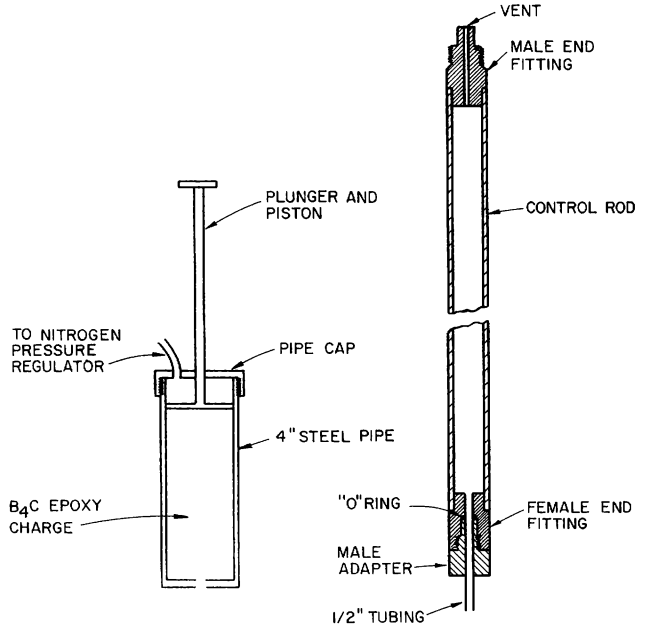

Fig. 42

Schematic of Charging Apparatus for Filling TREAT Control Rods

Each control rod had a void volume of approximately 100 in.^{3} Prior to adding the hardener to the mixture, 85 in.^{3} of B_4C was blended with 55 in.^{3} of ERL 2774 until a consistent slurry was obtained. The pipe cap was removed from the charging pipe and the apparatus was set up in a vertical position, as shown in Fig. 39. The hardener ZZL 0816 (11 in.^{3}) was added to slurry and mixed well.

The mixture was charged to the 4-in. steel pipe and the pipe cap was replaced. A nitrogen line from a pressure reducer was connected to a fitting in the pipe cap. The plunger and piston were then pushed down till the piston rested on the top of the charge. Approximately 50 psi of nitrogen pressure was applied to force the B_4C-epoxy mixture through the $\frac{1}{2}$-in. tubing and into the control rod. An O-ring was used to prevent leakage from the male adapter. The piston was kept in contact with the top of the charge to prevent the gas from pushing a hole in the slurry. As the rod filled with the mixture, the air was vented through a $\frac{1}{8}$-in. hole in the male fitting at the top of the rod. When the slurry started to come out the vent hole a small screw was inserted to prevent further escape. The nitrogen pressure was then increased to 250 psi to reduce the size of any entrained air bubbles. After pressuring for approximately 5 min, the $\frac{1}{2}$-in. tubing was pinched to close off the rod. The operation from pouring the charge into the pipe to the closing off of the tubing required about 15 to 20 min.

The rod was allowed to sit until the epoxy hardened completely. The male adapter was then removed and the charging orifice was tapped for insertion of a steel plug. X rays verified complete filling of the rods.

At first, two control rods were filled and tried in the reactor. The reactivity worth was essentially the same as the original rods. These rods were scrammed at least 50 times and then X-rayed again to examine them for internal physical changes. None were observed.

The remaining 8 control rods were then filled in a similar manner and placed in operation in the reactor.

V. Radiation Effects on Pressure Transducers (J. F. Boland and F. S. Kirn)

Unbonded, strain gauge-type pressure transducers have been used to indicate capsule pressure in a number of the experiments conducted in TREAT. Pressure transducers made by three leading manufacturers have been used in ranges between 15 and 1000 psi. Examination of the pressure vs time data obtained from a number of transients in the range of 2×10^{15} nvt showed that extraneous pressure signals, which varied between a few and many percent of maximum transducer range, were consistently observed. Therefore, a series of tests were made, in which the pressure transducers were open to atmospheric pressure, to attempt to isolate the cause of the extraneous pressure signals and to reduce or eliminate them if possible.

A schemetic block diagram of the circuit normally used for recording the pressure signals is shown in Fig. 43. This is a standard, direct-current circuit often used for recording the output of strain gauge bridges and therefore will not be discussed. A variation of this circuit was also used. In this case a low-impedance path to ground for common mode signals is provided by connecting a 500-ohm resistor from the power supply leads to ground. This is shown in dotted lines on Fig. 43.

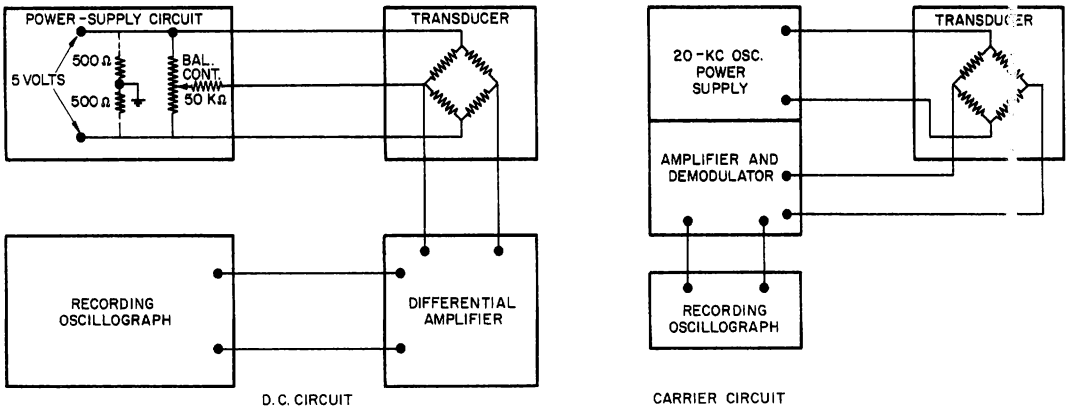

Fig. 43. Diagrams of Circuit and Carrier Circuit for Recording TREAT Pressure Signals

A standard, carrier-type strain gauge bridge instrument system was used in some of these tests, and the schematic block diagram of this circuit is also shown in Fig. 43.

Figure 44 shows the response of a 150-psi transducer obtained with the three measuring circuits described above. Also plotted are the instantaneous and integrated reactor powers, which are proportional to the instantaneous and integrated neutron and gamma fluxes at the transducer. As can be seen from this figure, the extraneous pressure signal is apparently a function of both instantaneous and integrated power when the ungrounded direct-current circuit is used; but the instantaneous power effect is essentially eliminated when either the carrier circuit or balanced-to-ground, direct-current circuit is used. It is postulated that the instantaneous effect is caused by ionization currents set up in the lead wires, or possibly in the transducer itself. S. Harris of Atomics International has reported[1] similar effects when lead wires without transducers were subjected to transients in KEWB. However, he did not report any integrated flux effects, possibly because the integrated flux in KEWB is from one to two orders of magnitude below that obtained in TREAT.

---

[1] S. Harris, Trans. ANS, Vol. 2, No. 2 (Nov., 1959).

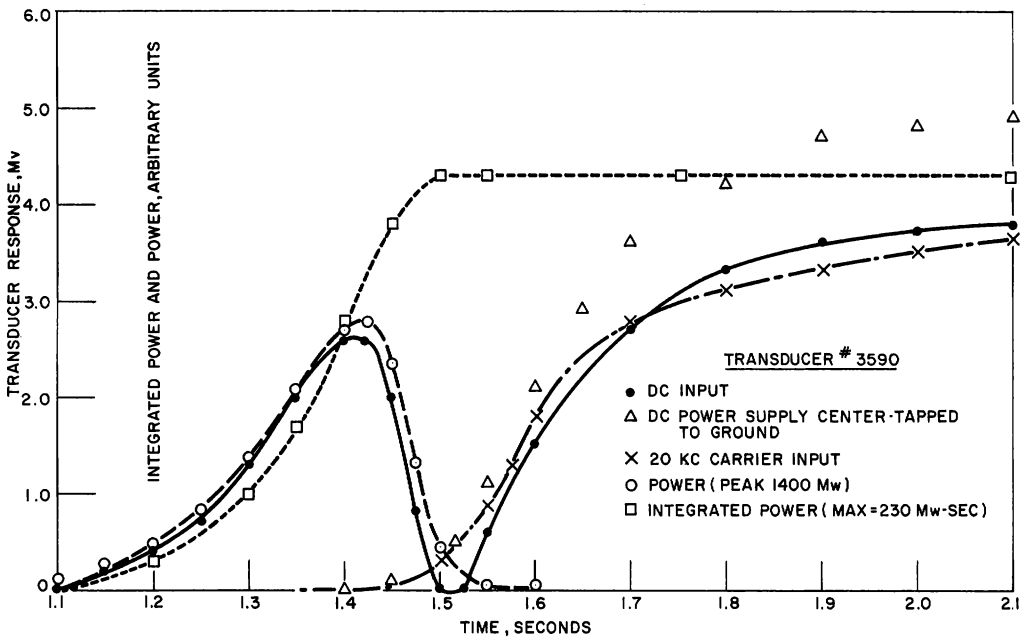

Fig. 44. Time vs Response for Three Measuring Circuits

To investigate further the integrated flux effect, a transducer was subjected to similar transients under normal conditions, when it was first contained in a 20-mil cadmium sheath and then later in a gamma shield consisting of 1 in. of lead surrounded by $\frac{1}{4}$ in. of steel.

Figure 45 shows the response of a transducer under these conditions, along with the instantaneous power and integrated power of the transients.

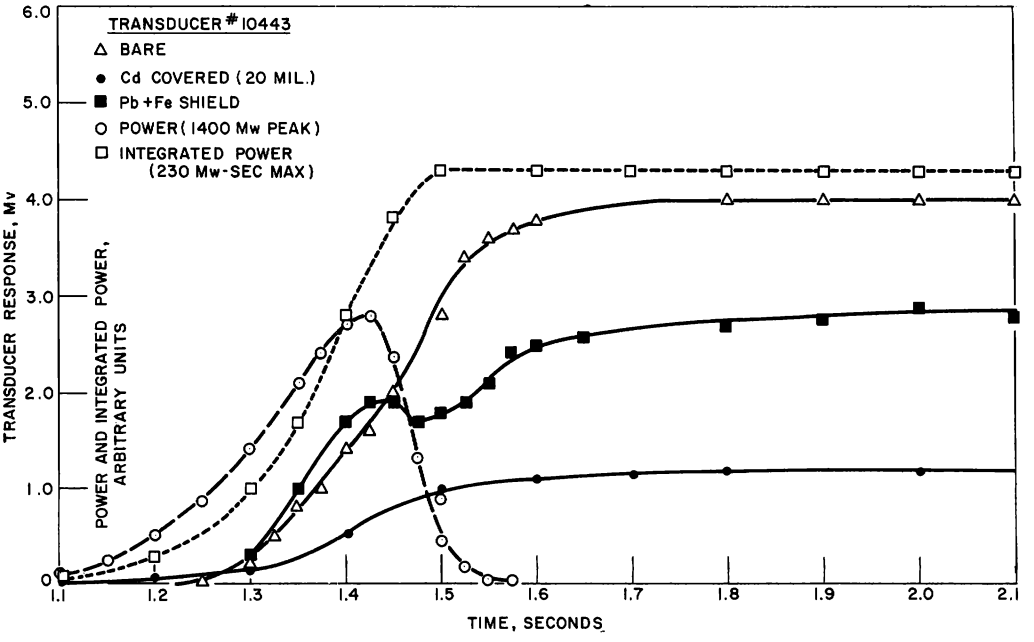

Fig. 45. Transducer Response, Power, and Integrated Power vs Time for TREAT Transients

The 20 mils of cadmium reduced the signal by a factor of three over that from the bare transducer. The gamma shield reduced the signal by about 30%. However, the effectiveness of the gamma shield could be accounted for by the reduction of neutron flux inside the shield as measured by neutron-sensitive foils. Therefore, it appears that the extraneous pressure signal which follows integrated power is primarily caused by neutrons.

In several runs the transducer signals were followed for several minutes after the transient. The transducers recovered in an apparently exponential manner. There also appeared to be a characteristic decay constant for each transducer.

Figure 46 shows typical recoveries of two transducers. Number 16691 displays an e-folding recovery time of about 10 sec, and #3590 a recovery time of 25-30 sec. There is considerable uncertainty in the decay rate because of the relative small deflection on the recorder traces.

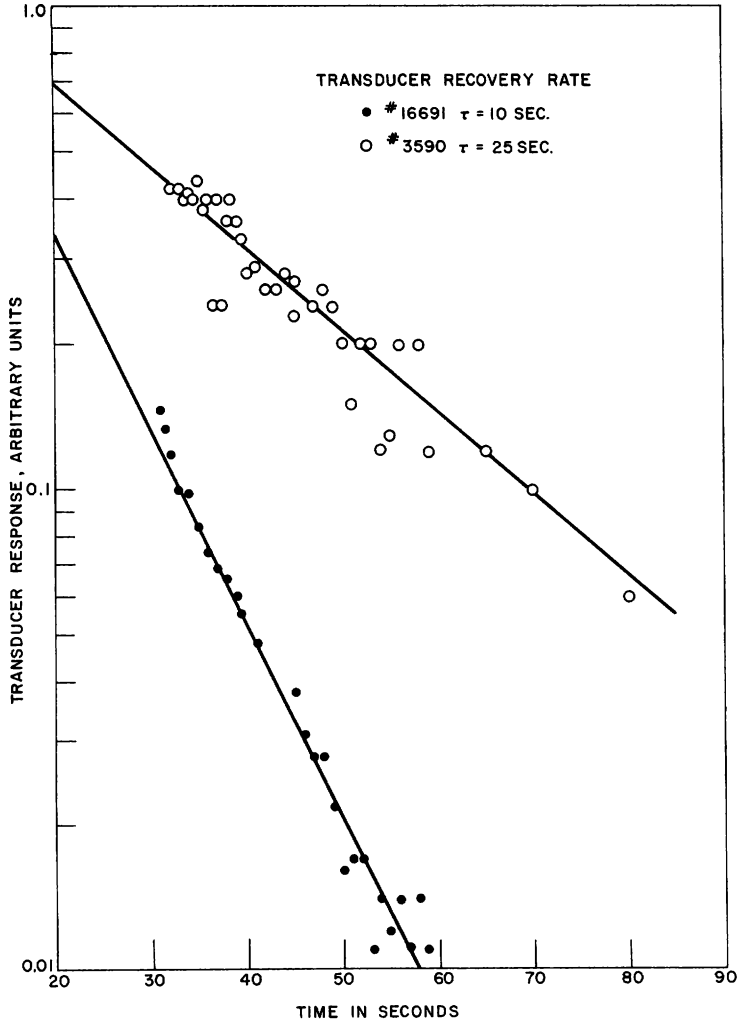

Fig. 46. Transducer Recovery Rate

In summary, the following qualitative results may be stated with regard to radiation sensitivity of the transducers:

1. The extraneous pressure signal which follows the instantaneous power can be essentially eliminated by using carrier-type circuits or by providing a balanced low-impedance path to ground for ionization currents if a direct-current-type circuit is used.

2. The extraneous pressure signal which follows the integrated power is primarily caused by neutrons. No way has been found to eliminate it except to provide adequate neutron shielding, which is very difficult if not impossible for many capsule-type experiments.

3. Differences in manufacturing methods or materials used by three manufacturers do not seem to make any appreciable difference in the neutron sensitivity of the transducers, nor does the pressure range of the transducer consistently affect this sensitivity. However, each transducer does have a characteristic rise and recovery time constant which may change considerably between transducers of the same range and type.

VI. Gamma Flux in TREAT Core (F. S. Kirn)

A series of experiments was undertaken to determine the gamma flux in the TREAT core for a given power level or total dose obtained during a transient. An Argonne-type IC 25B ion chamber with lead plates was the only non-neutron sensitive chamber available which had sufficient dynamic range. It was calibrated in the MTR gamma facility along with two other IC 25B chambers: one containing thorium plates, and the other B^{10}-coated aluminum plates.

The gamma facility consists of spent MTR fuel elements in a non-critical cluster under about 13 feet of water. Vertical instrument tubes, in which counter or samples to be irradiated may be placed, are provided at various distances from the assembly of fuel elements. The facility has established a secondary monitor by intercalibrating an ionization chamber against chemical dosimeters of both the Fe^{++} and Ce^{++++} ion type. Our three chambers were placed in a thimble about 6 in. from the edge of the cluster where, according to the MTR monitor, the flux was 3.86×10^6 r per hour. Table XXVII gives the results obtained for these chambers in terms of ionization current.

Table XXVII

IONIZATION CURRENTS OBTAINED FROM INTERCALIBRATING CHAMBERS

Chamber	Model No.	r/hour	Amperes	(Amp) hr)/r
Pb Plates	IC25-57348	3.86×10^{6}	1.26×10^{-4}	3.2×10^{-11}
Th Plates	IC25-57349	3.86×10^{6}	1.55×10^{-4}	4.0×10^{-11}
B^{10}-Al Plates	IC25- -	3.86×10^{6}	0.49×10^{-4}	1.27×10^{-11}

The noise level of the chambers was on the order of 10^{-11} amp.

The gamma chamber was then put in the center of the TREAT core, during both steady-state and transient conditions, and compared to the reactor power. Table XXVIII shows the results, using the calibration of Table XXVII.

Table XXVIII

CALIBRATION OF GAMMA CHAMBER

Run	Chamber Data	Reactor Data	r/(Mw)(sec)	r/hr/kw
S.S.	1.8×10^{-6} amp	10 kw	1.4×10^{3}	5.4×10^{3}
Transient (Flat top)	6.00×10^{-6} amp-hr	148 mw-sec	1.3×10^{3}	5.1×10^{3}
S.S.	1.74×10^{-7} amp	1 kw	1.4×10^{3}	5.4×10^{3}

The gamma flux as a function of position was also determined in the north face instrument hole. Figure 47 shows the r/(Mw)(sec) as a function of position measured in this hole.

In conjunction with the ionization chamber it was decided to measure the flux using chemical dosimeters. These solution-type dosimeters were supplied by E. Turk and J. Dunbar of MTR.

The dosimeters were the same type as were used in calibrating the monitor in the MTR gamma facility. Solutions of ceric sulphate are used in the range greater than 10^{5} r and ferrous sulphate in the range of 10^{5} r and less. These dosimeters were placed in the same relative position as the gamma chamber. Comparison between the dosimeter and the gamma chamber was not good. Table XXIX illustrates the disagreement.

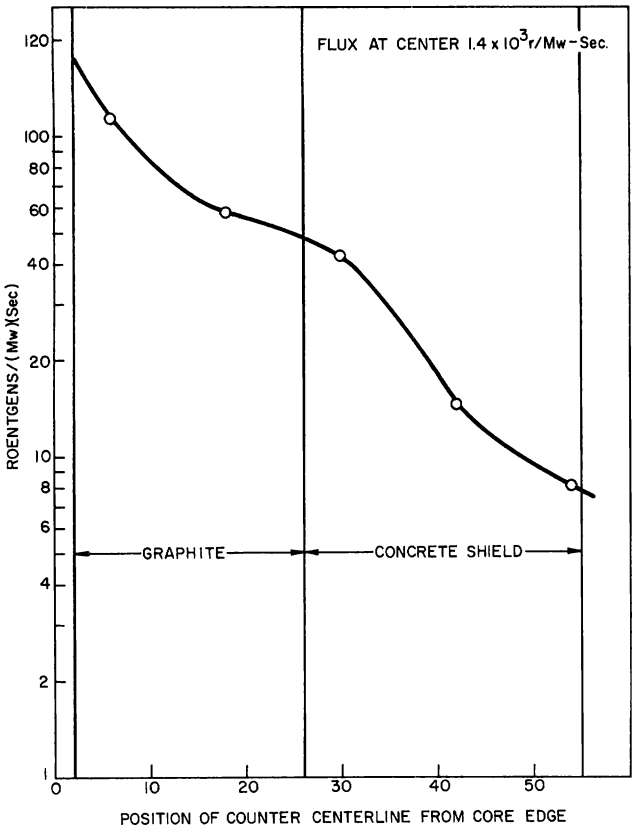

Fig. 47

Gamma Flux vs Position in North Face Instrument Hole of TREAT

It can be seen from Table XXIX that the gamma chamber reads below the iron dosimeter by a factor of 2 and below the cerium dosimeter by a factor of 4-5. Because of this disagreement, a few additional experiments are planned to determine the neutron sensitivity of the detectors, the possible effect of the gamma-energy spectrum on the different detectors, and a cross check of MTR chemical dosimeters with Argonne chemical dosimeters.

Table XXIX

COMPARISON OF DOSIMETER AND GAMMA CHAMBER CALIBRATION

Run	Integrated Power Mw-sec	Chamber		Fe Dosimeter		Ce Dosimeter	
		Dose(r)	r/(Mw)(sec)	Dose(r)	r/(Mw)(sec)	Dose(r)	r/(Mw)(sec)
Transient	100 Mw-sec					5×10^5	5×10^3
S.S.	(10kw)(3 min)		1.4×10^3				
Flat top	146 Mw-sec	1.95×10^5	1.3×10^3			10^6	7×10^3
S.S.	(100kw)(25 min)	2.1×10^5	1.4×10^3	4.6×10	3.1×10^3		

D. BOILING REACTOR EXPERIMENT V (BORAX V)

(Reviewed by R. E. Rice, Project Engineer)

D. BOILING REACTOR EXPERIMENT V (BORAX V)

I. Introduction (R. E. Rice)

Since this is the first quarterly report on the BORAX V project covering work in progress for some three years, a general review of work to date is presented, as well as a specific report of activities in the period during July-September, 1960.

The primary objectives of the proposed BORAX V program are to test nuclear superheating concepts and to advance the art of boiling water reactor design by performing experiments to improve the understanding of factors limiting the stability of boiling reactors at high power densities.

In 1957 the idea for another boiling reactor in the BORAX series was conceived by personnel of both the Idaho Division and Reactor Engineering Division of Argonne National Laboratory. In August, 1958, the Laboratory made a formal preliminary proposal to the AEC for construction of an extremely flexible boiling reactor experimental facility to be called BORAX V and operated as a modification of and addition to the existing BORAX plant at the National Reactor Testing Station in Idaho. In October, 1958, the preliminary proposal was approved and authorization to proceed with Title I design and cost estimation was given.

Norman Engineering Company, Beverly Hills, California, was selected as architect-engineer to perform the design and specification of the site, buildings, and plant with the exception of the reactor. The architect-engineer, in cooperation with the ANL Idaho Division staff, started work in late February, 1959. The Title I report was submitted in April, 1959; and approved by the AEC in May, 1959. The Title II design proceeded without delay and contract drawings and specifications were completed in September, 1959.

The Idaho Division of ANL has the prime responsibility for the BORAX V project. The BORAX V staff of the Idaho Division did the preliminary design of reactor and plant, and have done, or are doing, the detailed mechanical design and some development of fuel and core structure, reactor physics design and calculations, heat and hydraulics design, reactor control and instrumentation design, reactor vessel design, fuel handling, hazards reports, in-core instrumentation development, etc. In addition, the Reactor Engineering Division has assisted in the conceptual design stage, has run simulated boiling fuel element burnout and superheated steam heat transfer coefficient experiments, and has done development work on and modified the control rod drives. The Metallurgy Division prepared the specifications and will inspect the boiler and superheater fuel elements. Central Shops is continuing fabrication development work on both the boiler and superheater fuel assemblies.

II. Reactor and Plant (R. E. Rice)

1. Design Summary

Some of the plant utilized in the previous BORAX experiments is incorporated in the BORAX V system, but the reactor and its building, as well as the control building, located $\frac{1}{2}$ mile from the reactor, are new. A cutaway view of the BORAX V facility is shown in Fig. 48.

BORAX V is designed as an extremely flexible system. Three separate core configurations are provided: a boiling core with a centrally located superheater, a boiling core with a peripherally located superheater, and a boiling core without superheater. In all cases it is possible to operate with either natural or forced circulation of water through the core. Water serves as the moderator in both the boiler and superheater regions of the core, and as coolant in the boiling region. The superheater is cooled by steam.

The reactor vessel is a cylinder with ellipsoidal heads, $5\frac{1}{2}$ ft ID x 16 ft high internally, made of carbon steel clad internally with stainless steel. The core is centered about 4 ft from the bottom. The top portion of the vessel is used as a steam dome. Control rods are driven from below the vessel.

Each of the three cores is 24 in. high and has an effective diameter of 39 in. when containing the maximum of 60, four-inch-square fuel assemblies arranged in an 8 x 8 array with the corner assemblies missing. The central superheater core will contain 12 fuel assemblies in the central position, while the peripheral superheater core will contain 16 fuel assemblies, 4 in the middle of each outer row. Each square cell of 4 assemblies is surrounded by adjacent control-rod channels. Experiments will be run with the full complement of 60 fuel assemblies as well as with reduced numbers. The BORAX V reactor with a central superheater is shown in Fig. 49.

The coolant flow paths inside the reactor vessel are as follows: Water flows up through the boiling core and the riser above the core by either forced or natural circulation. The steam formed in the core continues up into the steam space while the water flows down through the annular downcomer area between the core and the reactor vessel. Feedwater, introduced at the top of the downcomer, subcools the recirculating water and helps to increase the rate of natural circulation. For the boiling core case, the steam leaves the pressure vessel through a 6-in. steam line. In the superheating cores, the steam from the steam dome enters the inlets to the superheater fuel assemblies, makes one pass down through half the superheater assemblies, mixes in the lower plenums, and makes a second pass up through the remainder of the superheater assemblies.

Fig. 48 BORAX V Facility

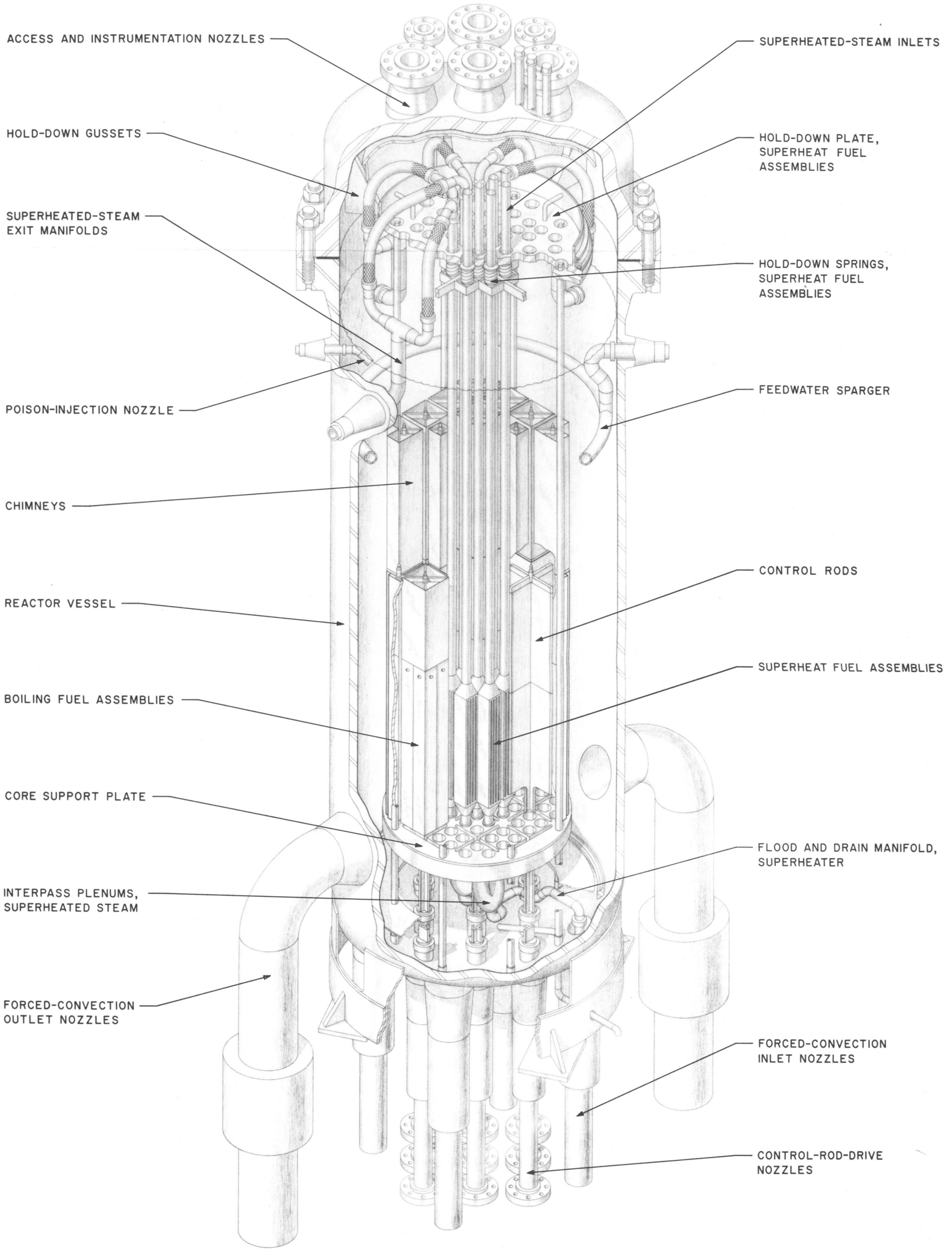

Fig. 49 BORAX V Reactor with Central Superheater

It then leaves the pressure vessel through flexible tubing and the superheated-steam outlet nozzles. Because BORAX V is using the turbine-generator-condenser system of its predecessors, the 600-psig steam must be reduced in pressure and temperature before entering the turbine.

Nine control rods, driven from below, are made of Alcoa X-8001, aluminum-clad Boral. The drive mechanisms are those formerly used on EBWR, modified for use in BORAX V.

A summary of some of the design characteristics of BORAX V is given in Table XXX.

Table XXX

DESIGN CHARACTERISTICS OF BORAX V

Operating pressure	600 psig
Maximum Steam Temp, Superheated	850°F
Maximum Steam Temp, Saturated	489°F
Nominal Design Full Power	20 Mw(th)
Maximum Plant Capacity	40 Mw(th)
Design Maximum Temp of Superheat Fuel Plate	1200°F
Limiting Temp of Boiling Fuel Rod Center	5000°F
Forced-circulation System Flow	10,000 gpm
Average Power Density at 20 Mw	
Boiling Zone	95 kw/l of core
Central Superheat Zone	80 kw/l of core

Further details of the reactor and plant design are given in Preliminary Design and Hazard Report - BORAX V, ANL-6120 (February 1960). Since this report was written the designs of the reactor fuel and a few other minor items have changed but, in general, ANL-6120 is still accurate.

2. Status

ANL personnel are installating reactor controls and instrumentation in the control building. Modifications to the existing turbogenerator plant have been minor. ANL has procured and installed a new steam separator. The cooling water side of the condenser tubes has been chemically cleaned, leak-tested, and inspected. To prepare for accidental or test defects in the superheater fuel elements, the air-ejector exhaust system has been redesigned to include an after cooler and de-mister for moisture removal, an AEC-type filter, an activated charcoal filter for iodine removal, and a stack radioactivity monitor. Also included will be a blower and air-dilution valve to assure that the free hydrogen in the system is kept below explosive limits.

III. Fuel and Core (R. E. Rice, J. D. Cerchione, R. W. Adamson,* and D. H. Drummond**)

The design of the fuel element for both boiler and superheater fuel has been changed since ANL-6120 was written. The diameter of the boiling fuel rod has been enlarged and the number of rods per assembly reduced to facilitate fuel handling and reduce cost. The superheat fuel assembly has been changed by reducing the number of fuel plates per element from 5 to 4.

1. Boiler Fuel

BORAX V has individually removable boiler fuel rods made of uranium oxide pellets clad with a 0.015-in.-thick, Type 304 stainless steel tube, as shown in Fig. 50. The rod OD is $\frac{3}{8}$ in., and there is a maximum radial gap of 2 mils between the pellet and clad. The rod, which is filled with helium at a pressure of 1 atm, has a fission gas expansion space which also contains an Inconel-X spring to allow for the differential expansion between the UO_2 pellets and the cladding tube. Latching pins are located in the tip of the rod, and a compression spring and manipulator fitting are on the head. The nominal enrichment of the UO_2 is 4.95%, although a number of rods with an enrichment of 9.9% will also be available to adjust reactivity and flatten the power distribution.

The individually removable fuel rod feature of the boiler fuel assemblies is shown in Fig. 51. The assembly is made of a square, X-8001 aluminum tube which has a square-to-round transition nozzle welded to its lower end. The 49 fuel rods are held between an upper grid and a lower grid, both made of Type 304 stainless steel. The upper grid is 4 in. long to guide the fuel rod into the proper hole in the lower grid. The fuel rod is latched in position and held in tension between the two grids by means of the pin on the tip and the compression spring on the rod head. This fuel assembly also has a removable orifice plate in the lower nozzle, which will be used in experiments to determine the effect of entrance orificing on reactor stability when natural circulation is employed. The individually removable rod feature permits changing of the water-fuel ratio, varying the fuel enrichment of rods within the fuel assembly, and the replacement of fuel rods with poison rods to adjust reactivity and flatten power distribution.

In April, 1960, a contract for the fabrication of 3000 boiling fuel rods of 4.95% enrichment and 500 of 9.90% enrichment was awarded to the Westinghouse Corp. Delivery is scheduled for November, 1960-January, 1961. Fabrication development and detailed design of the boiler

---

*On loan from California Polytechnic Institute, San Luis Obispo, Cal.

**On loan from Montana State College, Bozeman, Mont.

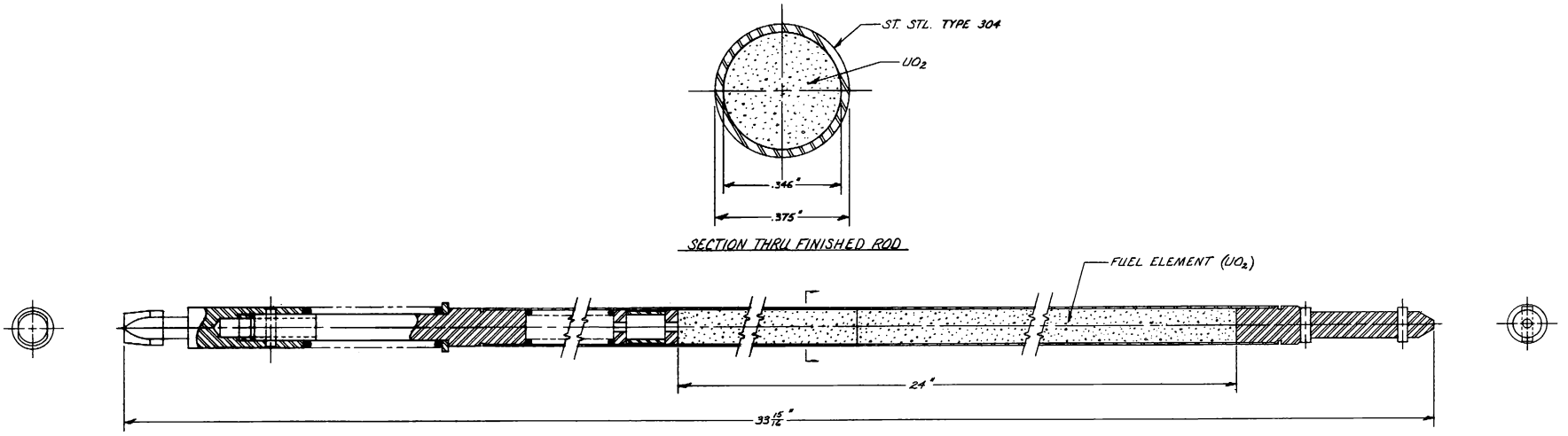

Fig. 50 Boiler Fuel Rod

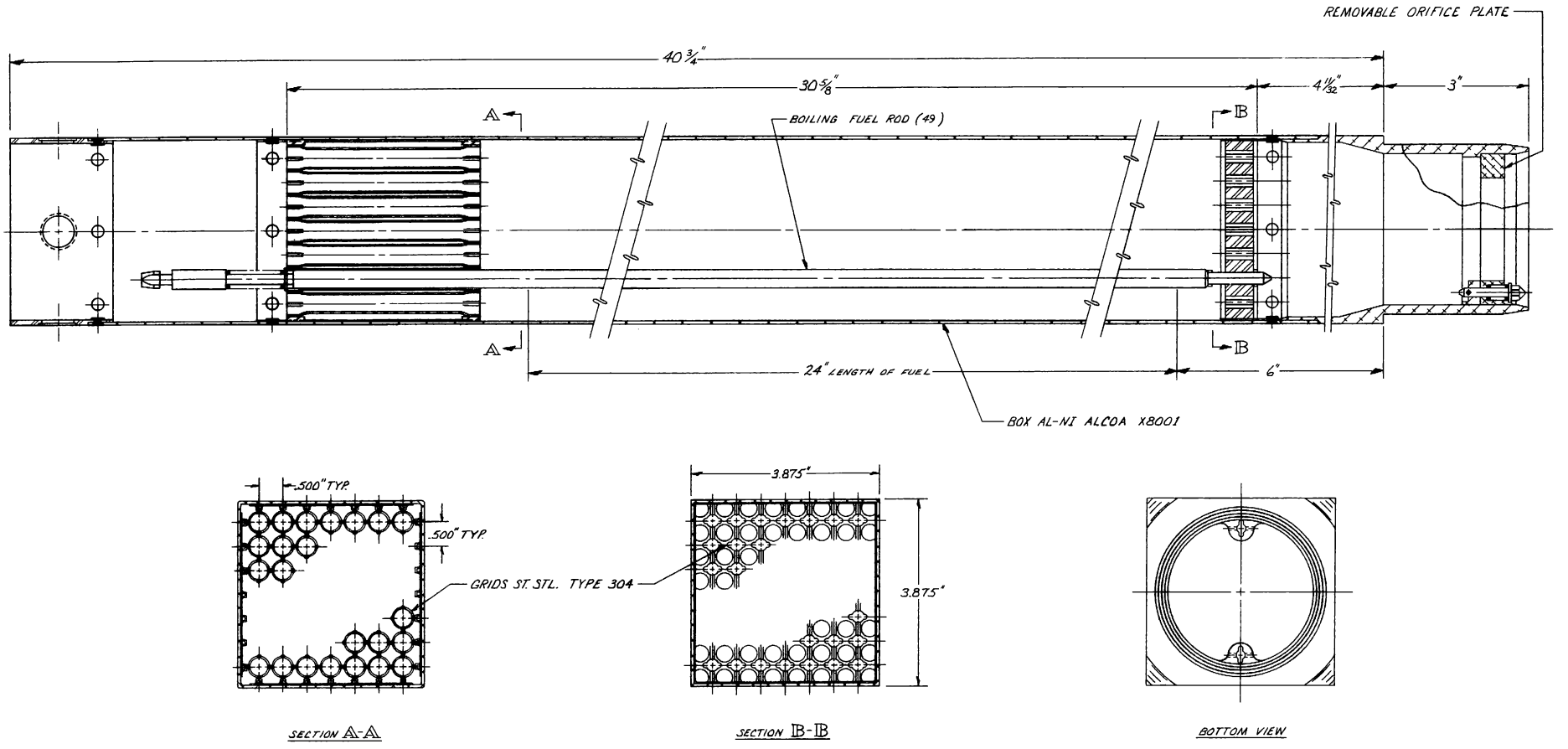

Fig. 51 Boiler Fuel Assembly

fuel assembly boxes was completed and material procurement is now under way in Central Shops. Seventy-five assemblies have been ordered.

2. Superheater Fuel

The superheater fuel assembly (see Fig. 52) is made of four fuel plates held in place by side plates and $\frac{1}{8}$-in.-diameter stainless steel spacer discs between the plates. The fuel plate has a core matrix of lightly enriched UO_2-stainless steel and is clad with Type 304 ELC stainless steel. Because they are cooled on one side only, the two outside fuel plates in each element have only about half the fuel loading of the inside plates. Each 4-plate element is contained in a rectangular, stainless steel tube which forms a static steam-insulating annulus between the outer fuel plates and the tube. Five fuel elements are welded into an assembly which has a long, double-walled downcomer, or riser tube, at the top and a short, double-walled nozzle at the bottom. The lower nozzle has a flange against which is seated a hollow-metal "O" ring seal, and on the upper tube is mounted a hold-down spring. The water moderator circulates between the fuel elements. One of the principal design features of this thin, flat-plate element is its excellent radiation and conduction shutdown cooling properties to the surrounding moderator.

Bids for the fabrication of 840 enriched superheat fuel plates were opened June 1, 1960. In late August, negotiations with the low bidder were concluded when the bidder refused to accept the terms of the proposed contract. Negotiations with the second low bidder were begun, but by the end of this report period a contract had not yet been signed.

Fabrication development work on the superheat fuel assemblies is proceeding at Central Shops and Metallurgy Division. Fabrication of the 4-plate element by both Nicrobraze and electron beam welding techniques has been tried. At present, the most promising assembly method is a furnace braze using GE 81 alloy with the element in a Hastelloy C brazing fixture sealed in a vacuum can. A mockup of a complete instrumented superheat fuel assembly is being made to develop fabrication methods and for later use in pressure-drop and vibration tests using air to simulate superheated steam.

3. Core Structure

A thorough stress analysis and design study was made on the superheater flood and drain manifolds and plenum chambers for both the central and peripherally located superheaters. The reference design manifold has sufficient flexibility without expansion joints to keep stresses well below allowable limits. Stress analyses of the geometrically complex core-support plates have been made both by modified tube sheet theory and grid beam theory. The struts, ring flanges, and hold-down plates for all three core structures have also been analyzed.

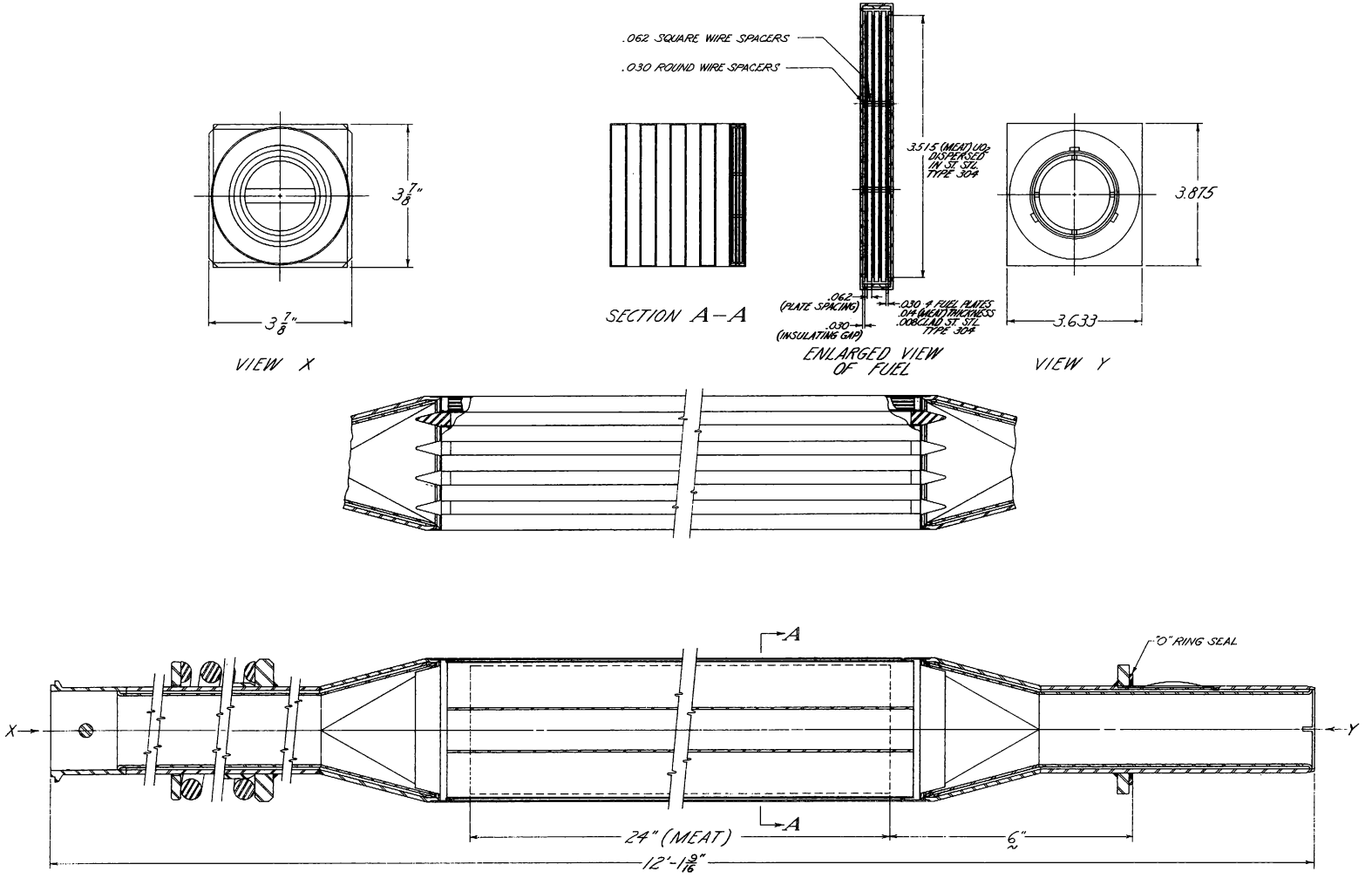

Fig. 52 Superheater Fuel Assembly for BORAX V

To facilitate easy reloading of complete core structures, no bolts are used to hold the core structures in place within the reactor vessel. Instead, the core structure is supported by eight tubular legs which slip over tapered guide dowels to rest on pads in the bottom of the reactor vessel. The core structures are centered at the top and held down by 6 gussets inside the top head of the vessel. Thus, when the top head is removed, the core structure is free to be lifted out by means of the remotely operated building crane.

To allow for the differential expansion between the core structure and reactor vessel a large Belleville spring is located between the gussets and core structure top-ring-flange. A schematic drawing of this arrangement is shown in Fig. 53. The deflections which have been considered in the design of the Belleville spring are:

1. the elongation of the reactor vessel due to the internal pressure of 600 psi;
2. the elongation of the carbon steel vessel due to the increase in temperature from 70°F to 500°F;
3. the shortening of the core structure due to the Belleville spring compressive load; and
4. the elongation of the stainless steel core structure due to the change in temperature from 70°F to 500°F.

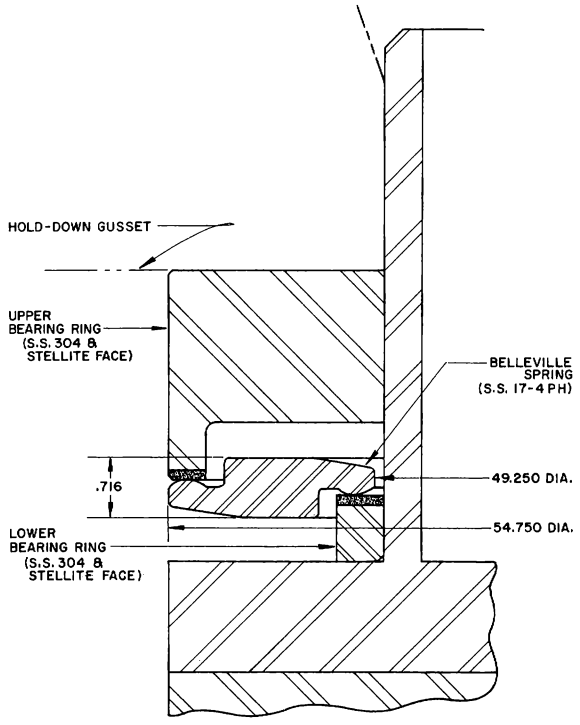

Fig. 53

Belleville Spring

For all three core structures, when natural circulation is being used, a spring force of 20,000 pounds has been selected to hold the structures firmly in place. For forced-circulation conditions, because of the hydraulic lifting force on the core structure and because of the gasket load required to seat the hollow metal "O" ring seal between the forced convection baffle and the core support plate, a Belleville spring load of 50,000 pounds is required. Springs for both conditions have been designed to exert the required force after heating and pressurization of the core structure and reactor vessel.

A summary of the design formula used in the Belleville spring calculations follows:

$$\beta = M_t \, r_0^2 / E I_x \tag{1}$$

$$\delta = 2 \, [\overline{OA} \, \sin(\beta + d) - \overline{AB}] \tag{2}$$

$$M_t = \frac{P}{\pi r_0} [\overline{OA} \cos (d + \beta) - \mu A] \tag{3}$$

$$d = \tan^{-1} (\overline{AB}/\overline{OB}) \tag{4}$$

$$I_x = I_x^1 \cos^2 \beta + I_y^1 \sin^2 \beta + I_{xx} \sin 2\beta \tag{5}$$

$$\sigma_t = M_t r_0 \, (y/I_x) \quad , \tag{6}$$

where:

β = angle of rotation of spring cross section

M_t = moment applied per unit of circumferential length of neutral axis of section

r_0 = radius of neutral axis

δ = deflection of load application points

P = total spring load

μ = coefficient of friction

A = absolute value of $[\overline{OA} \sin (B + \phi) - r_1]$

I_x^1 and I_y^1 = moment of inertia of the spring cross section about its own axis of symmetry

I_x = moment of inertia of the spring cross section about spring diameter through the neutral axis.

σ_t = hoop stress

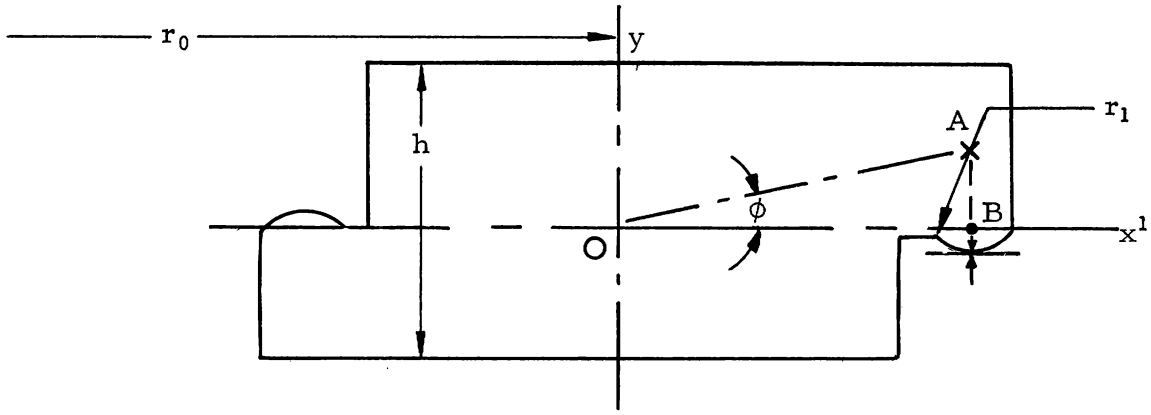

Detailed designs of all three core structures, hold-down boxes, chimneys, and superheater drain and flood manifolds have been completed. Material procurement for these items is proceeding in Central Shops.

IV. Heat and Hydraulics Engineering (R. A. Cushman)

1. Introduction

The work on heat and hydraulics performed through the end of 1959 is presented in ANL-6120, Preliminary Design and Hazards Report - BORAX V. Calculational techniques and design philosophy are presented in that report. This summary covers changes in the design of BORAX V since that time, as well as the additional work performed.

Two basic changes have been made in the core for BORAX V. The boiling fuel assembly now consists of 49 rods, each 0.375 in. in diameter, rather than of 100 rods, each 0.260 in. in diameter. The superheater fuel assembly remains similar in concept, but each of the 5 elements per assembly now contains four fuel plates rather than five, and each has three 0.062-in.-thick coolant channels rather than 4 coolant channels of 0.045-in. thickness. These basic changes will be discussed more fully later in this section.

2. Experimental Work

a. Boiling Burnout Tests

Results of natural circulation boiling burnout tests using parallel tubes with 0.332-in. ID to simulate flow outside of the fuel rods in the formerly planned 100-rod boiling assembly were reported in ANL-6120. Since that time R. P. Anderson and E. A. Spleha of Reactor Engineering Division have run additional natural-circulation boiling burnout tests with parallel tubes to simulate the performance of the 49-rod assembly. Using two parallel tubes, each 24 in. long and of 0.562-in. ID

(corresponding to the equivalent diameter of the fuel rods away from the side walls of a boiling fuel assembly when the rods are uniformly spaced within the assembly), heat fluxes up to 514,000 Btu/(hr)(ft^2) were obtained without the occurrence of burnout. This heat flux was the maximum obtainable from the power supply on the test loop. A further test was made on the same tubes after slightly flattening the middle 18 in. to produce an equivalent diameter in this region of 0.474 in. (the equivalent diameter of the rod in a boiling fuel assembly when a square pitch of 0.500 in. was used to make the equivalent diameter of the edge, corner and interior rods equal). Once again a heat flux of 514,000 Btu/(hr)(ft^2) was obtained without the occurrence of burnout.

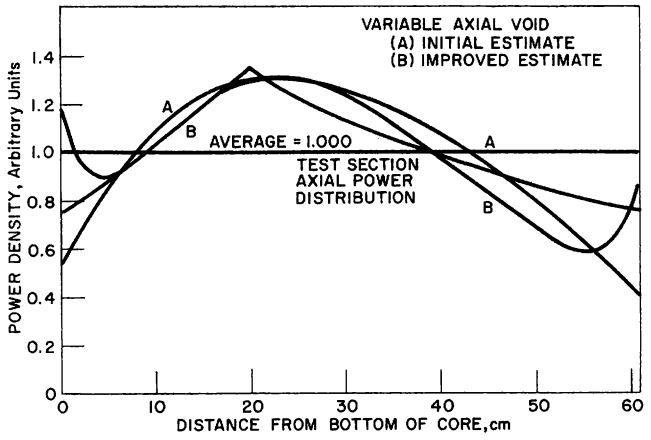

Fig. 54 Axial Power Density of the Boiling Core of BORAX V

In order to overcome the limitation on the power supply, a different test loop and test section were used for the next test. The earlier test section had a uniform wall thickness over the heated length and therefore produced a uniform heat flux. For this final test, in an effort to produce an axial power distribution similar to that of the reactor (see Fig. 54), the two parallel tubes had variable wall thicknesses as a function of length. The minimum wall thickness occurred 8 in. from the inlet end of the section, and the thickness increased uniformly from that point to each end. There was consequently an axial variation in heat flux, with a peak-to-average heat flux of 1.35. The results of the test are given in Table XXXI. Instability was first observed during Run #11, and the amplitude of the oscillations increased with increasing power levels on successive runs until burnout occurred during Run #14, with a peak heat flux of 1.09 x 10^6 Btu/(hr)(ft^2) and an average of 8.05 x 10^5 Btu/(hr)(ft^2).

Table XXXI

RESULTS OF BOILING BURNOUT TEST

Run No.	Power (kw)	Average Power Density (kw/l)	Maximum Power Density (kw/l)	Average Heat Flux x 10^{-3} [Btu/(hr)(ft^2)]	Maximum Heat Flux x 10^{-3} [Btu/(hr)(ft^2)]	Makeup Water Flow Rate (lb/sec)	Steam Flow Rate (lb/sec)	Inlet Sub-cooling (^{o}F)	Exit Quality (%)	Total Flow Rate (lb/sec)	Inlet Water Velocity (ft/sec)	Makeup Water Temp (^{o}F)
1	30.4	226	306	212	287	-	0.0086	24	1.4	0.620	5.28	100
2	30.4	226	306	212	287	-	0.0086	17	1.4	0.6139	5.23	100
3	40.56	301	408	282	382	0.0193	0.0171	20	2.8	0.6203	5.28	100
4	50.02	371	503	350	447	0.0259	0.0250	20	4.0	0.6276	5.34	100
5	60.8	451	611	425	576	0.0328	0.0333	37	5.3	0.6230	5.31	100
6	72.1	536	726	505	684	0.0453	0.0597	33	10.3	0.5804	4.94	400
7	79.9	594	805	556	753	0.0489	0.0660	38	12.2	0.5417	4.62	370
8	90.1	669	906	630	854	0.0774	0.0772	49	14.9	0.5164	4.40	370
9	90.1	669	906	630	854	0.0796	0.0771	42.8	14.9	0.517	4.40	370
10	94.8	704	954	663	898	0.0850	0.0855	44.9	17.5	0.488	4.16	397
11	100.0	744	1008	697	944	0.0987	0.0921	46.7	20.2	0.455	3.87	404
12	105.8	786	1065	736	997	0.1111	0.0978	47.1	20.1	0.487	4.15	396
13	110.5	820	1111	772	1046	0.1169	0.1018	48.9	21.6	0.471	4.01	386
14	115.1	855	1161	805	1090	BURNOUT						

b. Superheated Steam Heat Transfer Experiments

Work was completed, and a report [J. B. Heineman, An Experimental Investigation of Heat Transfer to Superheated Steam in Round and Rectangular Channels, ANL-6213,(Sept. 1960)] issued on the subject of convective heat transfer coefficients for superheated steam. The following is quoted from the report:

SUMMARY AND CONCLUSIONS

"Forced convection heat transfer to superheated steam in turbulent flow was experimentally investigated, utilizing two channel geometries: a round tube, 0.333 in. ID x 12.00 in., and a thin rectangular channel, 0.047 in. wide, aspect ratio, 26.6:1, and 12.00 in. in length. The experiments encompassed a Reynolds number range from 20,000 to 370,000, pressure range from 300 to 1500 psia, inlet superheat from 5 to 160 F°, and film temperature differences from 30 to 550 F°.

"Concerning the round channel experiments, the following conclusions may be drawn:

1. Convection coefficients may be predicted within ±10 per cent, using the following equations and the properties found in Tables 1 and 2:

$$\frac{hD_e}{k_f} = 0.0157 \left(\frac{GD_e}{\mu_f}\right)^{0.84} \left(\frac{c_p\mu}{k}\right)_f^{1/3} \left(\frac{L}{D_e}\right)^{-0.04}$$

for $(6 < L/D_e < 60)$

and

$$\frac{hD_e}{k_f} = 0.0133 \left(\frac{GD_e}{\mu_f}\right)^{0.84} \left(\frac{c_p\mu}{k}\right)_f^{1/3}$$

for $(L/D_e > 60)$.

2. Particular attention should be paid to the type of unheated entrance section preceding the heated length of channel. The first of the above equations is applicable when this precedent section is 16 diameters in length. It may be safely used (with respect to limiting surface temperatures) for shorter unheated sections and should closely apply for a more fully developed velocity profile (unheated $L/D_e > 16$), because of the relatively weak influence of L/D_e.

3. Making allowances for the unheated entrance section, the data substantiates the experiments of McAdams, Kenne., and Addoms[4] within ±5 percent even to a Reynolds number of 370,000.

4. The Dittus-Boelter equation,

$$\frac{hD_e}{k_f} = 0.023 \left(\frac{GD_e}{\mu_f}\right)^{0.80} \left(\frac{c_p\mu}{k}\right)_f^{1/3} ,$$

when compared to the present study, yields values of the coefficient which are 11.5 percent, high in the lower Reynolds range (35,000) and 1.8 percent high in the upper range (370,000). It is conjectured that this is due, in part, to the unsettled question of correct steam conductivity values.

"Concerning the thin rectangular channel experiments, the following observations are made:

1. The vena contracta caused by the sharp-edged entrance condition influences the heat transfer coefficient to a length of approximately 75 equivalent diameters, including the unheated entrance length of 13 diameters.

2. There is no observable difference between the rectangular data and the round channel correlation in the L/D_e range from 60 to 121. Even if it is postulated that the flow is not fully established in this region, there is no evidence that any serious decrease in coefficient will occur beyond this range, even according to the data of Levy, Fuller, and Niemi,[16] whose data run to an L/D_e of approximately 180."

3. Thermal Distortion of Superheater Fuel Element

The effects of temperature gradients in the superheater fuel element are being investigated. A simulated superheater fuel element with stainless steel rather than stainless steel plus UO_2 fuel plates was heated to 550°F, and then one side of the element was dipped into liquid nitrogen at -320°F. No measurable distortion resulted.

Apparatus has been constructed for additional tests of thermal distortion. A two-plate simulated fuel element can be radiantly heated on the outer surfaces of the two plates while air is forced through the enclosed coolant channel. Thermocouples are attached to the outer surfaces of the plates. It is possible to measure the variation of the overall thickness (two plates plus coolant channel) of the assembly while heating is in process and thus determine the distortion, if any. Preliminary results indicate no serious distortions.

4. Flow Through a Boiling Fuel Assembly

The air-water flow test loop which was built for check out of in-core instrumentation was used to determine the accuracy of the core pressure-drop calculational techniques. For the flow of water at the loop temperature, fairly good agreement between calculated and experimental pressure drops was obtained, with the difference represented by a constant factor. Good agreement was also obtained on the value of the flow of water which would lift the boiling fuel assembly (see Table XXXII).

Table XXXII

TEST FLOW THROUGH A BOILING FUEL ASSEMBLY

Flow, gpm	Pressure Drop, psi		Weight, in Addition to Fuel Assembly, Required to Resist Lifting, lb	
	Calculated	Measured	Calculated	Measured
100	0.38	0.46		
200	1.5	1.8		
300	3.4	4.1		
400	6.1	7.2		
500	9.4	10.6		
390	5.8	6.8	12	10
465	8.2	9.0	31	26
7500	-	12.0	57	49
7500	-	13.2	68	62
7500	-	14.0	75	78

Preliminary tests have been made to determine the effect on the fuel assembly performance of the pressure drop caused by flowmeters in the boiling fuel assembly. Early results indicate that the orificing action will not seriously affect the capability of the assembly to deliver its power in the reactor.

5. Analytical Work

a. Boiling Core

The change in the boiling fuel assembly, from one-hundred, 0.260-in. diameter rods to forty-nine, 0.375-in. diameter rods, which was dictated by fuel-handling and fuel-fabrication considerations, resulted in revisions in the heat transfer and hydraulic analysis of the boiling core. The flow area per assembly was unchanged, but the heat transfer surface was reduced. The resultant increase in equivalent diameter increased the burnout heat flux so that the total power production was unchanged. The two rods with different diameters are compared in Table XXXIII. The most recent boiling burnout test results indicate that the maximum allowable heat flux can safely be set at 600,000 Btu/(hr)(ft^2) (corresponding to a calculated fuel rod center temperature of 5000°F).

Table XXXIII

COMPARISON OF BOILING FUEL RODS WITH DIFFERENT DIAMETERS

Rod OD (in.)	No. of Rods Per Assembly	Total Rod Cross-sect Area (in.^{2})	Flow Area (in.^{2})	Heating Surface (ft^2)	Friction D_e (in.)	q" Burnout [Btu/(hr)(ft^2)]	q" Design Maximum [Btu/(hr)(ft^2)]	Max. Temp (°F)
0.260	100	5.31	8.64	13.65	0.364	390,000 (based on D_e = 0.332 in.)	300,000	2,000
0.375	49	5.41	8.59	9.60	0.474	1,090,000	600,000	5,000

Problems have been submitted for IBM 704 machine calculation using the RECHOP code to determine the operational characteristics of the boiling fuel assemblies under widely varied conditions of inlet subcooling, power level, and pressure drop due to orificing the flow. These calculations are based on the present upper and lower boiling assembly fuel support grids and should not change markedly from earlier calculations.

The spacing of the rods within the boiling fuel assembly has been established. If the rods are spaced uniformly, i.e., if each rod has associated with it $\frac{1}{49}$ of the flow area within the assembly, the edge and corner rods have lower equivalent diameters than the interior rods due to the presence of the wall of the fuel assembly box. Figure 55 shows the variation of the equivalent diameter of the edge, corner, and central rods as a function of rod spacing.

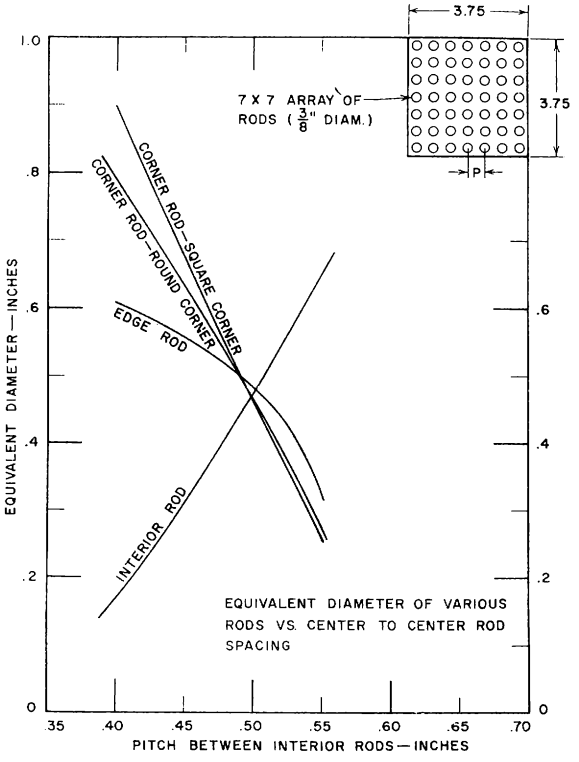

Fig. 55

Equivalent Diameter of Various Rods vs Center to Center Rod Spacing

A $\frac{1}{2}$-in. rod-spacing was selected for BORAX V with a resultant 0.47-in. equivalent diameter for rods in all three locations. This spacing tends to bunch the rods within the box and leaves an additional water gap around the outside of the 7 x 7 array. The additional water gap causes an increase in the peak-to-average flux within a fuel assembly, as shown in Fig. 56. The peak-to-average flux in the assembly goes from 1.17 with uniform spacing to 1.26 with the $\frac{1}{2}$-in. pitch, but the combined effect of the improved burnout heat flux and more severe flux peaking allows an increase in the maximum reactor power.

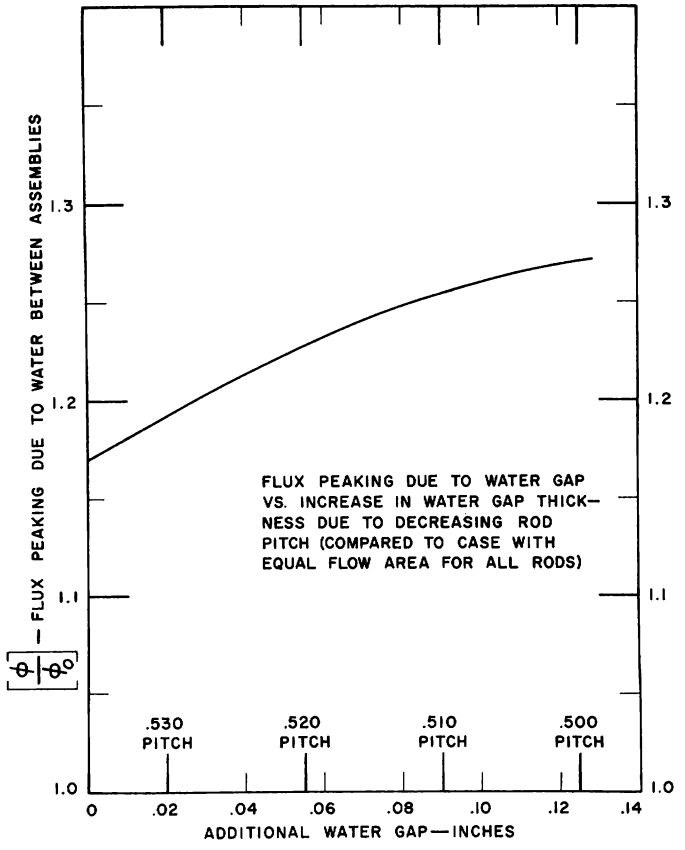

Fig. 56

Water Gap Flux Peaking vs Rod Pitch

b. Superheating Region

The design of the superheater fuel assembly has been changed from that presented in ANL-6120, as has been mentioned earlier. The chief reason for revising the design was the fact that the calculated maximum surface temperature with the five-plate element was only 1100°F, rather than the 1200°F design limit. This indicated that the design was overconservative and failed to take maximum advantage of the properties of the fuel element materials.

Because of the characteristics of a gas-cooled reactor, which cause much of the approach to the maximum permissible temperature to be taken up by the temperature rise of the coolant, it is possible

to decrease the amount of heat transfer surface without as great a corresponding increase in the fuel element surface temperature. In the present case, a reduction of 25 percent in the heat surface accompanied by an increase in the channel thickness from 0.045 to 0.062 in. (which results in a reduced heat transfer film coefficient) caused only a 100°F rise in the maximum surface temperature. This, together with a reappraisal of hot channel factors, resulted in a maximum surface temperature of 1160°F with the four-plate element. An additional beneficial result was a decrease in pressure drop from 40 to 26 psi through the two passes of the superheater. Also, the number of fuel plates to be fabricated was decreased 20 percent, from 5 to 4 plates per element, with a consequent reduction in fabrication costs. The neutron economy has been improved since there has been a reduction in the amount of stainless steel and a slight increase in the moderator associated with each element. The ability to dissipate the shutdown heat by radiation cooling has been increased since there is one less radiating surface to be considered. The differences between the two elements are summarized in Table XXXIV, which applies to the central superheater when the reactor is operating at 40 Mw.

Table XXXIV

COMPARISON OF 4- AND 5-PLATE SUPERHEAT FUEL ELEMENTS

	5-plate Element	4-plate Element
Maximum Surface Temperature (°F)	1100	1160
Pressure Drop through 2-pass Core (psi)	40.5	26
Thickness of Water between Elements (in.)	0.335	0.367
Approximate Stainless Steel in Elemental Cell (v/o)	28.1	24.4
Average Heat Flux [Btu/(hr)(ft^2)]	75,700	101,500

Figure 57 presents the steam temperature and fuel element surface temperature as a function of axial position for the hottest and average channel in the central superheater when the reactor is operating at 40 Mw. A machine program for the IBM 704 has recently been prepared and is currently being checked out on the machine to calculate individual fuel plate and coolant channel temperatures as a function of axial position for any power level and combination of hot channel enthalpy rise and film temperature drop factors.

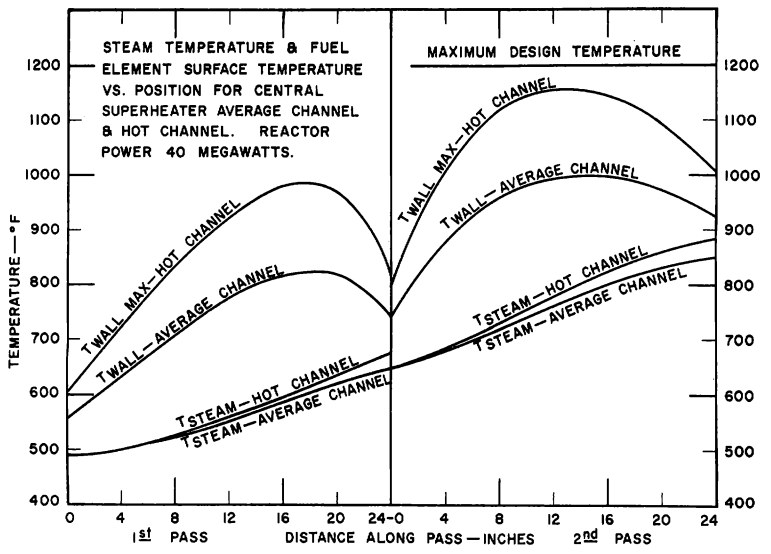

Fig. 57

Axial, Steam and Fuel Plate Temperature Profiles

V. Reactor Physics (J. I. Hagen and A. W. Solbrig, Jr.)

1. Introduction

The nuclear design effort for BORAX V is outlined in this section. Prior to the quarter covered by this report, the final or "reference" fuel loadings were established for all three configurations, i.e., all boiling core, central superheater with peripheral boiler, and central boiler with peripheral superheater. The just-critical loadings for the hot, power-producing condition (15% average steam voids in the boiler with 19% of the total power of 30.5 Mw being produced within the superheater) were obtained by analysis of a matrix of one-iteration, two-group, Univac RE-6 problems. A range of constants was obtained for these problems by the use of the MUFT IV and SOFOCATE codes. Homogenized number densities (adjusted for disadvantage factors) and self-shielding factors were supplied as input for these codes.

The two-group RE-6 problems were compared with four-group RE-6 and three-group, two-dimensional PDQ problems. The only significant disagreement occurred in the power distribution between the central boiler and the peripheral superheater. (Apparently this configuration is not well represented by the concentric cylinders of RE-6.) It was necessary to decrease the source integral for the superheater obtained from the one-dimensional RE-6 code to 16.6% to bring about agreement with the PDQ results. An increased loading was then calculated to provide sufficient reactivity for equilibrium xenon and samarium override.

2. Design Progress during the Reporting Quarter

Several aspects of the design problem were undertaken. Tables XXXV and XXXVI accompanying this section present the principal

results as of the close of this period. Table XXXV is a general summary of the reactor calculations and Table XXXVI presents data obtained for use in possible critical experiments as well as for use when first assembling the BORAX V core.

Table XXXV

NUCLEAR DESIGN OF BORAX V

	All Boiling		Central SH		Peripheral SH	
	Just Critical	Ref.	Just Critical	Ref.	Just Critical	Ref.
Loading						
g U^{235}/Fuel Rod, Boiler	11.1	16.2	13.85	16.2	11.2	16.2
% Enrichment		5		5		5
Total Loading, kg U^{235}		47		38.1		34.4
g U^{235}/Subassembly, Superheater	-	-	400	430	600	680
% Enrichment	-	-		93		93
Total Loadings, kg U^{235}	-	-		5.2		10.9
Stainless Steel Poison Rods						
Number of Rods Required to Depress Reactivity		15		0		17
Control Rods						
ρ Hot, Operating - ρ Cold Flooded Superheater	0.210	*	0.194	*	0.171*	*
Superheater Flooding Worth						
Hot - 15% Voids in Boiler	-	-		2.6		1.1
Hot - 0% Voids in Boiler	-	-		1.8		0.8
Cold - 0% Voids in Boiler	-	-		0.5		0.4
% $\Delta\rho$ in Boiler Voids						
Hot, 15% Average Voids to 0% Unflooded Superheater	-	4.2		3.5		4.1
Hot, 15% Average Voids to 0% Flooded Superheater		-		2.7		3.8
%$\Delta\rho$ in Temperature (Boiler 0% Void)						
Hot to Cold, Unflooded SH		6.5		7.2		7.4
Hot to Cold, Flooded SH		-		5.9		7.0
Boiler Only, Hot to Cold, Unflooded Superheater		-		6.7		6.9
Boiler Only, Hot to Cold, Flooded Superheater		-		5.7		6.5

*Calculations incomplete.

**Calculated with 16.2-g U^{235}/rod (depressed with B^{10}) and 655-g U^{235}/SH subassembly.

Note: Changes in reactivity, ρ, are given as

$$\Delta\rho = \rho_1 - \rho_2 = \frac{K_{eff_1} - 1}{K_{eff_1}} - \frac{K_{eff_2} - 1}{K_{eff_2}}$$

Table XXXVI

CRITICAL SIZES AND WORTHS OF ASSEMBLIES

Core Description	Critical Radius (cm)	No. of Assemblies in Critical Core	Worth of 1 Assembly at Core Edge (%Δρ)	Worth of Central Assembly (%Δρ)	Critical Mass (kg)
Boiler Assemblies only, 16.2 g U^{235}/rod (cold, clean, 0% void)	21.4	11.2	2.5	7.4	8.9
SH Assemblies only, 430 g U^{235}/assembly (cold, clean, flooded)	37.0	33.4	0.5		14.4
SH Assemblies only, 680 g U^{235}/Assembly (cold, clean, flooded)	19.3	9.0	3.4		6.2

a. Fuel Rods

It was decided, primarily for economic reasons, that the same set of fuel rods should serve for all three cores and that the loading for these rods should be that required in the central superheater, as this case required the highest enrichment. It was also decided that a number of stainless steel and/or boron-stainless steel poison rods would be used to substitute for fuel rods as needed in the pure boiling and peripheral superheater cores. During the present report period, calculations were made to obtain the worth of these poison rods. The approximate numbers required for suppression of reactivity are listed in Table XXXV.

b. Two-dimensional Calculations

Two-dimensional flux plots were obtained in x-y geometry for all three cases and in r-z geometry for the central superheater-peripheral boiler. In the latter problem the variation in steam voids was taken into account by use of discrete regions with different void fractions. The overall average was the same 15% used for all one-dimensional problems on the reactor at power. The stainless steel structure in the water reflector above and below the core was homogenized with the water and similarly represented in discrete regions. The reactivity for this problem was, however, in good agreement with previous results.

c. Control Rod Calculations

PDQ problems were run to check the ability of the control rods to provide adequate shutdown in all three configurations. In the superheating reactor, it is particularly important that there be sufficient shutdown when the superheater is flooded and the reactor cold. Preliminary results are listed in Table XXXV.

d. General Factors Affecting Reactivity

Several RE-6 problems were run to simulate the flooded superheater, hot and cold, and to establish temperature and steam void worth. Other problems are being run to obtain information at an intermediate temperature. Results available at the end of this quarter are listed in Table XXXV.

3. Final Design and Hazards Report

Studies directed toward the writing of the Final Design and Hazards Report have been initiated. These studies include a survey of the literature to assess the danger and probability of a metal-water reaction, and to find a suitable method of treating the kinetics problem in the event of an excursion.

a. Metal-Water Reaction

While the probability of a stainless steel-water reaction actually occurring is remote because of many interlocks and operational care, an excursion under some conditions could bring about melting of superheater plates. Live steam passing across these at high velocity is a factor that requires investigation. From results obtained with TREAT (Chemical Engineering Division experiments) and other sources, a pessimistic guess would suggest between a 4 to 10% reaction possible.

b. Nuclear Excursion Analysis

Studies of the SPERT excursion experiments together with a general survey of related work were carried on in order to investigate methods of treating the kinetics problem and, in particular, to obtain a quantitative description of probable shutdown mechanisms under excursion conditions. An exceedingly unlikely chain of events could lead to rather rapid injection of cold water into the hot boiler by the forced convection pump. The resulting ramp-rate of reactivity addition could be as high as 20% per second.

Univac problems were submitted to obtain the prompt neutron lifetime by the $1/v$ thermal poison method. Preliminary problems to obtain adjoint fluxes have been prepared. The adjoint fluxes will be used as input to the RE-185 code, which calculates effective delayed neutron fraction and prompt neutron lifetime.

4. Coupling Theory

Some investigation into the application of coupled reactor theory was begun. It is felt that some semi-empirical relationships might be established which would enable a prediction of the overall effect of a change

in one region, as well as possibly to obtain an insight into the future experimental behavior of BORAX V when operated as a superheating reactor. During the past quarter, several special Univac problems were run to obtain source dependence of one region on the other for selected cases.

VI. Reactor Control and Instrumentation (W. R. Wallin and R. N. Curran)

1. Reactor Control

Three features of the electrical part of reactor control differ from previous BORAX reactors and EBWR:

a. Control rods may be operated in groups, as described in ANL-6120. Two-speed reversing motors with starters are employed to drive the four intermediate control rods surrounding the center rod individually at a given speed or in the group of 4 at one-fourth speed. This is a convenience to the operator in that only three lever switches are needed to manipulate control rods.

b. There are three scram interlocks required for superheater operations: Low main-steam flow, High superheat fuel temperature, and Superheater flood-valve open. Alarms provide a warning that the first two scrams are being approached.

c. A scanning system provides a warning if any one of 40 superheater fuel thermocouples indicates a fuel temperature above 1250°F. The scanning system consists of a stepping switch with action initiated by a motor-driven switch. The system samples at the rate of one thermocouple every 1.5 sec. The thermocouple selected is balanced against a standard voltage equal to the desired alarm or scram point. When a voltage difference, created by the thermocouple output exceeding the standard output, is seen by an amplifier, the scram or alarm relay is actuated. The scram thermocouple is selected manually, not by the scanner. Using the same 40 thermocouples, a selecting system using a manual rotary switch, relay tree, and stepping switch permits one of these thermocouples to be recorded continuously. All of this is accomplished remotely using only 16 conductors, whereas 80 conductors, $\frac{1}{2}$ mile long, would be required without these switching and scanning systems.

2. Nuclear Instrumentation

The log power amplifier used on BORAX IV has been modified to use a semiconductor log converter in a temperature-controlled atmosphere to provide long-time stability. The linear power amplifier 8-decade range switch has been changed to use a Ledex system. This reduced the number of wires required to the remote control building. Potentiometers have been installed on the control console so the operator can observe and adjust the trip level setting of the safety high-flux circuits.

3. Radiation Monitors

A commercially available fission product monitor to monitor continuously a condensed steam sample or a reactor water sample has been purchased. This unit collects activated particles on a resin column which is monitored with a scintillation counter feeding a log rate meter through a pulse-height analyzer.

As a result of the redesign of the air-ejector-exhaust system, a new stack monitor has been purchased. This unit will monitor for both particulate and gas activity.

4. Process Instrumentation and Control

The major portion of the process instrumentation and control was ordered from the Minneapolis Honeywell Company on a performance-type specification. To use the main control valves as driving function controls for transfer function experiments, high-speed operation was desired. The valves were specified to be capable of following oscillations up to a frequency of one cycle per second with amplitudes as follows:

Main Feedwater-Control Valve	- 10% of 120 gpm
Main-Steam, Back-Pressure-Control Valve	- 20% of 60,000 lb/hr at 600 psig
Vent-Steam, Back-Pressure-Control Valve	- 20% of 45,000 lb/hr at 100-600 psig

This is equivalent to 10% and 20%, respectively, of full power at 20 Mw. These valves were subcontracted to the Fisher Governor Company to obtain the fastest electropneumatic valves available.

Underload testing of these valves using water at 735 psig for the feedwater valve and compressed air at 300 psig for the steam valves revealed that the steam valves have a flat response to 0.2 cps. By increasing the electrical control signal 20 to 30 percent above that required for flat response, these valves can be made to oscillate at one cps. No improvement beyond this point is possible without sacrificing the requirement for tight shutoff.

The water-level control system is specified to maintain recorded water level to within 1 in. of set point in the 66-in.-ID reactor vessel during normal operation with a maximum deviation of 3 to 4 in. for a 60,000 lb/hr load change. This is equal to closing the main steam valves at full power (20 Mw). To perform a computer analysis of this control system, Honeywell required response characteristics of the transmitters. Special underload testing of these transmitters showed that the response of the process pressure-to-current transmitter is flat to one cps, and the differential pressure-to-current signal will be down about 2 db for the 400-in.-of-H_2O transmitter and about 5 db for the 100-in.-of-water transmitter. With a knowledge of the responses of amplifiers, recorders, and other components, the control system response can now be determined and settings of control devices can be established.

Measurement of water level in the reactor will be accomplished by means of a differential pressure device connected to the standpipe outside the reactor vessel. To improve the accuracy of this device, two features are added to the system used previously. The measuring column and reference leg will be heated by a steam-tracing line to maintain the temperature equal to that of reactor water. A density-compensating signal taken from the reactor pressure recorder will correct the output of the differential pressure transmitter.

The automatic water level control is a three-element, all-electric system similar to that used for ALPR and EBWR, but designed by Minneapolis Honeywell especially for BORAX V. The back-pressure-control system uses two valves, each taking its control signal from the reactor pressure transmitter when in automatic control. When the main-steam, back-pressure-control valve has opened to provide maximum permissible steam flow to the turbine the vent valve opens to exhaust steam to atmosphere for powers higher than 20 Mw. These valves can also be controlled manually.

Valves and transmitters required by the construction contractor for installation have been received. The recorders, indicators, and control components are being installed as they are received.

VII. Control Rods (R. E. Rice)

The control rods for BORAX V consist of five 14 x 14-in. cruciform rods, one located in the center, with four equispaced in an intermediate ring, and four 7 x 14-in. T-shaped rods located on the core edge, one in the center of each flat. These rods are made of Boral, clad with X-8001 aluminum alloy and have an X-8001 aluminum follower and a stainless steel extension shaft. In the preliminary design, these rods were $\frac{3}{8}$ in. thick and were made with $\frac{1}{4}$-in.-thick Boral which had 35 w/o B_4C in the "meat."

In order to increase the clearance between rods and the $\frac{1}{2}$-in. channels in the core structure shroud, the overall thickness of the rods has been reduced to $\frac{5}{16}$ in. and the Boral is now $\frac{3}{16}$ in. thick, but has 50 w/o of B_4C in the "meat." The cladding of X-8001 aluminum is still $\frac{1}{16}$ in. thick.

SNG problems were run to ascertain the effect of an increased water thickness in the control rod channels. Thermalization appeared to increase only slightly with the thinner rod.

Two sets of control rods are needed. The rods for the boiling core have a stroke and follower length of 29 in., and the poison can be moved 5 in. above the core for certain clean core experiments. The rods for the two superheat cores have a stroke and follower length of only 24 in. because the superheater flood and drain manifolds limit the stroke.

Detailed design of the control rods was completed this quarter and materials procurement is under way at Central Shops.

VIII. Control Rod Drives (M. Trillhaase)

BORAX V will use the control rod drives originally used on EBWR, but modified to meet the requirements of BORAX V. Before it was decided to modify and use the EBWR control rod drives on BORAX V, all known American manufacturers of reactor control rod drives were contacted in an effort to select the best drives available at reasonable cost. Screw and nut drives with linear seals, rack and pinion drives with rotary seals, and even one novel design utilizing a worm gear with generated rack, were considered. However, when the EBWR drives were made available to BORAX at no cost, the choice became obvious. These drives are of the screw and nut type, with linear seal. Modifications have been made to satisfy BORAX characteristics, to improve performance, and to achieve simplification where experience showed this to be practical.

Of primary importance are the improvements made in the seal housing to achieve more effective flushing. This was a problem with EBWR, and the buildup of radioactive crud resulted in a high level of radiation at the drives. An improved bushing and a baffle in the housing should eliminate this trouble in BORAX.

To insure more positive unlatching, the stub shaft has been altered. The notch is now circumferential and a slight bevel ($2\frac{1}{2}°$) eliminates hesitation by the latch rollers when scramming. The external dashpot on the EBWR drives was found to be superfluous and has been eliminated. Performance has been improved by modifying the shape of the internal dashpot plunger. Other changes made include shortening the stroke from 48 to 29 or 24 in., and installing mechanical stops. The stroke is set by limit

switches and can be readily changed again merely by repositioning these switches. The possibility of damage to reactor internals caused by defective limit switches failing to limit the stroke is eliminated by mechanical stops which back up the switches.

All drives complete with motors and change gears will be shipped to the BORAX site. For flexibility in control it was decided to have two speeds available on the intermediate control rods and new two-speed gear motors have been bought for this purpose. The change gears provide a choice of three gear ratios between the gear motors and drives.

The control rod drives for BORAX V are now almost complete and ready for shipment to Idaho. Work remaining to be done consists of installing baffles in seal housings, installing "rod down" indication switches, and completing assembly.

IX. Reactor Vessel (R. W. Thiel and R. P. Hearn)

1. Introduction

The conceptual design of the pressure vessel is based on five prime requirements: it should be capable of operating with superheating cores; it should be suitable for forced-circulation experiments; the operating pressure should be high enough so data gathered are commercially meaningful; there should be many vessel openings to provide versatility; and the vessel should have a useful life of about five years. The vessel size was based upon core design and hydraulic requirements.

Final design consisted of a vessel of 5 ft 6 in. ID x 16 ft long. The shell thickness was $1\frac{7}{8}$ in. and the heads were $3\frac{1}{4}$ in., all of A-212-B carbon steel made to fine-grain practice. A $\frac{3}{16}$-in. internal cladding of Type 304 stainless steel was provided. A total of 40 nozzles was provided, including 9 for control rods.

Sufficient detail design was done to prove the feasibility of the vessel, to provide the necessary correlation to related equipment and structures, to permit the writing of a specification, and to provide a basis for cost estimates and bid evaluation. (A detailed description of the pressure vessel and its functions is set forth in ANL-6120, Preliminary Design and Hazards Report, Boiling Reactor Experiment V.)

In April, 1959, the invitation-to-bid package was released and on August 3, a contract was signed with the Nooter Corporation of St. Louis, Missouri for $123,900 for a February 15, 1960, delivery date.

The fabricator's design work was sufficiently complete by early September to permit ordering the shell plate and heads and flanges, which were the first items needed by their shop.

In the meantime a general steel strike started on July 2, 1959, and continued until November 7th (116 days). Foreign steel sources were investigated but nothing useful was developed. As a result of the strike, the contract delivery date was extended to June 19, 1960.

Later-than-scheduled deliveries to the fabricator of the above-mentioned basic parts further complicated the procurement schedule. AEC expediting assistance, a DMS E-2 priority rating, and BDSA directives were of little help in this regard.

General fabrication started in mid-March, 1960, on receipt of the main closure flanges. Boiler shop work proceeded at good pace, but machining work peculiar to this type of vessel was new to the fabricator and was a source of considerable trouble, both procedurally and timewise. However, the quality of finished work from all departments was excellent.

A noteworthy item was observed during fabrication. The top and bottom heads had been ordered to be dished $\frac{3}{4}$ in. beyond the usual 2:1 ellipsoidal shape to allow for expected shrinkage due to the welding-in of the several nozzle reinforcements. Actual shrinkage was of the order of $\frac{1}{16}$ in.

ANL inspection has been on an intermittent rather than a resident basis, since Nooter has a capable and conscientious inspection group who operate with virtually unquestioned authority within the company. The ANL inspectors served more as advisers and expediters than as monitors.

2. Report Period

a. Fabrication

By the beginning of the report period, all materials were on hand at the fabricator's shop, except some recently revised "O" rings for D.S.D. Couplings. These were received during the quarter.

During this quarter, the welding-in of the several nozzle reinforcements was completed and the vessel was stress-relieved. No appreciable distortion was found after stress relief. Subsequent to this operation, the reinforcements were machine-bored, the nozzles fitted and welded, machining was completed, all bolts were fitted, radiography was completed, and the 1% boron-stainless steel thermal shield was fitted. The feedwater spargers and the vessel lifting devices were completed.

It became necessary to build up a portion of the thermal shield in order to provide the specified plate thickness. This was accomplished satisfactorily through the use of boron-stainless filler strips applied by the Heliarc process. Later machining was found to be possible, though somewhat difficult. Workmanship continued to be generally excellent, and machining continued to be the fabricator's principal problem.

The "plow-through" welded cladding process, developed for this job, gave some trouble and procedural revisions had to be developed.

When stainless steel having a moderately low carbon content is electrode-deposited on a higher-carbon steel backing, the carbon from the backing material diffuses into the stainless deposit and results in a higher-than-desired carbon content in the finished deposit.

In the "plow-through" process an ELC stainless steel sheet is first laid against the backing material. The stainless steel electrode is then applied over the sheet in a manner that burns through the sheet and penetrates the backing. This method is capable of producing a stainless steel cladding surface with a carbon content of the order of 0.08%.

b. Cleaning, Final Inspection and Testing

General fabrication was completed on September 16th and the cleaning and final inspections were started. Some difficulty was encountered in removing the free iron inclusions from the surface of the Lukens stainless steel clad. Repetitive sandblasting, grinding, and passivation finally produced the required cladding surface. As-built dimensions were all found to be within the specified tolerances.

In preparation for hydrostatic testing, a number of strain gages and a brittle coating were applied. Testing was done with demineralized water. The vessel specifications require leakage at a test pressure of 1275 psig. During several tests, leakage occurred at the main closure flanges at about 900 psig. Several corrective measures were attempted, unsuccessfully, including the use of gasket shimming material borrowed from EBWR. The attending representative of the gasket manufacturer then recommended modifications of the flange gasket grooves. The vessel was dismantled and remachining began on September 30th. ANL inspectors were at the Nooter plant for 10 visits with a total of 38 days during this quarter.

c. Contract Amendments

During this quarter, the final contract amendment was negotiated and the contract price was increased, thereby, to $128,235. This represents a total increase of 3.5% over the original price. The major portion of this increase resulted from additions to the scope of work.

X. Fuel-handling System (D. Brown)

The fuel-handling system for BORAX V may be divided into three subsystems:

1. reloading of fuel with the reactor vessel head on;
2. reloading of fuel and core structures with the vessel head removed; and
3. the storage and handling of fuel, core structures and core components.

1. For reloading through nozzles in the top head of the reactor vessel, the preliminary design of a tool with an extendable grappler has been completed. This tool will be used primarily with the boiling core. The grappler is novel in that a waterproof push-pull type of solenoid is used to actuate the grappler. A model of the grappler head has been made and tested continuously under water for three days. Due to limitations of building height, the crane hook has a maximum height of fifteen feet above the main floor. If a one-piece rod with grappler were used to remove fuel assemblies, the length of such a rod would be twenty feet. So the tool height has been reduced by combining a telescoping rod with an extendable arm. The tool is mounted on top of a coffin, which in turn is mounted on a frame directly above one of the fuel-handling nozzles in the vessel head. The coffin support frame may be adjusted so that the coffin can be mounted over any one of the five fuel-handling nozzles.

This tool will operate as follows: The telescoping rod is inserted through the nozzle, and the grappler is lowered to approximately shroud height. The grappler then may be extended to a maximum radius of ten inches from the nozzle centerline by means of a ball screw drive. The grappler may also be rotated about the nozzle centerline, enabling the grappler to grip any fuel element within a ten-inch radius of the nozzle centerline. By using all five fuel-handling nozzles, fuel assemblies from the entire boiling core may be removed with the vessel head on.

The fuel-handling coffin, used for both head-on and head-off operations, will be a modified version of an existing BORAX coffin. Modification is necessary so that the superheat elements can be accommodated and so that the fuel-handling tool can be mounted on the coffin. The natural uranium portion of the old coffin will be used to conserve on space requirements. Also, the doors of the existing coffin will be redesigned so that more positive closing is obtained after the fuel element is hoisted into the coffin. This will make for safer transportation of the fuel assemblies.

2. When retrieving either boiler or superheater assemblies with the vessel head removed, the coffin will be placed directly over the fuel element to be removed. A grappler similar to the one used on the vessel head-on handling tool will retrieve the boiling assemblies. The design of the superheat fuel assembly grappler is not yet complete. A spool piece, which bolts onto the reactor flange, is provided so that the water level in the vessel may be raised to provide adequate shielding when raising fuel into the coffin.

3. A mockup of a portion of the core in a water tank is being fabricated to check the feasibility of the fuel-handling tools, and the underwater lighting. Another use of the tank is to determine if a periscope is necessary for viewing the grappling head and fuel element with the vessel head on.

The water-storage pit will be used for fuel handling and for cooled or temporary storage of the fuel assemblies and the boiling fuel rods. The boiling fuel assemblies will be stored in the BORAX IV storage racks. New holders have been designed for the individual fuel rods. Tools and fixtures for inserting and removing the fuel rods in the fuel assembly submerged in the water storage pit have been designed. The old BORAX reactor pit and vessel will be converted to a dry storage area for fuel assemblies and miscellaneous radioactive core components.

The three core structures: peripheral superheat, central superheat and boiling, will be stored in the dry storage pit. Preliminary designs of the lifting fixture and storage stands have been completed. The control rods will also be stored in the dry storage pit during core changes. Lifting hooks have been designed for this operation.

Hand tools and a concrete block shield have been considered to remove the flood and drain manifold from the superheater core structures. Preliminary design of hand tools has been completed for the miscellaneous operations of removing the core structure and components. These tools encompass the following operations: uncoupling of the temperature-compensated coupling, removal of flow bushings in the core support plate, operation of boiler fuel assembly hold-down latches, and removal of chimneys and hold-down boxes.

XI. Superheater-fuel Assembly-seal Test Program (J. D. Cerchione)

When installed, BORAX V superheater fuel assemblies must have a nearly perfect, watertight seal between the individual assemblies and the reactor core-support plate. This seal will prevent excessive water leakage from the reactor moderator into the superheated steam circuit.

A program to test seals was initiated in 1959, and the testing of standard, commercially available, metallic-type seals was undertaken to determine which would give the best performance in BORAX V. A 600-psig seal test vessel and mockup superheat fuel element were constructed for the test, as shown in Fig. 58. The advantages of using static metallic seals result from the low compressive forces required for proper sealing and the ability to meet the temperature requirements. For seals of the size necessary for BORAX V, compressive loads range from about 150 to 800 lb, while for ordinary Flexitallic-type gaskets of comparative size a load of about 10,000 lb would be required. Disadvantages of metallic seals results from the considerations that they require very parallel seating surfaces (because the seals only deflect 0.005 to 0.030 in. when compressed), that they require extremely smooth mating surfaces (16 to 32 microinches rms), and that the seals must be kept as clean and smooth as possible. The manufacturers recommend that all of the seals be silver-plated to overcome slight deformities in seating surfaces. Most seals of this type may be used over and over again; however, the thin-walled metallic "O" rings have a limited life of about 6 or 7 compressions.

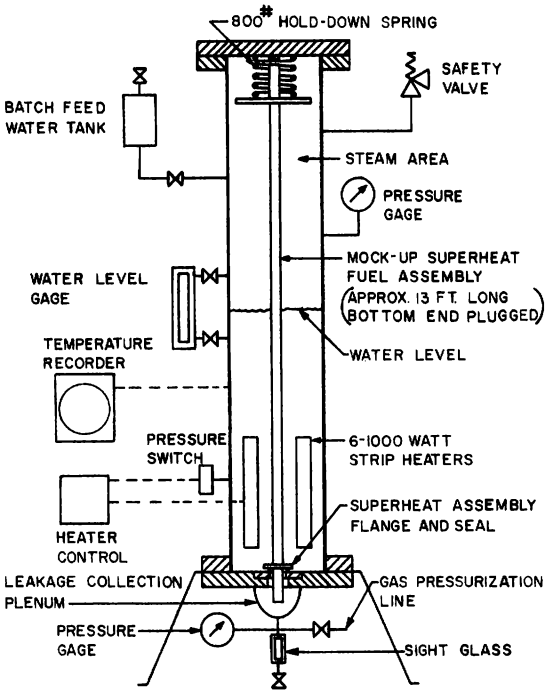

Fig. 58 Seal Test Rig

The tests were conducted on three different types of seals from five different manufacturers; the Cadillac Gage Company, Costa Mesa, California; the Hydrodyne Corporation, North Hollywood, California; the Advanced Products Company, North Haven, Connecticut; The D.S.I. Manufacturing Company, Hamden, Connecticut; and the United Aircraft Products Company, Dayton, Ohio.

The various seals were placed on a mockup fuel element in the test vessel, and rates of seal leakage were measured while varying compressive forces on the seals and pressure differentials across the seals. A hydraulic cylinder mounted on top of the test vessel was the source of the varying hold-down load, while a high-pressure gas bottle was used to adjust the pressure in the plenum below the seal to give the required pressure differential across the seal.

The preliminary results of the seal tests definitely established the feasibility of using one or more of the seals on the BORAX V superheater fuel element. Good data were obtained as to the hold-down loads required on the various seals, and these data agreed quite favorably with the respective manufacturer's recommendations. The Cadillac, Hydrodyne "Skinner," and Advanced seals, respectively, required about 16, 53, and 100 lb load per linear inch of seal for acceptable sealing.

To simulate actual operating conditions more closely, four large springs of varying loads were purchased to replace the hydraulic cylinder as the hold-down force on the seal-test vessel. As a result of tests conducted during April and May, 1960, the silver-plated hollow-metal "O" ring was selected as the most desirable seal for BORAX V, and testing of other types of seals was discontinued. This selection was based on the fact that the "O" ring gave by far the best seal and was not appreciably affected by the pressure differential across the seal. In addition, the "O"-ring seals are considerably more economical. With an 800- to 900-lb spring hold-down load, which was slightly less than the manufacturer's recommendations, leakage rates on the "O"-ring seal averaged 1 to 2 cc/hr.

For proper sealing and to prevent overstressing, the "O" rings must be deflected a specified amount, controlled by groove depth. They must further be backed up on either the ID or OD to prevent overstressing of the "O" ring.

The current reference design makes use of a standard $2\frac{5}{8}$-in. diameter, silver-plated "O" ring, press fitted inside its own integral retainer ring. This retainer ring satisfies both of the above requirements and eliminates the necessity of machining seal grooves for the "O"-ring seal, into either the core support plate or the fuel element flange, which could collect dirt and be difficult to clean. Several manufacturers will supply the "O" rings in this manner.

Extensive testing of the stainless steel, silver-plated "O" rings, with pressure-equalizing holes, press fitted inside an integral retainer ring, was conducted with excellent results. This type seal is shown on the mockup superheat fuel assembly in Fig. 59. Leakage rates with a 20 to 30-psi pressure differential across the seal and a hold-down force of 600 to 800 lb averaged 1 to 4 cc/hr over prolonged periods of time.

In order to facilitate remote seal replacement on the fuel assembly and ease of insertion and removal into the reactor, three equally spaced stainless steel leaf springs are installed on the fuel element nozzle to retain the "O"-ring seal. A special "sliding door" jig will be used for removal and replacement of seals on superheat fuel assembly nozzles remotely under water in the water storage pit. Preliminary tests of the nozzle leaf springs and seal removal and replacement jig proved very satisfactory.

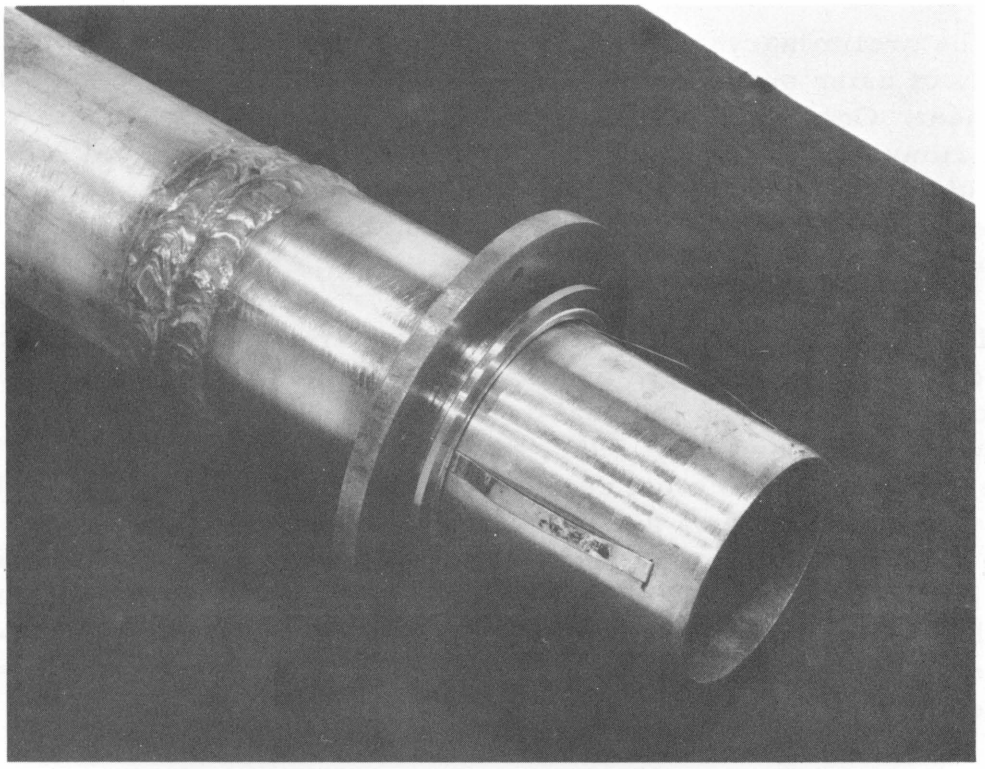

Fig. 59 Superheater-fuel Assembly Seal

To insure a minimum spring relaxation at the elevated temperatures in BORAX V, and to resist the corrosive atmosphere, the superheater-fuel-assembly-hold-down springs which apply the sealing load will be made of Inconel X material.

XII. In-core Instrumentation Development (E. J. Brooks)

1. Introduction

An extensive program of in-core instrumentation is being developed for the BORAX V reactor, with the intent of determining parameters of reactor operation to advance the design of boiling water types of reactors.

The measurements described below illustrate the variables which will be monitored. The use to which these measurements will be placed can be briefly described as follows:

Fuel Temperatures

Such data will provide the operator with safety information, and will give information for calculating power distribution

and generation in the fuel. Overall heat transfer coefficients for the boiler fuel rods may be determined from measurements of center fuel and water temperatures, thus giving some indication of the physical condition of the fuel.

Water Temperatures

Measurements of water temperature will be used to help obtain data on average boiling length (boiler fuel assembly), downcomer recirculation rate, and water subcooling.

Flow Measurements

Measurements of flow in individual assemblies will allow calculation of power production at various assembly locations in the core. Flowmeters in instrumented boiler fuel assemblies, in addition to the above, will also give data to determine the rate of generation of steam voids.

Pressure Measurements

Measurements of steam pressure during transient testing will be made to correlate void generation, water temperatures, flow rates, and other data obtained simultaneously.

Flux Mapping

These physics measurements are to be used in obtaining radial and axial flux distribution and neutron spectra within the core.

2. Fuel Temperature Measurements

Boiler Fuel Rod Thermocouples

For measurement of the UO_2 temperatures at points along the axis of the fuel, tungsten vs 74% tungsten/26% rhenium thermocouples have been specified. Sample pieces of material have been procured, and are now undergoing resistance and calibration tests at temperatures up to 4200°F. The thermocouples are insulated with magnesium oxide or beryllium oxide, and sheathed with 0.063-in. diameter tantalum tubing in the fuel area. For passage through the boiling water region, the insulation used will be aluminum oxide, and the sheathing will be 0.085-in. diameter stainless steel tubing. On the basis of the test results, the vendor and final type of insulation will be selected for fabrication of production thermocouples for the fuel rods.

Superheater Temperatures

Sample thermocouples representative of final design have been procured commercially and are currently being fabricated into mocked-up superheat fuel plates by Central Shops. The thermocouple design selected is a chromel-alumel type with aluminum oxide insulation and a 0.040-in. diameter stainless steel sheath. The tip is bent to a 90° angle and flattened to 0.020-in. for insertion into a hole in the edge of the fuel plate, where it is brazed in place. Difficulties in this final assembly stage have now been overcome, and the design appears to be feasible to construct.

3. Water Temperature Measurements

Saturation and Subcooled Regions

Absolute temperatures will be determined with chromel-alumel, stainless steel-sheathed thermocouples, and temperature differentials will be determined by means of thermopiles constructed of specially selected and aged chromel-alumel thermocouples. Construction drawings of these instruments are nearly completed, and it is intended to have a reliable thermocouple vendor fabricate these items.

Tungsten resistance thermometers, now commercially available, are being considered as a back-up for the above thermocouples and thermopiles. Data available indicate excellent stability and sensitivity, and it appears that the only problem is that of obtaining suitably long extension leads on the thermometers. The vendor is currently working on a proposal regarding such instruments.

Boiler Fuel Assembly Water Temperatures

A dummy fuel rod will be used to insert 12 thermocouples into the flowing stream within a boiler assembly. Construction drawings must yet be made on this "rake." The dummy rod will be furnished to a thermocouple vendor for assembling the thermocouples into it.

4. Flow Measurements

Boiling Assembly

A turbine-type meter, as is shown in Fig. 60, is currently undergoing air-water tests at the entrance of a boiler fuel assembly mockup. An exit meter of similar design is on order, with delivery expected during November. Both meters will undergo further testing to verify their performance in measuring flow rate and in determining void ratio in the assembly.

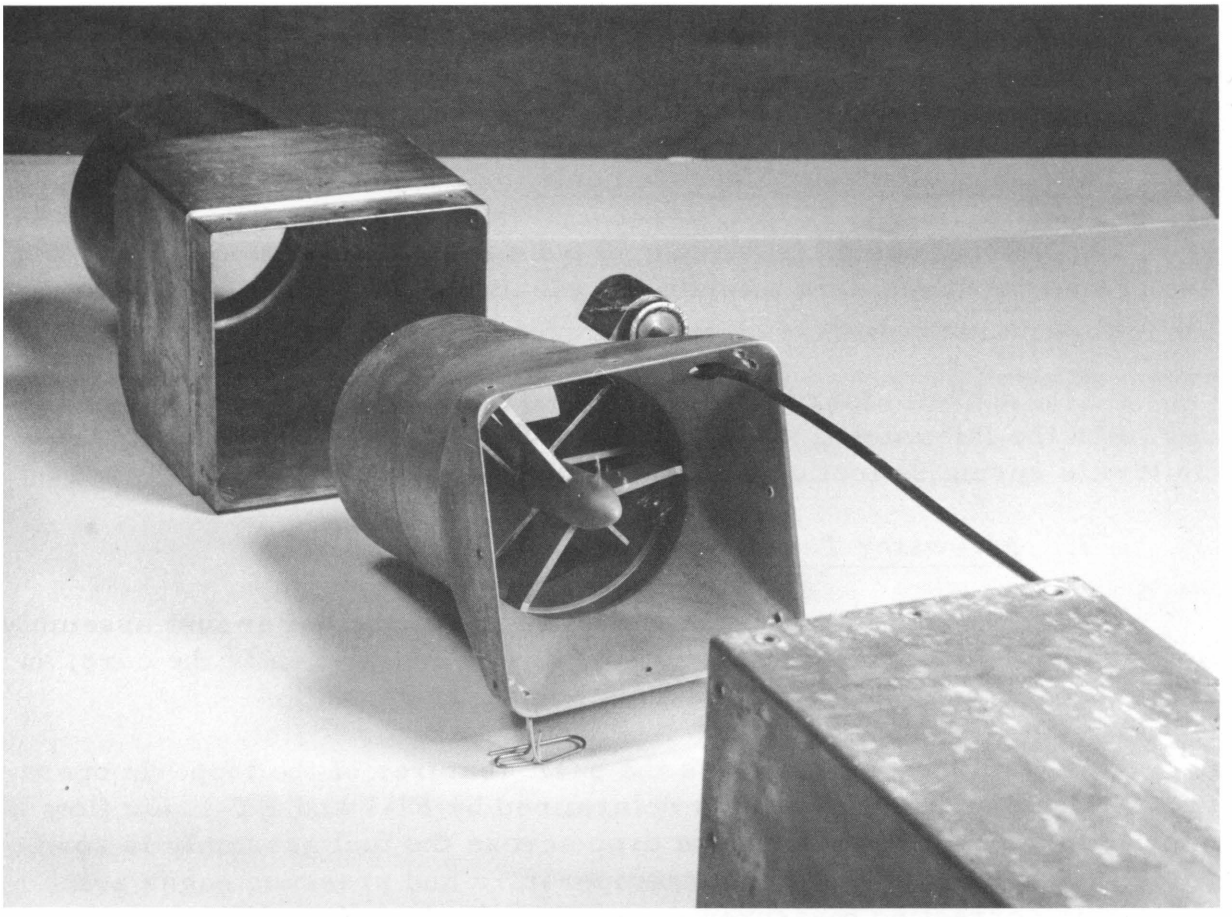

Fig. 60 Boiler Fuel Assembly Flowmeter

A drag-disk type of flowmeter for the entrance has been received, but was returned to the vendor for repair of damage in shipment. This meter will be compared with the turbine meter to determine which is most useful for the final design. The construction of the flowmeter is such that it may be easily modified to obtain velocity measurements in the reactor downcomer, should it not be satisfactory for use in the boiler assemblies.

Superheater Assembly

Three sets of proposed designs on a superheater fuel assembly flowmeter have been exchanged between ANL and Potter Aeronautical with Potter's latest proposal being unsatisfactory because of interferences between the pickup coil and core hold-down plate.

5. Pressure Measurements

Final design is not complete on the method of mounting the pressure transducer in the vessel; however, it is planned to seal a standard

strain gage-type transducer or a newly developed variable-reluctance transducer in a pressure-tight housing which will operate in the reactor vessel.

6. Miscellaneous Measurements

Final design is not completed on flux-mapping equipment, but use of wire activation and miniature ionization chamber techniques are planned.

A preliminary design proposal has been discussed with a vendor, with the intention of making measurements on the core structure Belleville spring deflection while at temperature and pressure.

7. Air-water Test Loop

In order to verify the performance of the boiler fuel assembly flow and void-measuring instruments prior to installation in the core, an air-water test loop has been constructed and operated.

Figure 61 illustrates the basic features of the loop. In operation, the rate of flow of water is determined by FI-1 and FT-1, air flow by FI-2 and FT-2. The pressure drop across the fuel assembly is read on ΔP-1 and ΔP-2. The various temperature and pressure gages are utilized in correcting measurements to standard conditions.

The air-water mixture is introduced at the fuel-assembly entrance, and for this reason loop operation differs from actual reactor conditions. To calibrate the flowmeter pair for voids, two sets of runs are necessary: one set with water flow only, and the second set with air-water mixture. Also, because of this difference, two-phase pressure-drop measurements will show greater loss than actually occur in the reactor and must be corrected by a factor related to the equivalent boiling length.

The void fraction is measured by the gamma attenuator technique, which consists of using a synchronous motor-driven thulium-170 source and photomultiplier combination to measure attenuation of the air-water column. Data are presented on a strip chart recorder. Operation of the system was verified by interposing attenuation paths of known density. In actual use, "empty" and "full" attenuation readings are obtained on the test section to compensate for source decay.

Hydraulic data obtained to-date are reported elsewhere in this report (see Section IV).

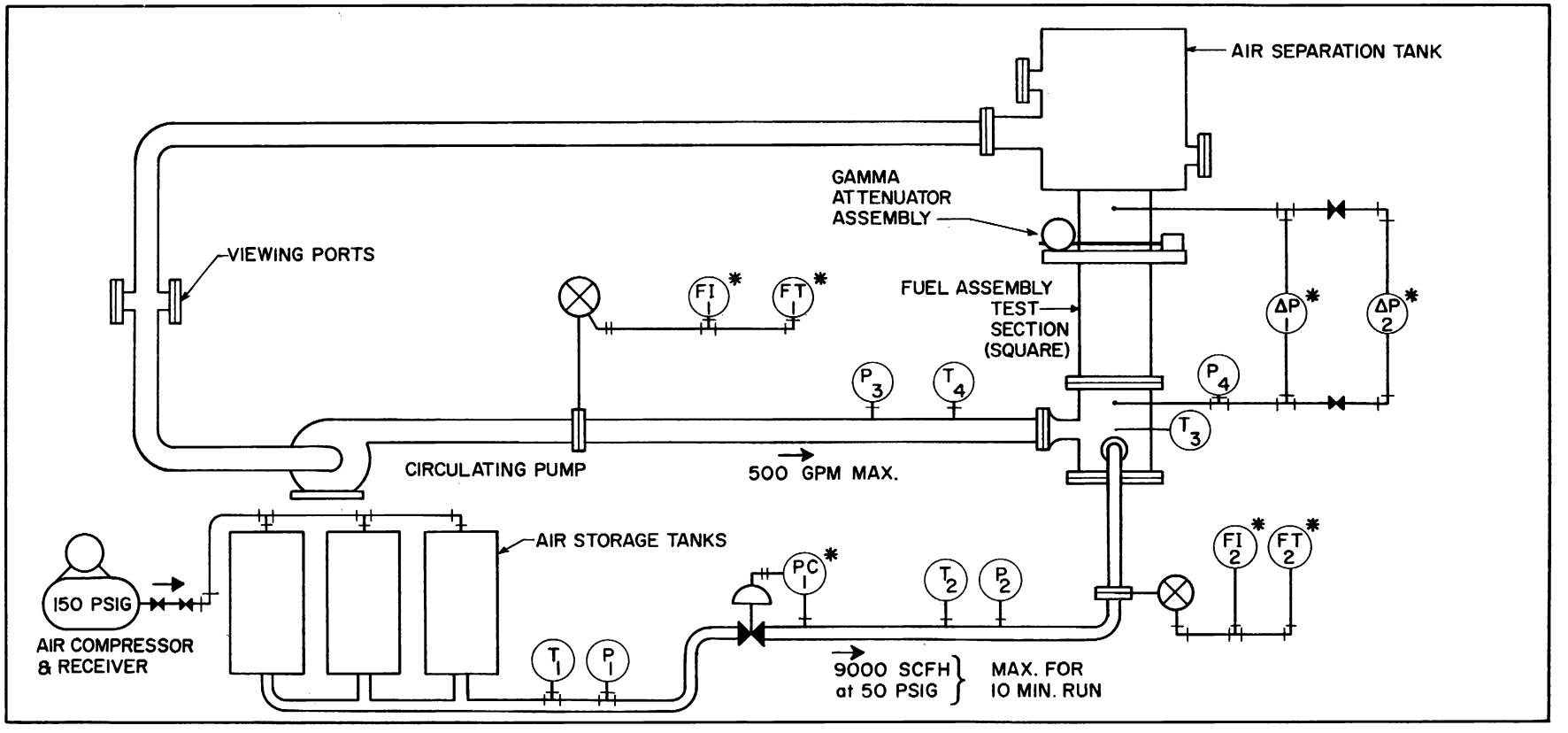

P_1 LOCAL PRESSURE GAGE 0-200 PSIG

P_2 LOCAL PRESSURE GAGE 0-200 PSIG

P_3 LOCAL PRESSURE GAGE 0-60 PSIG

P_4 LOCAL PRESSURE GAGE 0-60 PSIG

ΔP-1* PANEL-MOUNTED DIF. PRES. GAGE 0-30 PSI

ΔP-2* PANEL-MOUNTED DIF. PRES. GAGE 0-2 PSI

T_1 LOCAL THERMOMETER 0-200 °F

T_2 LOCAL THERMOMETER 0-200 °F

T_3 LOCAL THERMOMETER 0-200 °F

T_4 LOCAL THERMOMETER 0-200 °F

PC-1* PANEL-MOUNTED PRESSURE CONTROLLER

FI-1* PANEL-MOUNTED WATER FLOW RATE INDICATOR 0-500 OR 0-125 GPM

FT-1* PANEL-MOUNTED WATER FLOW TOTALIZER 25 COUNTS PER MIN. AT MAX. FLOW

FI-2* PANEL-MOUNTED AIR FLOW RATE INDICATOR 0-9000 OR 0-4500 SCFH

FT-2* PANEL-MOUNTED AIR FLOW TOTALIZER 1500 COUNTS PER HOUR AT MAX. FLOW

NOTE: * = PANEL MOUNTED INSTRUMENT

Fig. 61 Schematic of Air-water Loop

XIII. Water Chemistry (D. Cissel and C. Miles)

Chemistry activities for the BORAX V reactor plant will be conducted to control water conditions to the greatest practical extent and to observe the effects of basic processes occurring in the plant, viz:

(1) corrosion;
(2) neutron activation;
(3) radioactivity transport and deposition;
(4) water dissociation; and
(5) radiation-induced chemical reactions.

These effects are related to practical problems in the operation and testing of the plant, such as component reliability, personnel radiation exposure, plant maintenance, and radioactive waste disposal. Knowledge of the effects is also essential to the correct analysis of component malfunction or failure.

The BORAX V power plant water treatment components will be operated to maintain maximum attainable water purity under all operating conditions, with the following objectives:

1. To maintain halide (especially chloride) concentrations in the reactor coolant as low as possible, thus reducing the danger of halide-induced stress-corrosion cracking of austenitic stainless steel fuel element cladding and structural members.
2. To maintain concentration of all water impurities, subject to neutron activation, as low as possible, thereby reducing coolant specific activity and curtailing the formation of long-lived activities which can pose problems of plant maintenance, accessibility, and waste disposal.
3. To maintain concentrations of all water impurities as low as possible, thereby reducing the carryover of such impurities in the saturated steam from the boiling region with possible deposition in the superheat region.
4. To reduce the danger of localized electrochemical corrosion due to deposition and reduction of heavy metals on cladding and core structures.
5. To reduce concentrations of ionic and particulate impurities which promote the dissociation of water under irradiation.

Against this background of controlled water conditions, chemistry test work can be conducted, and comprises the following:

1. radiochemical studies to identify and determine fission products and neutron-activation products in the plant streams;

2. studies of corrosion-product species and concentrations in the plant streams;

3. radioactivity deposition studies;

4. water dissociation studies; and

5. studies of radiation-induced chemical reactions.

The implementation of chemistry control and testing activities requires a system for sampling the various plant streams and for making certain chemical measurements. Accordingly, a preliminary design of a sampling system for the BORAX V plant, which has the following capabilities, has been completed:

1. intermittent sampling of the major plant streams for laboratory chemical and radiochemical analyses of contained gases and solids;

2. semicontinuous filtration of selected sample streams to permit determinations of suspended solids concentrations and to provide samples of accumulated solids for chemical and radiochemical analyses;

3. semicontinuous flow of selected sample streams through ion-exchange columns to concentrate dissolved solids for laboratory analysis;

4. continuous measurement of electrolytic conductivity in selected plant sample streams;

5. continuous measurement of pH in selected plant sample streams; and

6. continuous measurement of dissolved oxygen concentrations in selected plant sample streams.

During this report period, procurement of equipment items for the BORAX V chemistry sampling panel was initiated.

XIV. Contruction Status (R. E. Rice)

1. History

Bid invitations for the BORAX V construction contract were sent out in early September, 1959, and the low bidder, Arrington Construction Co. of Idaho Falls, Idaho, was awarded the contract on November 12, 1959. Scheduled completion date was October 15, 1960, and initial contract price was $721,275.

In April, 1960, the control building was completed and accepted by ANL. The new underbuilt power line between the Central Facilities Area and the BORAX site was completed and turned over to the Phillips Petroleum Co. for operation.

The following "Schedule X" items designed and specified by ANL or NECO and procured by ANL are being furnished to the contractor:

Item	Vendor
Reactor Vessel	Nooter Corp.
10,000-gpm Forced Convection Pump	Worthington Corp.
150-gpm Circulating Pump	Peerless Div. of Food Mach. Corp.
Two 150-gpm Reactor Feed Pumps	Byron Jackson Co.
150-kw Reactor Water Preheater	Mongomery Bros.
Process Control and Instrumentation System and Control Valves	Minneapolis Honeywell
Solenoid Trip Valves	Ruggles-Klingman
Condensate Demineralizer	Nooter Corp.

In addition, several items such as air compressors, reactor water demineralizer system, makeup water demineralizer system and storage tank, feedwater storage tank, and sump pump, from the existing BORAX plant are being reused. A portion of the 14 and 16-in. stainless steel piping and valves originally fabricated for a forced-circulation system in EBWR is being used on BORAX V. By the end of this report period all of the above-listed items were on hand, with the exception of the reactor vessel.

2. Status

At the start of this report period, July 1, 1960, all excavation, including the 56-ft-deep reactor pit in solid rock, was complete. The concrete work for the reactor pit, subreactor room, access shaft, piping trench between reactor and turbine building, and new footings and grade beams for the reactor building were complete, and some of the high-density concrete shielding slabs had been poured. Most of the piping was installed, welded, and radiographed in the trench between buildings, and installation of equipment and piping in the equipment pit had begun. The transformer and controls for the 10,000-gpm pump were installed on the new substation slab, and wiring had begun. Materials for the prefabricated metal reactor building were on the site. At this time, the overall construction project was 53.5% complete, as compared with 67.5% scheduled.

By the end of this report period, October 1, 1960, most of the concrete work was completed, including the piping trenches and floor slab in the reactor building, the high-density shielding slabs, the foundation and

floor slab for the H&V building, and most of the piping-trench cover slabs. The concrete block heating and ventilating building was finished, and installation of the reactor building heating system and reactor pit exhaust systems was well advanced. The prefabricated metal reactor building was completed with the exception of a portion of the roof left off for the installation of the reactor vessel, and the interior wainscoting. The spiral staircase and floor levels of gratings were installed in the access shaft and subreactor room.

The 10,000-gpm forced convection pump was installed in the subreactor pit. Installation of equipment such as feed pumps, condensate filters and demineralizers, reactor ion-exchange heat exchangers, control valves and piping, was near completion in the equipment pit. Installation of piping and valves in the east and west piping trenches in the reactor building was well along, and the batch emergency feed system and boron-addition system were in place.

The electrical subcontractor had completed all exterior electrical work, including the new substation and branch power line, with the exception of the line between reactor and turbine building, and was installing wiring, conduit, and controls inside the reactor building.

At this time the construction contract was 79.5% complete, versus 93% scheduled. Because of delays caused by the unexpected large amount of pressure grouting in the fractured lava beneath the reactor pit and by miscellaneous small changes and additions to the contract, the contract completion date was officially extended to November 4, 1960 and the contract price was up to $817,000. However, because of delay in construction the actual completion date will obviously be later.

E. ARGONNE FAST SOURCE REACTOR (AFSR)

G. S. Brunson

The Argonne Fast Source Reactor went critical late in October, 1959. After a brief checkout period for determination of the permanent fuel loading and for the calibration of control and shim rods, the lower core section was returned to Argonne for canning. The final core loading was 21.52 kg of enriched uranium.

Early in January, 1960, the canned fuel was re-installed and the reactor again was loaded to critical. Mechanical tune-up, such as a remodeling of the plug position indicator, continued.

Shielding was found to be inadequate at various places. The nominal thickness of 4 1/2 in. of dense concrete was sufficient, but the hardness of the neutron spectrum made all penetrations a much greater problem than had been anticipated. As a result, special shielding has been added over the access tunnel, in a girdle around the reactor shield at the floor level, and at the end of the thermal column. In addition, the manhole cover was rebuilt.

The fluxes available have been explored and are shown in Table XXXVII for those who might want to make use of AFSR fluxes. Figure 62 shows the location of the experimental holes. Table XXXVIII lists the dimensions of these facilities.

Table XXXVII

FLUXES AVAILABLE IN AFSR

Position	Flux Characteristics: Cadmium Ratio for				One Watt-hour Gives the Following Number of Fissions per Gram of				One-watt Power Level Gives the Following Fluxes ($n/cm^2/sec$)
	B^{10}	$\frac{\sigma_{f28}}{\sigma_{f25}}$	$\frac{\sigma_{f24}}{\sigma_{f25}}$	$\frac{\sigma_{f49}}{\sigma_{f25}}$	U^{235}	U^{238}	$U_{enriched}$	Pu^{239}	
Center of core (glory hole and foil recess)		0.147		1.26	6.0×10^9	8.8×10^9	5.6×10^9	7.6×10^9	5.0×10^8
Center of grazing hole		0.050		1.27	1.8×10^9	9.0×10^7	1.7×10^9	2.4×10^9	1.5×10^8
*Inner end of beam hole		0.059	0.39	1.27	2.3×10^9	1.4×10^8	2.2×10^9	2.8×10^9	2.0×10^8
Inner end of beam hole liner	1.17	0.027	0.31	1.51	1.0×10^9	2.75×10^7	9.4×10^8	1.5×10^9	8.0×10^7
Center of graphite hole #1	34						8.2×10^9	1.1×10^{10}	1.5×10^6
Center of graphite hole #2	~800			1.28			1.0×10^9	1.4×10^9	1.9×10^5
Beam hole	Beams available 1 foot out from face of reactor shield								1.0×10^4
Grazing hole									1.8×10^3
Glory hole									1.3×10^3
Vertical cooling duct									3.3×10^3

*Not normally accessible

Table XXXVIII

DIMENSIONS OF EXPERIMENTAL FACILITIES

Core including 0.005-in. nickel can	diameter	4.51 in.
	height	4.55 in.
Glory hole	diameter	0.50 in.
Horizontal axis of hole intercepts axis of core 0.15 in. above center of core. Center point of hole is $66\frac{3}{16} \pm \frac{1}{16}$ in. from face of shield Glory hole #1, $66\frac{1}{4} \pm \frac{1}{16}$ in. through Glory Hole #2.	effective dia (with thimble)	0.470 in.
Grazing hole	diameter	1.078 in.
Horizontal axis of hole passes axis of core at a distance of 3.875 in. and lies 1.277 in. below center of core. Minimum blanket thickness between grazing hole and core is 0.984 in. Center point of grazing hole is $66\frac{3}{16} \pm \frac{1}{16}$ in. from face of shield through Grazing Hole #1 and $66\frac{1}{4} \pm \frac{1}{16}$ in. through Grazing Hole #2.		
Beam hole	diameter	2.218 in.
Horizontal axis of hole intercepts axis of core 0.15 in. above center of core. Hole itself terminates in blanket 2.852 in. from axis of core. Minimum blanket thickness between beam hole and core is 0.500 in. The beam hole liner prevents insertion of anything farther than 4 in. from inner end of hole.	effective dia (with liner)	2.128 in.
Graphite thermal column	4 ft high	
Reactor is embedded ~1 ft into end of thermal column. Minimum thickness of graphite between 1st hole and reactor is 1 ft, between 2nd hole and reactor is 3 ft. Holes have been reamed to $2\frac{3}{8}$ in. Stringers can be removed along axis of thermal column to accept equipment up to 16 x 16 in. Center of thermal column is $66\frac{1}{4} \pm \frac{1}{4}$ in. from either shield face in either hole.	4 ft wide 5 ft 8 in. long	
Miscellaneous		
Rossi α at delayed critical	3.65×10^5 sec^{-1}	
Prompt neutron lifetime (assuming $\beta_{effective} = 0.0068$)	1.86×10^{-8} sec	
Operational core loading	21.524 kg enriched U	
Estimated critical mass	21.25 kg enriched U	
Coolant flow	~76 cfm	

115-v outlets for instrument use are white; black outlets are for utility use.

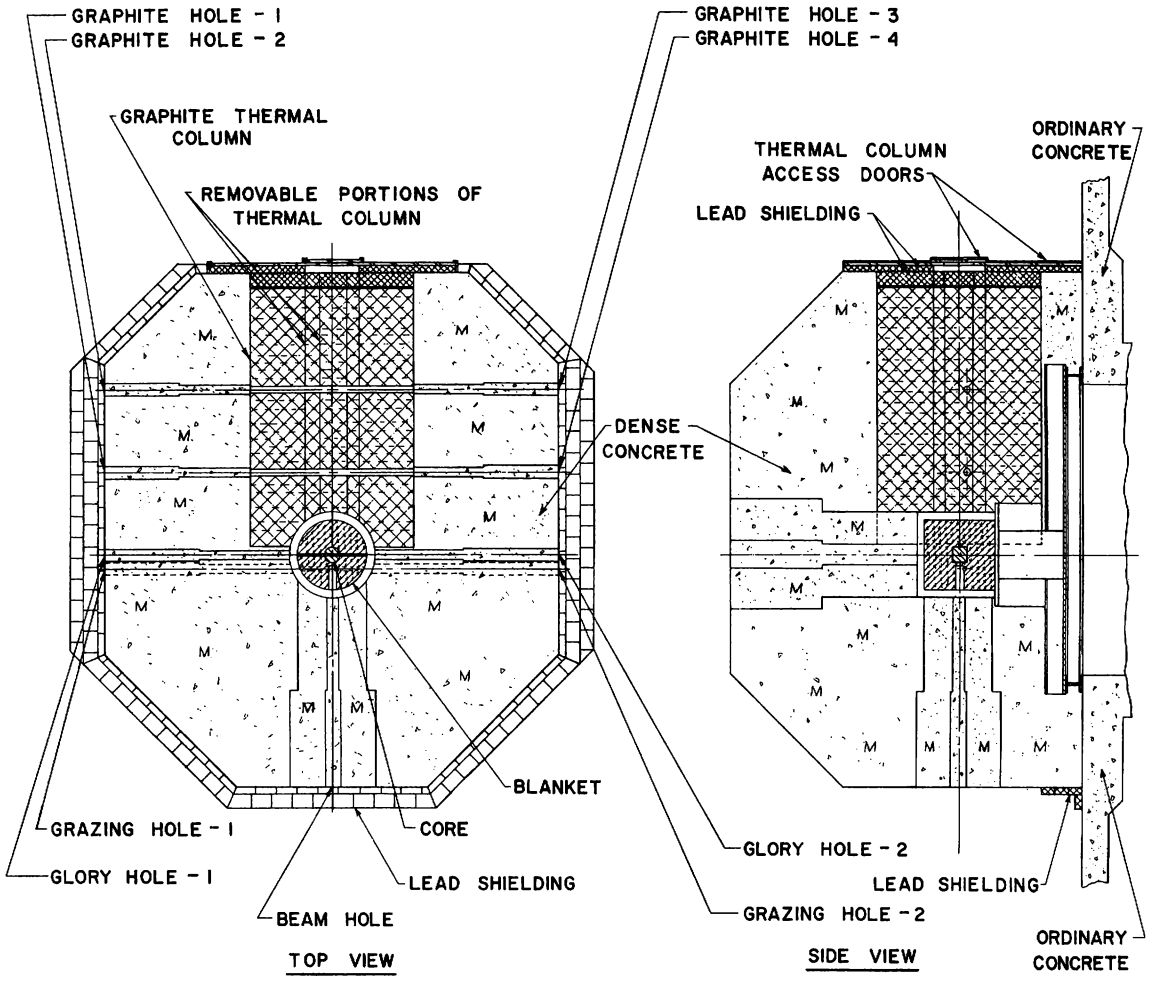

Fig. 62 Experimental Facilities at the AFSR.

A Rossi-alpha measurement on the reactor gave results in excellent agreement with those obtained on TOPSY at Los Alamos. The alpha is 3.69×10^5 sec^{-1}, corresponding to a neutron lifetime of about 1.9×10^{-8} sec.

The operating instructions have been revised in the light of experience and will be published shortly.

The experimental program associated with AFSR is just getting under way. A first model of a neutron spectrometer has been built, utilizing proton recoil from one scintillator to another.

Currently we are working to bring background noise down to an acceptable level by improving the electronics and chilling the phototube with dry ice.

A second type of proton-recoil spectrometer is to be fabricated soon. This counter is designed to accept for analysis only those proton recoils which travel in a narrowly defined volume in the direction of the neutron beam.

A third type of spectrometer based on the principle of total absorption is to be tested. Its main component is a large, annular $B^{10}F_3$ counter which has already been procured.

The program for irradiation of materials which might be used as spectral indicators has begun. Samples of gold, copper, nickel, and manganese were irradiated over a range of neutron spectra.

Soon a representative of Reactor Engineering Division will be using AFSR to test a Perlow counter which, if successful, will be used in ZPR-III. Other work in the future, as now planned, will pursue the four ideas outlined above.